EVALUATION OF 15[1]-HYDROXYPURPURIN-7-LACTONE (G2) DERIVATIVES, BORON DIPYRROMETHENE (BODIPY) AND ROSAMINE ANALOGUES AS PHOTOSENSITISERS FOR PHOTODYNAMIC CANCER THERAPY

LIM SIANG HUI

FACULTY OF MEDICINE
UNIVERSITI MALAYA
KUALA LUMPUR

2014

EVALUATION OF 15[1]-HYDROXYPURPURIN-7-LACTONE (G2) DERIVATIVES, BORON DIPYRROMETHENE (BODIPY) AND ROSAMINE ANALOGUES AS PHOTOSENSITISERS FOR PHOTODYNAMIC CANCER THERAPY

LIM SIANG HUI

THESIS SUBMITTED IN FULFILMENT OF
THE REQUIREMENTS FOR THE DEGREE OF
DOCTOR OF PHILOSOPHY

FACULTY OF MEDICINE
UNIVERSITI MALAYA
KUALA LUMPUR

2014

UNIVERSITI MALAYA

ORIGINAL LITERARY WORK DECLARATION

Name of Candidate: LIM SIANG HUI (I.C/Passport No: 801012-08-6471)

Registration/Matric No: MHA 100010

Name of Degree: DOCTOR OF PHILOSOPHY

Title of Project Paper/Research Report/Dissertation/Thesis ("this Work"):

EVALUATION OF 15[1]-HYDROXYPURPURIN-7-LACTONE (G2) DERIVATIVES, BORON DIPYRROMETHENE (BODIPY) AND ROSAMINE ANALOGUES AS PHOTOSENSITISERS FOR PHOTODYNAMIC CANCER THERAPY

Field of Study:

I do solemnly and sincerely declare that:

(1) I am the sole author/writer of this Work;
(2) This Work is original;
(3) Any use of any work in which copyright exists was done by way of fair dealing and for permitted purposes and any excerpt or extract from, or reference to or reproduction of any copyright work has been disclosed expressly and sufficiently and the title of the Work and its authorship have been acknowledged in this Work;
(4) I do not have any actual knowledge nor do I ought reasonably to know that the making of this work constitutes an infringement of any copyright work;
(5) I hereby assign all and every rights in the copyright to this Work to the University of Malaya ("UM"), who henceforth shall be owner of the copyright in this Work and that any reproduction or use in any form or by any means whatsoever is prohibited without the written consent of UM having been first had and obtained;
(6) I am fully aware that if in the course of making this Work I have infringed any copyright whether intentionally or otherwise, I may be subject to legal action or any other action as may be determined by UM.

Candidate's Signature Date

Subscribed and solemnly declared before,

Witness's Signature Date

Name:
Designation:

Evaluation Of 15[1]-Hydroxypurpurin-7-Lactone (G2) Derivatives, Boron Dipyrromethene (Bodipy) And Rosamine Analogues As Photosensitisers For Photodynamic Cancer Therapy

Abstract

Photodynamic therapy (PDT) is a therapeutic strategy that utilises the administration of a photosensitiser along with light irradiation to generate reactive singlet oxygen that destruct pathological lesions. However, the current clinically approved photosensitisers for the treatment of cancer present several limitations such as a lack in ideal photophysical and photochemical properties, poor solubility and adverse effects i.e. prolonged photosensitisation or pain following PDT. Therefore, it is necessary to discover and develop new classes of photosensitiser with more ideal properties. From our earlier data, we had shown that 15[1]-hydroxypurpurin-7-lactone dimethyl ester (G2), a semisynthetic cyclic-tetrapyrrole, was a potent photosensitiser. In this study, aspartyl and lysyl amino acids conjugated G2 analogues were prepared and evaluated with the aim to further improve its PDT efficacies. Also included in this study, were two series of non-tetrapyrrolic photosensitisers: boron difluoride dipyrromethene (BODIPY) and rosamine photosensitisers. Both classes of compounds have many characteristics of an ideal photosensitiser and their syntheses are relatively easy to perform and scale-up. For the G2 analogues, results from the study indicated that conjugation of aspartyl or lysyl amino acids was able to modify its properties including light absorption coefficient, singlet oxygen quantum yield, cellular uptake and intracellular localisation. Both conjugations were able to improve the aqueous solubility but resulted in reduced *in vitro* PDT potency. Further evaluation showed that G2-aspartyl (G2-Asp) was able to achieve similar potency compared to G2 in terms of vasculature occlusion efficiency in chorioallantoic membrane (CAM) model and tumour growth inhibition in a syngeneic mouse model. Meanwhile for the BODIPYs, *in vitro* data indicated that BODIPY with

iodinated core exhibited potent photo-induced cytotoxicity at sub-micromolar IC_{50} concentrations. Further studies on a lead BODIPY showed exclusive mitochondria localisation, induction of G_2/M-phase cell cycle block and onset of apoptosis. The BODIPY molecules also extensively occluded the vasculature of the CAM model. Conversely for the rosamines, they were found to be minimally photoactive, even though several of the derivatives exhibited potent cytotoxicity (average $IC_{50} < 0.5$ μM) which was found to be associated with their ability to compromise mitochondrial membrane potential and to inhibit the oxidative phosphorylation complexes primarily the ATP synthase. Preliminary *in vivo* studies on 4T1 murine breast cancer-bearing female BALB/c mice indicated that treatment with a lead rosamine in a single dosing of 5 mg/kg or a scheduled dosing of 3 mg/kg once every two day for six times (q2d×6) exhibited only minimal tumour growth delay. In conclusion, G2-Asp given its hydrophilic nature, is a pharmaceutically advantageous candidate to be developed into a clinical photosensitiser as it can be formulated easily for administration. Meanwhile for the non-tetrapyrrolic photosensitisers, BODIPY with an iodinated core structure may have potential as new PDT agents for cancer, while the rosamine analogues may be further developed as mitochondrial targeting agents that either directly kill or deliver cytotoxic drugs to selectively kill cancer cells.

Evaluasi Derivatif 15[1]-Hidroksipurpurin-7-Lakton (G2), Boron Dipyrromethane (BODIPY) dan Rosamin Sebagai Fotosensitiser Untuk Terapi Kanser Secara Fotodinamik

Abstrak

Terapi fotodinamik (PDT) merupakan strategi terapeutik yang melibatkan penggunaan molekul fotosensitif (fotosensitiser) bersama-sama dengan penyinaran cahaya untuk menjana molekul oksigen singlet yang reaktif yang berupaya memusnahkan lesi patologi. Walau bagaimanapun, fotosensitiser semasa yang diluluskan untuk rawatan klinikal kanser mempunyai beberapa batasan contohnya; kekurangan ciri-ciri fotofizikal and fotokimia yang ideal, tahap kelarutan yang rendah dan kehadiran kesan sampingan seperti fotosensitiviti yang berpanjangan dan kesakitan berikutan PDT. Oleh itu, penemuan kelas fotosensitiser yang baru dengan ciri-ciri yang lebih ideal harus diberi keutamaan. Kajian terdahulu kami telah menunjukkan bahawa 15[1]-hidroksipurpurin-7-lakton dimetil ester (G2) merupakan fotosensitiser tetrapirol bersiklik separa sintetik yang poten. Dalam kajian ini, analog G2 yang dikonjugasikan dengan asid amino seperti asid aspartik dan lisin telah disediakan dan diuji dengan tujuan meningkatkan keberkesanan PDT. Kajian ini juga merangkumi dua siri fotosensitiser bukan tetrapirol iaitu *boron difluoride dipyrromethene* (BODIPY) dan rosamin. Kedua-dua kelas sebatian ini mempunyai ciri-ciri fotosensitiser yang ideal dan kaedah sintesis mereka adalah mudah untuk melaksanakan. Hasilan daripada kajian ini menunjukkan G2 yang dikonjugasi dengan asid aspartik atau lisin mengubah parameter termasuk koefisian molar penyerapan, kuantum penghasilan oksigen singlet, penyerapan sel dan intra-selular lokalisasi. Kedua-dua konjugasi ini berupaya meningkatkan kelarutan akueus tetapi dengan pengurangan potensi PDT *in vitro*. Kajian selanjutnya menunjukkan bahawa G2-aspartil (G2-Asp) mampu mencapai potensi yang sama berbanding dengan G2 dari segi efikasi oklusi vaskular dalam model membrane

korioalantoik (CAM) model dan perencatan pertumbuhan tumor dalam model mencit syngenik. Sementara itu, bagi sebatian BODIPY, data *in vitro* menunjukkan bahawa BODIPY berteraskan iodin mempamerkan foto-sitotoksiksiti yang tinggi dengan nilai IC_{50} pada kepekatan sub-mikromolar. Kajian lanjutan keatas BODIPY pilihan menunjukkan lokalisasi mitokondria secara eksklusif, menghalang kitaran sel pada fasa G_2/M dan apoptosis. Molekul BODIPY ini juga menyebabkan oklusi vaskular CAM secara menyeluruh. Sebaliknya, rosamin didapati mempamerkan fotoaktiviti yang minima, tetapi beberapa terbitannya menunjukkan sitotoksiksiti yang tinggi (purata IC_{50} < 0.5 μM). Aktiviti ini dikaitkan dengan keupayaan mereka untuk mengkompromasikan potensi membran mitokondria dan merencat kompleks pemfosforilan oksidatif terutamanya ATP sintase. Kajian awalan *in vivo* menggunakan mencit BALB/c betina yang diinokulasi dengan kanser payudara 4T1 menunjukkan bahawa rawatan rosamin utama dengan dos individu (5 mg/kg) atau dos berkala (3 mg/kg sekali setiap dua hari untuk enam kali, q2d×6) melewatkan pertumbuhan tumor hanya pada kadar yang minimum. Kesimpulannya, G2-Asp yang bersifat hidrofilik, adalah calon farmaseutikal yang berpotensi untuk dibangunkan sebagai fotosensitiser klinikal kerana ia boleh diformulasikan dengan mudah untuk pentadbiran. Sementara itu, bagi fotosensitiser bukan tetrapirol, BODIPY dengan struktur berteraskan iodin mempunyai potensi sebagai agen baru PDT untuk kanser, manakala analog rosamin boleh terus dibangunkan sebagai agen sasaran mitokondria yang sama ada secara langsung membunuh atau sebagai agen penghantaran sebatian sitotoksik untuk membunuh sel-sel kanser.

Acknowledgements

Many individuals have generously contributed their time and support in making the completion of this project possible. I would like to take this opportunity to extend my sincere gratitude to those who have provided guidance and assistance in every step of the way. Without them, this thesis could not have been written.

My foremost appreciation is to Dr. Lee Hong Boon, who introduced me to photodynamic therapy. I would also like to heartily thank her for her continuous guidance and help during my research work. It has been a real pleasure and a positive learning experience working with her. My appreciation is also extended to Prof. Dr. Chung Lip Yong and Dr. Kiew Lik Voon for their invaluable advice and constructive criticisms throughout the course of this project. In addition, I would like to thank all three of them for their help in reviewing the chapters of this thesis.

A special note of thanks to the Medical Photonics Group, Swiss Federal Institute of Technology (EPFL) Prof. Dr. Hubert van den Bergh, Dr. Georges Wagniéres, Dr. Patrycja Nowak-Sliwinska, Dr. Elodie Debefve, Dr. Filippo Piffaretti and Dr. Tanja Gabrecht from EPFL, Switzerland for sharing their expertise in PDT and for making my six months attachment in their laboratory fruitful while equally enjoyable and unforgettable. I am also indebted to Prof. Dr. Kevin Burgess and his research team, especially Wu Liangxing, Cliferson Thivierge and Anyanee Kamkaew at Chemistry Department of Texas A&M University, USA for their generosity in providing us the compounds/photosensitisers for this study.

Special thanks are also expressed to Prof. Dr. Teo Soo Hwang at Cancer Research Initiatives Foundation (CARIF) for the opportunities she has provided me during my time with CARIF. The team from Photodynamic Therapy/Drug Discovery group, CARIF, especially Mr. Fadzly Azhar Kamarulzaman, Ms. Yam Mun Li, Ms.

Lam May Lynn and Ms. Norazwana Samat for their contribution to parts of the research work, and everyone in CARIF for being a friend, a labmate and for providing many wonderful time and memories. In addition, my appreciation is also sincerely extended to Mr. Andrew Leong at Monash University Sunway Malaysia for his contribution.

Lastly, I would like to thank my family especially my parents for their constant and loving support over the years. I am forever grateful. I would also like to extend my deepest gratitude to Ms. Teoh Hoon Koon for always being there and understanding and believing in everything that I do. Her relentless support and devoted companionship during the course of my study are greatly appreciated.

Table of Contents

List of Figures

Chapter 2

Chapter 3

Chapter 4

Chapter 5

List of Tables

Abbreviations

ε	Molar extinction coefficient
λ_{abs}	Wavelength absorption maxima
λ_{em}	Wavelength emission maxima
ALA	5-aminolevulinic acid
ATP	Adenosine triphosphate
BODIPY	Boron difluoride dipyrromethene
CAM	Chorioallantoic membrane
CO_2	Carbon dioxide
COMPARE	Computerised pattern-recognition algorithm
CrEL	Cremaphor EL
DAMPs	Damage-associated molecular patterns molecules
DLCs	Delocalised lipophilic cations
DMSO	Dimethyl sulphoxide
DNA	Deoxyribonucleic acid
DPBF	1,3-diphenylisobenzofuran
DTP	Development Therapeutic Programme
EDD	Embryo development day
EDTA	Ethylenediaminetetraacetic acid
EGTA	Ethylene glycolbis(aminoethylether)-tetra-acetic acid
ELISA	Enzyme-linked immunosorbent assay
EtOH	Ethanol
EWG	Electron withdrawing groups
FBS	Feotal bovine serum
FDA	U.S. Food and Drug Administration
FITC	Fluorescein isothiocyanate
IC_{50}	50% inhibition concentration
IL	Interleukin
i.v.	Intravenous
LED	Light emitting diode

MHC-I	Major histocompatibility class I
MOPS	3-(N-morpholino)propanesulfonic acid
MTT	3-(4,5-dimethylthiazol-2-yl)-2,5-diphenyltetrazolium bromide
NCI	U.S. National Cancer Institute
NMR	Nuclear magnetic resonance
PBS	Phosphate-buffered saline
PDT	Photodynamic therapy
PhA	Pheophorbide a
PpIX	Protoporphyrin IX
ref.	Reference
Rh123	Rhodamine-123
RNase A	Ribonuclease A
RTV	Relative tumour volume
SAR	Structure-activity relationship
TMR	Tetramethylrosamine
UV	Ultra-violet light
VIS	Visible light
v/v	Volume to volume

CHAPTER 1

Introduction

1.1 Overview

Photodynamic therapy (PDT) is a therapeutic strategy that utilises the administration of a photosensitiser along with irradiation of light to generate reactive singlet oxygen that destruct pathological lesions. PDT is a clinical modality approved mainly for palliative and curative treatment of some forms of cancers (superficial and luminal carcinomas), precancerous lesions and the treatment of age-related macular degeneration. The advantages of PDT over conventional treatment such as surgery, chemotherapy or radiotherapy are their potential for dual selectivity i.e. preferential accumulation of photosensitisers in diseased over normal tissues, and focusing of light to confine damage to the targeted region thus minimising collateral damage to normal tissues (Dolmans et al. 2003; Castano et al. 2004; Agostinis et al. 2011). So far, there are only five photosensitisers, namely Photofrin®, Levulan®, Foscan®, Laserphyrin® and Photolon® that have been approved for PDT treatment of cancer and they are all cyclic-tetrapyrroles. However, these photosensitisers have several limitations such as lack of long and strong light absorbance which is essential for effective light penetration into tissues, poor solubility and prolonged photosensitisation or pain following PDT.

Furthermore, the majority of photosensitisers being investigated in clinical trials share a common cyclic-tetrapyrrole structure, probably due to the fact that modern PDT has evolved from the naturally derived cyclic-tetrapyrroles such as haematoporphyrin (Nyman and Hynninen 2004; Wainwright 2009). However, challenges in synthesis and purification of cyclic-tetrapyrroles have restricted modulation of their photophysical and

biological properties through chemical derivatisation during drug development. For example, functionalisation of tetrapyrrole is often limited to *meso*-position with unsatisfactory yields that required laborious chromatographic separation (Feng and Senge 2001). Hence, there is an interest among photodynamic research groups in discovering other cyclic-tetrapyrrole or non-tetrapyrrole photosensitisers that might be synthetically more accessible.

We had previously shown that 15[1]-hydroxypurpurin-7-lactone dimethyl ester (G2), a semisynthetic cyclic-tetrapyrrole, was a potent photosensitiser and was found to be a promising clinical PDT candidate (Lim et al. 2011). However, like many tetrapyrrole photosensitisers, G2 is highly conjugated and therefore its solubility in aqueous media is poor. To overcome this, hydrophilic amino acids conjugated G2 analogues had been prepared with the aim to improve its solubility and efficacies. In this study, these G2 analogues were evaluated for their photophysical properties, *in vitro* photo-killing efficacy, single oxygen generation quantum yield, photobleaching, intracellular uptake and subcellular localisation. The most promising G2 analogue was further evaluated in a mouse tumour allograft model to establish its *in vivo* efficacies.

Additionally, two alternative classes of non-tetrapyrrole photosensitisers, namely boron difluoride dipyrromethene (BODIPY) and rosamine were also evaluated as potential PDT agents. Both BODIPY and rosamine are widely used as fluorescence imaging probe and have many characteristics of an ideal photosensitiser including, high extinction coefficients, high quantum efficiencies of fluorescence, relative insensitivity to the environment and resistance to photobleaching (Gorman et al. 2004). The synthesis of BODIPY and rosamine analogues is relatively straightforward, thus facilitating compound series preparation and scale-up (Loudet and Burgess 2007; Wu and Burgess 2008b). The capability for derivatisation is crucial in improving the selectivity and therapeutic efficacy of photosensitiser as this process may change their

photosensitising properties and their pharmacology/pharmacokinetic profiles by altering the hydrophilic/lipophilic balance. In terms of photodynamic action, only a few examples of BODIPYs and rosamines have been investigated even though a great range of derivatives could be easily synthesised.

In the initial part of this study, BODIPYs and rosamines were screened for their *in vitro* photocytotoxicity efficacy and their structure-activity relationship was analysed. The effects of the most promising candidates from both classes of compounds were further investigated in intracellular localisation, cell cycle arrest and onset of apoptosis experiments. Subsequently for the BODIPY series, their photosensitising properties were evaluated in terms of their PDT-induced vascular occlusion efficacy in a preclinical model using the chick chorioallantoic membrane (CAM). Meanwhile, due to the poor photo-induced cell killing of the rosamines and their selective accumulation in mitochondria, these compounds were further evaluated as a mitochondria targeting drug. As potential mitochondrial drugs, the effects of rosamines on cellular redox systems in terms of induction of mitochondrial transmembrane potential loss and oxidative phosphorylation enzymes inhibition were evaluated. The *in vivo* antitumour activity of the most potent rosamine was then investigated in a syngeneic mouse tumour model. Selected rosamines were also tested in the NCI-60 cell lines panel of the National Cancer Institute's (NCI) Developmental Therapeutics Program in their *in vitro* screening platform.

The overall strategies used to evaluate the three different classes of photosensitiser were slightly different as they have unique design features to enhance PDT efficacy. For example, G2 was not tested for its ability to induce cell cycle arrest or apoptosis as both the experiments had been previously reported (Lim et al. 2011). Instead, this work is a continuation to evaluate the effects of ionic amino acid conjugation on the solubility of G2 where experiments such as Log D, photostability

and cellular uptake studies were carried out. As for the rosamines which were found to be cytotoxic, a different approach was used to study their effects on mitochondrial transmembrane potential and oxidative phosphorylation enzymes activities. NCI-60 screening was also performed on the rosamines to elucidate their possible mechanism(s) of action. While the *in vitro* experiments were done using human-derived cancer cell lines, the *in vivo* experiments were carried out using 4T1-mouse mammary carcinoma in syngeneic BALB/c mouse model instead. The reason is because BALB/c syngeneic model has intact systemic immunity which is lacking in nude mice xenograft, and therefore, it is relevant for interrogating the activation of the immune system by PDT in the future. Furthermore, PDT is not known to have species-specific effects as the cytotoxic agents of PDT are reactive singlet oxygen.

1.2 Aim and Objectives

The main aim of the study is to investigate the *in vitro and in vivo* PDT efficiencies of hydrophilic amino acids conjugated G2 analogues and two series of non-tetrapyrrole photosensitisers namely BODIPY and rosamines. Rosamines were later evaluated for non-PDT antitumour activities given their interesting antitumour potency and lack of photodynamic activity. The specific objectives of this study are as follows:

1) To compare the PDT efficacies of a series of hydrophilic amino acids conjugated G2 in terms of their:
    a) photophysical properties such as molar extinction coefficient, absorption maxima and fluorescence quantum yield, as well as their photochemical properties such as singlet oxygen generation, distribution coefficiency (Log D in octanol/PBS pH 7.4) and photostability.

b) *in vitro* bioactivities such as cellular uptake, intracellular localisation and photo-induced cytotoxicity.

c) *in ovo* PDT-induced vasculature occlusion efficiency using CAM model and *in vivo* PDT antitumour efficacy in BALB/c mice bearing 4T1-mouse mammary tumour.

2) To evaluate the PDT efficacies of differently substituted BODIPYs in terms of their:

a) photophysical properties such as molar extinction coefficient, absorption maxima and fluorescence quantum yield, as well as their photochemical property such as singlet oxygen generation.

b) *in vitro* bioactivities such as photo-induced cytotoxicity potency, intracellular localisation, cell cycle arrest and onset of apoptosis.

c) *in ovo* PDT-induced vasculature occlusion efficiency using CAM model.

3) To investigate the PDT/antitumour efficacies of cyclic-amine substituted rosamine in terms of their:

a) photophysical properties such as molar extinction coefficient, absorption maxima and fluorescence quantum yield.

b) *in vitro* bioactivities such as photo-induced cytotoxicity potency, intracellular localisation, cell cycle arrest and onset of apoptosis.

c) effect on the cellular redox systems, namely mitochondrial transmembrane potential and oxidative phosphorylation enzymes activity.

d) *in vivo* antitumour efficacy in BALB/c mice bearing 4T1-mouse mammary tumour.

CHAPTER 2

Literature Review

2.1 Photodynamic Therapy

Photodynamic therapy (PDT) is a well-recognised and an approved modality for the palliative and curative treatment of some forms of cancers (refer to Table 2.1), premalignant lesions such as actinic keratosis and the treatment of neovascularisation-related disorders such as age-related macular degeneration (Dolmans et al. 2003). The application of PDT requires three key components, namely a non-toxic photosensitising drug, known as photosensitiser, non-damaging light and tissular oxygen. PDT is a two-step procedure (Figure 2.1) involving the administration of photosensitiser either topically or systematically, in which the photosensitiser will selectively accumulate in the tumour after a period of systemic distribution. The tumour lesions are then focally irradiated with light at a specific wavelength (mostly in red or far-red, 600-800 nm region) to activate the photosensitiser. Through a series of photochemical reaction, highly reactive singlet oxygen molecules are generated from molecular oxygen by the activated photosensitiser that subsequently cause damage to lesion tissues (Dolmans et al. 2003; Agostinis et al. 2011). This effect is highly localised given the short half-life of singlet oxygen ~0.6 μs (Moan and Berg 1991). In cancer treatment, PDT is capable of inducing cellular death of tumour, the shutting down of blood vessels feeding the tumour and the activation of immunological responses against tumour cells (Juarranz et al. 2008). These detailed mechanisms of tumour ablation induced by PDT will be discussed in Section 2.5.2.

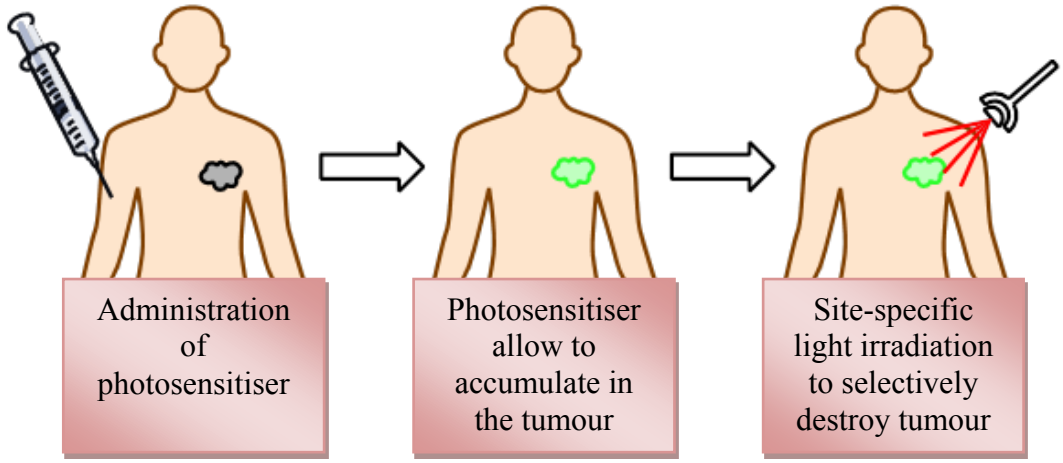

Figure 2.1 Treatment protocol of PDT. PDT is a two-step procedure, where a drug known as photosensitiser is first injected into the patient body and allowed to accumulate at the tumour site. In the second step, the tumour site is irradiated with light in order to activate the photosensitiser to selectively destroy the tumour.

The main attribute of PDT is the potential for dual selectivity, i.e. preferential accumulation of photosensitiser in diseased over normal tissues, and focusing of light to confine damage to the targeted region thereby minimising collateral damage to normal tissue (Castano et al. 2004). This makes PDT less invasive compared to conventional treatments such as surgery, by preserving tissue structure and retaining anatomical functions and mechanical integrity of hollow organs such as tongue, larynx and bladder. PDT is a suitable modality for treating patients with tumour occurring in complex regional anatomy or close proximity to vital structures which is often inoperable with surgery (Lou et al. 2004). Besides that, the excellent post-treatment cosmesis outcome i.e. minimal scarring, makes PDT the preferred modality for treating skin cancers (Wang et al. 2001).

Unlike chemotherapy and radiotherapy, PDT has no cumulative toxicity as photosensitisers are non-toxic in the absence of light. None of the clinically approved photosensitisers accumulate in cell nuclei, thereby eliminating DNA damage that can

potentially cause cancer or lead to the induction of resistant clones (Agostinis et al. 2011). Therefore, PDT can be repeated without development of resistance (Dolmans et al. 2003). Moreover, immunosuppression commonly present in conventional therapy is not observed in PDT but in fact, PDT is known to trigger activation of both innate and adaptive immune system (Castano et al. 2006; Garg et al. 2010).

In cancer therapy regimens, PDT can be used before or after surgery or, in combination with chemotherapy or radiotherapy, without compromising their treatment modalities (Agostinis et al. 2011). The sensitivity of PDT is not affected by chemoresistance or radioresistance, therefore PDT is useful to treat recurrent tumours, especially in patients who have previously been treated by chemotherapy or radiotherapy, but are unsuitable for other treatment options. In addition, PDT procedures can be performed on an outpatient basis, which is more cost-effective and patient-friendly (Agostinis et al. 2011).

PDT has several limitations. Due to the limited tissue penetration of light, PDT is more effective for thin, superficial tumours and for tumours situated within hollow organs. PDT in general is ineffective for treating metastases due to their highly localised effect. However, studies have demonstrated that PDT can activate the adaptive immune response and resulted in regression of distant untreated tumours in patients who received PDT (Thong et al. 2007). The common adverse effects of PDT are pain during treatment and photosensitivity, and because of this, local anesthesia or painkiller is given to manage the pain, whereas photosensitivity can be prevented by avoiding direct exposure to sunlight or bright indoor light for a period of time post-treatment.

2.2 Light in PDT

PDT is a type of radiation therapy but unlike radiotherapy which utilises ionising radiation such as x-ray and gamma-ray, the radiation used in PDT is non-ionising and therefore does not cause tissue damage on its own. The spectrum of light relevant to PDT covers the limited range of the visible light between 400 to 800 nm. While non-ionising, photon energy from visible light may still be able to induce certain molecules to become electronically-excited. In order to achieve optimal photosensitiser excitation, the ideal irradiation light wavelength used should correspond with the absorption maxima of the photosensitiser. However, the nature of light penetration depth into biological tissue (tissue optical window) needs to be considered for successful PDT outcome.

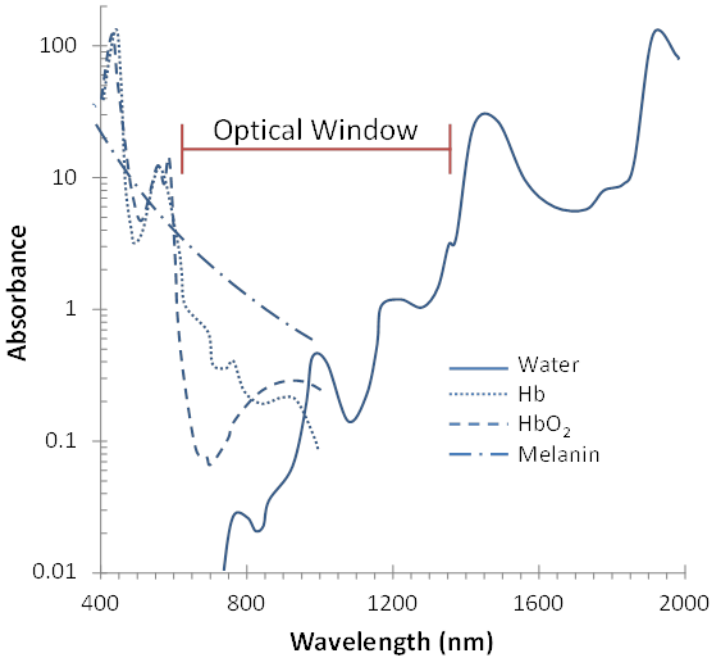

Figure 2.2 Tissue optical window. The absorption spectra of tissue interference components such as water, oxy- and deoxyhemoglobin and melanin which limit the light penetration of tissue. The figure was adapted from Castano et al. (2004).

The light penetration in tissue generally is limited by the presence of light interfering components of tissues such as water that absorbs infra-red light, and oxy-/deoxyhemoglobin and melanin that absorb UV light as shown in Figure 2.2 (Castano et al. 2004; De Felice 2010). Therefore, tissue to some extent is much more transparent at longer wavelengths 600-1400 nm (red to infra-red), while blue light penetrates least efficiently. Even though wavelengths up to 1400 nm have good penetration, the use of wavelengths beyond 800 nm is restricted given its insufficient energy to initiate photochemical reaction (Juzeniene et al. 2006). The choice of light wavelength used also depends on the depth and size of lesion tissues (Agostinis et al. 2011). For an instance, shorter wavelengths such as blue and green light have lesser tissue penetration depth of approximately 0.5-2.5 mm, are much preferred for treatment of thin, superficial cancer such as basal cell carcinoma, melanoma, cutaneous T-cell lymphoma in order to minimise photodamage on healthy tissues underneath these cancers. Meanwhile, the use of longer red light wavelengths, which have deeper tissue penetration of about 8-10 mm, allowed treatment of larger or deep-seated tumours as shown in Figure 2.3 (Tuchin 1997).

The light source for PDT can be either from lasers, incandescent- and LEDs-(light emitting diodes) lights, and is mostly delivered or directed to the target area using endoscopes coupled with fiber optics with a diffusing tip (Brancaleon and Moseley 2002). Light dosimetry is crucial in PDT for successful eradication of cancerous lesions, while causing minimal injury towards normal tissues. Nevertheless, the optimum light dose is difficult to quantify due to the reflecting, scattering and absorbing characteristics of light, and the divergent tissue optical density that varies for each individual (Zhu and Finlay 2008; Agostinis et al. 2011). Given the complexity of measuring these factors, in current clinical practice, light delivered to the target site exceeds the dose pre-determined in prior clinical trials and is in accordance with standard light doses (Mang

2008; Zhu and Finlay 2008). For example, the standard light dose used in clinical PDT is 200 J/cm^2 is illuminated with light at a typical fluence rate of 150 W/cm^2.

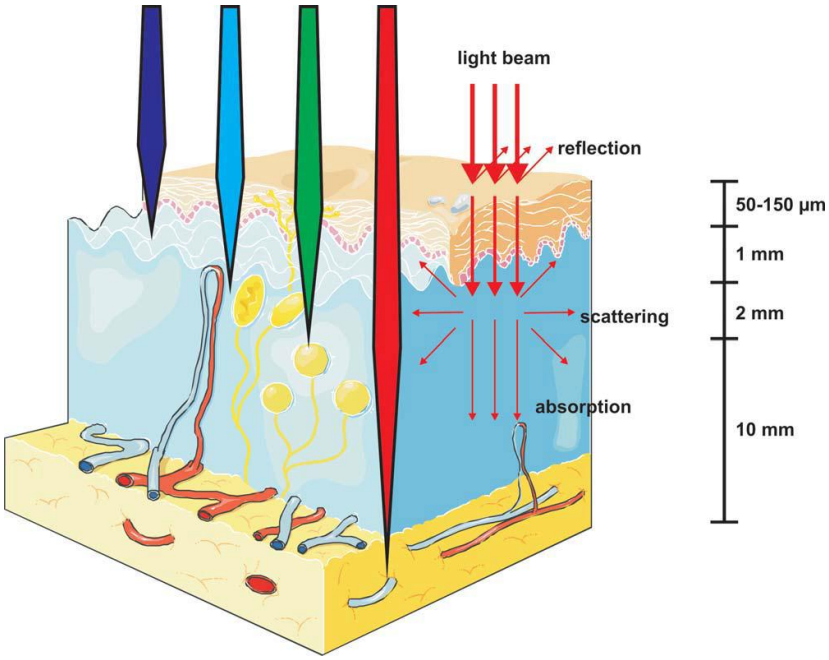

Figure 2.3 Tissue penetration depth of light at violet, blue, green and red wavelengths (as indicated by different colour bars). The scale bar on the right shows the depth of light penetration through tissues which increased with longer wavelengths. While the light beam travel through the tissue, part of the light will be reflected, scattered and absorped. The figure was adapted from Agostinis et al. (2011).

2.3 Photosensitisers

A photosensitiser is a compound with the ability to absorb light and subsequently initiates photophysical or photochemical reactions. For instance, a photosensitiser for PDT can be promoted to an excited state upon absorption of light and react with oxygen to produce singlet oxygen. The typical chemical structure of photosensitisers consists of a multiple planar-aromatic moiety known as chromophore, that is conjugated with peripheral groups known as auxochrome (Wainwright 2009). The chromophore comprise of π–electron system which is crucial for the photosensitisers ability to absorb

visible light and to mediate the conversion of absorbed light to other forms of physical or chemical energy. Meanwhile, the auxochromes participate in delocalising the electron system around the structure, thereby varying the photophysical and photochemical properties of the photosensitisers.

2.3.1 Ideal Photosensitiser Characteristics

In general, certain characteristics of photosensitiser are considered ideal for PDT as outlined by Allison and Sibata (2010), and Garland et al. (2009). An ideal photosensitiser for PDT must have relatively high absorption extinction coefficients (>20000-30000 $M^{-1}cm^{-1}$), at wavelength between 650-800 nm in order to achieve sufficient excitation energy and effective tissue penetration. As discussed in Section 2.2, absorption bands at shorter wavelengths (< 600 nm) have lower tissue penetrationdepth, whereas photons with wavelengths longer than 800 nm will not have sufficient energy to excite a photosensitiser to its singlet state and to yield substantial reactive oxygen species. Furthermore, a photosensitiser with low fluorescence quantum yield is preferred as fluorescence occurs through relaxation from singlet excited states, since high quantum yields for fluorescence means much of the energy absorbed on excitation does not crossover to triplet states for effective singlet oxygen generation. Other properties, such as low photobleaching quantum yield as photobleaching reduces the availability of photosensitiser, and high singlet-to-triplet intersystem crossing efficiencies, are desirable for optimal singlet oxygen generation.

Table 2.1 Clinically approved or in trials photosensitisers for cancer treatment.

Photosensitisers	Trade name	Structure	Indication
Porfimer sodium, (hematoporphyrin derivative)	Photofrin	Porphyrin	*Approved*: early and advanced lung cancer, esophagus and bladder cancer *Clinical trials*: cervical, bile duct, brain, ovarian and breast cancer
5-aminolevulinic acid (ALA)	Levulan	Porphyrin precursor	*Approved*: esophagus cancer *Clinical trials*: skin, bladder and brain cancer
ALA-ester	Metvix, Hexvix	Porphyrin precursor	*Approved*: Non-melanoma skin cancer, basal cell carcinoma *Clinical trials*: bladder cancer
Temoporfin, m-tetrahydroxyphenylchlorin (mTHPC)	Foscan	Chlorin	*Approved*: recurrent head and neck cancer *Clinical trials*: lung, brain, skin and bile duct cancer
Verteporfin (benzoporphyrin derivative monoacid ring A)	Visudyne	Chlorin	*Approved*: age-related macular degeneration (ophthalmic) *Clinical trials*: pancreatic, basal and squamous cell carcinoma
Mono-(L)-aspartylchlorin-e6	Talaporfin, Laserphyrin	Chlorin	*Approved:* early lung cancer *Clinical trials:* liver, head and neck, colorectal, brain and breast cancer
Chlorin e6-polyvinylpyrrolidone (Ce6-PVP)	Photolon	Chlorin	*Approved:* skin and mucous membrane cancer *Clinical trials:* nasopharyngeal cancer, sarcoma, brain cancer
Tin ethyl etiopurpurin (SnEt2)	Purlytin	Chlorin	*Clinical trials*: Kaposi's sarcoma, metastatic breast cancer, prostate cancer
Pyropheophorbide-a hexyl ether (HPPH)	Photochlor	Chlorin	*Clinical trials*: head and neck cancer, Barett's esophagus, lung cancer
Padoporfin	Tookad	Bacteriochlorin	*Clinical trials*: prostate cancer
Motexafin texaphyrin	Lutex	Texaphyrin	*Clinical trials*: lung, cervical, prostate cancer
Silicon phthalocyanine	Pc4	Phthalocyanine	*Clinical trials*: cutaneous T-cell lymphoma
Rose Bengal	PV-10	Fluorescein	*Clinical trials*: metastasis melanoma, liver and breast cancer
Hypericin	-	Anthraquinone	*Clinical trials*: brain cancer, cutaneous T-cell lymphoma

Source from http://clinicaltrials.gov and Agostinis et al. (2011)

In terms of bioactivity, a photosensitiser must have little or no toxicity in the absent of light and must be eliminated from the body immediately after treatment to reduce PDT side-effects such as skin photosensitivity after irradiation. Preferably, the photosensitiser selectively accumulates and retains in the disease tissues to avoid irradiation injury to surrounding healthy tissues. In pharmaceutics standpoint, the photosensitiser should be a pure compound with constant composition to ease dose standardisation and it should be easy to synthesise and manipulate for derivatisation. Other properties such as stability, good solubility in accepted pharmaceutical formulation and low tendency to aggregate following dosing are ideal. Table 2.1 lists the photosensitisers that have been approved or in clinical trials for anticancer PDT. These photosensitisers can be classified based on their chemical structures to two distinct groups, namely cyclic-tetrapyrrole and non-tetrapyrrole.

2.3.2 Cyclic-Tetrapyrrole Photosensitisers

To date, most of the photosensitisers used in cancer therapy or being investigated in clinical trials have a common cyclic-tetrapyrrole structure, which is similar to hemoglobin and chlorophyll. This is probably due to the fact that modern PDT has evolved from the use of porphyrins and ultraviolet light in image-guided surgical resection of neoplastic tissue (Nyman and Hynninen 2004; Wainwright 2009). This class of photosensitisers includes porphyrins, chlorins, bacteriochlorins, phthalocyanines, and related chromophore structures.

2.3.2.1 Porphyrins

(a) Hematoporphyrin

One of the earliest therapeutic successes in clinical PDT was the discovery of porfimer sodium (Figure 2.4), a water-soluble mixture of oligomers of up to eight units of hematoporphyrin formed by ester and ether linkages (Brown and Truscott 1993). A purified form of the porfimer sodium was marketed as Photofrin^{TM} and to date is the most commonly use photosensitiser in the clinic. Photofrin was first approved in Canada (1993) for the treatment of bladder cancer and subsequently approved by the United States Food and Drug Administration (FDA) for the indication of esophageal cancer (1995), non-small cell lung cancer (1998) and Barrett's esophageal disease (2003).

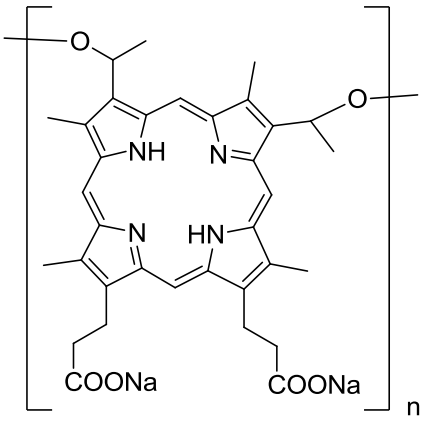

Figure 2.4 Structure of hematoporphyrin.

In clinical practice, porfimer sodium is activated by red light at a wavelength of 630 nm. The disadvantage with this short wavelength is that the tissue penetration of light is poor, thus making porfimer sodium only suitable for superficial tumour. Moreover, the low absorbance of porfimer sodium at 630 nm (molar extinction coefficient, $\varepsilon = 3000\ M^{-1}cm^{-1}$) necessitates the use of high energy and long irradiation of light which often leads to irradiation site discomfort and pain. Other disadvantages of

porfimer sodium are their prolonged skin photosensitivity of up to 10 weeks as a result of their complex mixture that tends to break down slowly over time (Sharman et al. 1999). Due to the disadvantages of porfimer sodium, there has been a major effort in PDT research to develop second generation photosensitisers which are more effective.

(b) Protoporphyrin IX

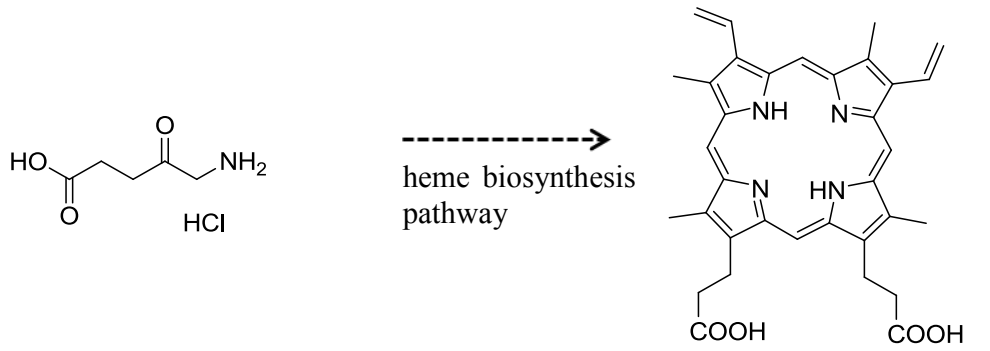

5-aminolevulinic acid (ALA) protoporphyrin IX (PpIX)

Figure 2.5 Structures of protoporphyrin IX photosensitiser and its precursor 5-aminolevulinic acid (ALA).

One notable second generation photosensitiser was 5-aminolevulinic acid (ALA), a non-photoactive precursor for the biosynthesis of the protoporphyrin IX (PpIX) photosensitiser (Figure 2.5) (Kennedy and Pottier 1992). Both ALA and PpIX are endogenous components that occur naturally as part of the heme biosynthesis as illustrated in Figure 2.6. Unlike other photosensitisers which accumulate in tumour through hydrophilic/hydrophobic balance, administration of exogenous ALA leads to build up of PpIX because of the inherent lower enzymatic activity of ferrochelatase in tumours which converts PpIX to heme (Kloek et al. 1998; Wachowska et al. 2011).

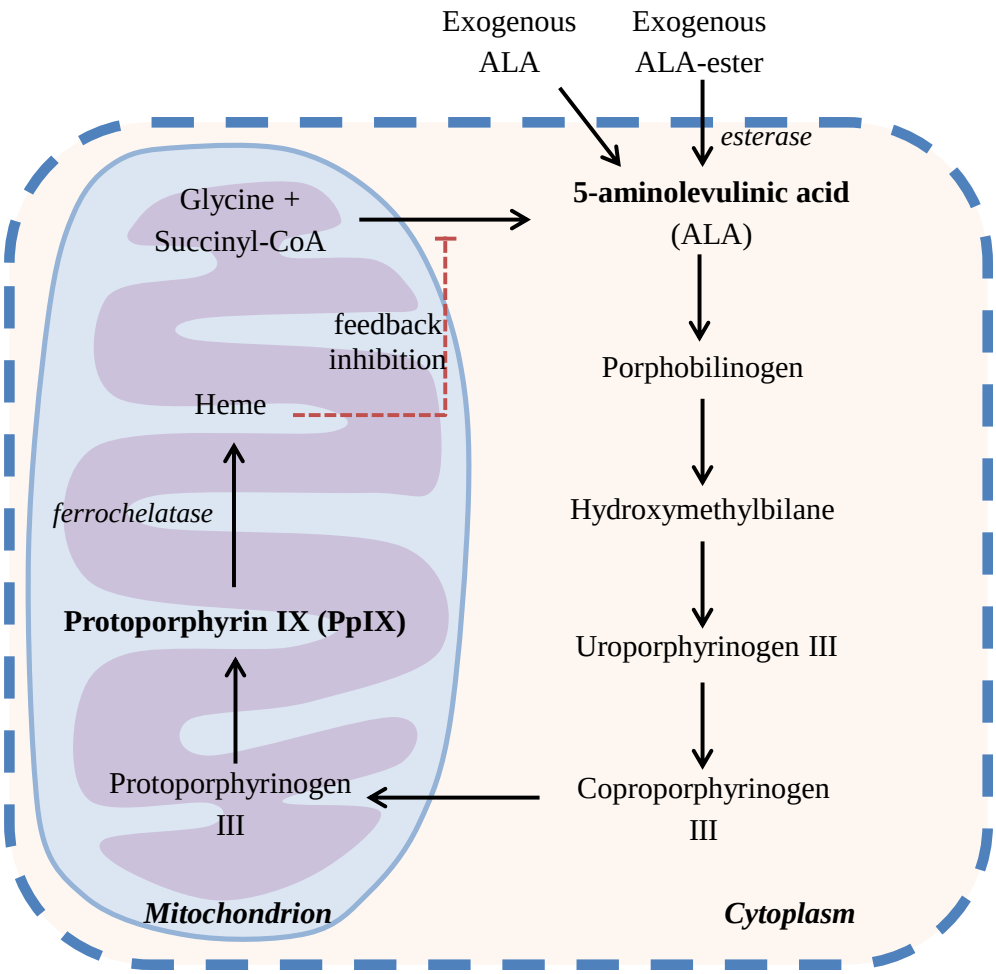

Figure 2.6 The heme synthesis pathway in cells using endogenous/exogenous 5-aminolevulinic acid (ALA) or exogenous ALA-ester as a precursor. Given the inherent lower ferrochelatase activity in tumours which converts protoporphyrin IX (PpIX) to heme, lead to a build-up of protoporphyrin IX (PpIX). Illustration was adapted from (Wachowska et al. 2011).

ALA (Levulan^{TM}) received U.S. FDA approval for the treatment actinic skerolosis in 1999 and esophageal dysplasia in 2007 (Wachowska et al. 2011). The advantages of ALA are its rapid clearance from the body and high selectivity for malignant lesions. The rapid systemic clearance of ALA induced-PpIX within 24 h through the formation of heme by healthy tissues minimises the risk of prolonged photosensitivity (Webber et al. 1997; Wachowska et al. 2011). However, ALA is hydrophilic and has limited penetration into biological barriers with lipophilic

characteristics especially the highly lipophilic stratum corneum, the outermost layer of epidermis, given that ALA is administered topically in PDT treatment of basal cell carcinoma (Fotinos et al. 2006). To overcome this shortcoming, a methyl-aminolevulinic acid (MAL, Metvix^{TM}) which is more lipophilic was synthesised (Godal et al. 2006). MAL was approved for the treatment of actinic keratosis and non-melanoma skin cancers, namely basal cell carcinoma in Australia, New Zealand and some European countries. Nevertheless, the absorption spectrum and absorbance for PpIX (λ_{abs} = 630 nm, ε = 5000 $M^{-1}cm^{-1}$) is very similar to porfimer sodium and therefore has not improved light-tissue penetration and is always associated with pain at irradiation site as high energy light is applied (Warren et al. 2009).

2.3.2.2 Chlorins

Other than porfimer sodium and PpIX (from ALA) which are porphyrin-based, the other clinically approved photosensitisers are all chlorin structures. When compared to porphyrins, the structure of chlorins are more reduced, contain two extra hydrogens in one pyrrole ring. This structural change leads to a bathochromic shift in the absorption band (640-700 nm) and gives $\varepsilon \sim 40000$ $M^{-1}cm^{-1}$, allowing better photosensitizing efficiency and deeper tissue light penetration.

(a) Temoporfin

The first of these is 5,10,15,20-tetra(3-hydroxyphenyl)-2,3-dihydroporphyrin, temoporfin, which is a pure synthetic compound (Figure 2.7). Temoporfin (Foscan^{TM}) is currently approved for PDT treatment of advanced head and neck cancer in Europe and has much more desirable properties compared to porfimer sodium and ALA in terms of

better potency, strong absorption at wavelength of 652 nm and shorter skin photosensitivity of 2-4 weeks (Senge and Brandt 2011).

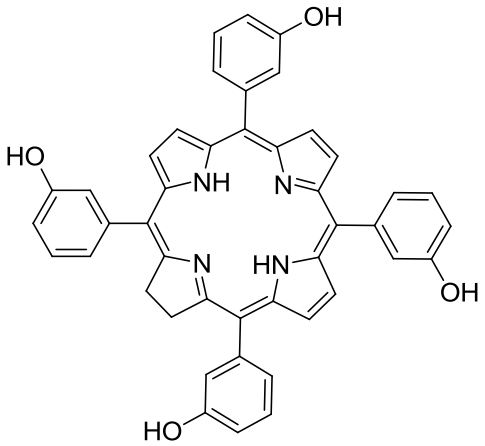

Figure 2.7 Structure of temoporfin.

Temoporfin displays 100-200 fold better potency than Photofrin that even in the presence of very dim light will lead to severe skin photosensitivity (Allison and Sibata 2010). The downside of temoporfin is its highly hydrophobicity causing it to precipitate easily upon administration (Kiesslich et al. 2007). As a consequence, temoporfin follows a very slow distribution pharmacokinetic attributed to its slow release from the aggregates to monomeric form (Hopkinson et al. 1999). This has resulted in a four-day delay between injection of the photosensitiser into the bloodstream and activation with light (Sasnouski et al. 2006). During this period, patients are highly photosensitive to light and therefore appropriate light exposure precautions should be followed.

(b) Verteporfin

The verteporfin, a benzoporphyrin derivative monoacid ring A (Figure 2.8), is one of the more ideal photosensitisers among the list with long activation wavelength at 690 nm, rapid clearance from the body and short periods (only few hours) of skin

photosensitivity than Photofrin (Houle and Strong 2002). This photosensitiser is vascular acting and is particularly useful for treating highly vascularised lesions (Chen et al. 2006b). In clinical verteporfin-PDT, light treatment is initiated within 30 min of photosensitiser infusion. This together with its rapid body clearance thereby makes them suitable for use in outpatient setting.

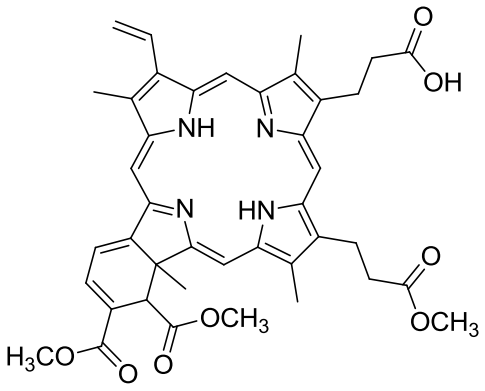

Figure 2.8 Structure of verteporfin.

Verteporfin is a lipophilic compound that will self-aggregate in aqueous solution (Aveline et al. 1995), but following formulation with liposome (Visudyne^{TM}), this compound becomes one of the most successful photosensitisers used for the treatment of age-related macular degeneration caused by abnormal blood vessel growth of the retina (Cruess et al. 2009). Present clinical trial data showed that verteporfin is particularly useful for the PDT treatment of non-melanoma skin cancer (Lui et al. 2004) and pancreatic cancer (Celli et al. 2011).

(c) Chlorin e6 derivatives

Two other chlorin-based photosensitisers approved for clinical applications are the mono-aspartyl-L-chlorin e6 (also known as talaporfin) and chlorin e6-polyvinypyrrolidone (Figure 2.9). Talaporfin is marketed in Japan as Laserphyrin^{TM} for

the treatment of lung cancer (Usuda et al. 2006) whereas chlorin e6-polyvinypyrrolidone (Photolon^{TM}) is approved in Belarus and Russia for the treatment of skin tumours and mucosal malignancies of hollow organs (Shliakhtsin et al. 2009), respectively. Both photosensitisers are highly efficient with excellent singlet oxygen generation and high absorbance at longer wavelengths (~660 nm, 40000 $M^{-1}cm^{-1}$). However, these chlorin e6-based photosensitisers have high photobleaching rate which reduces their availability for efficient PDT (Hongying et al. 1999).

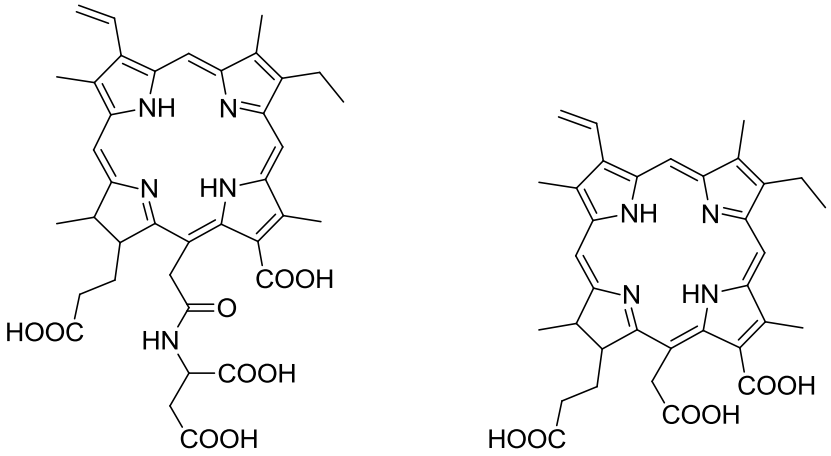

mono-aspartyl-L-chlorin e6 chlorin e6

Figure 2.9 Structures for mono-aspartyl-L-chlorin e6 (talaporfin) and chlorin e6.

Based on the literature review, it is clear that the spectroscopic and physicochemical properties such as absorption maxima, molar extinction coefficient, fluorescence quantum yield, photobleaching quantum yield, singlet oxygen generation quantum yield and octanol/water partition coefficient play an important role in determining the potency of a photosensitiser. Therefore, the spectroscopic and physicochemical parameters for these clinical PDT agents are summarised in Table 2.2 for better comparison.

Table 2.2 Spectroscopic and physicochemical properties of clinically approved photosensitisers for cancer treatment

Photosensitiser	λ_{abs} (nm)	λ ($M^{-1}cm^{-1}$)	λ_{em} (nm)	Φ_{fl}	Φ_{PB}	Φ_{Δ}	Log $P_{o/w}$
Porfimer sodium (Photofrin ™)	630[a]	3000[a]	NA	NA	5.4 x 10^{-5} (PB)[b]	0.25 (PB + 1% TX100; 630 nm; oxygen depletion with FFA)[c]	3.96 (calc.)[d]
Protoporphyrin IX (Levulan ™)	635[a]	5000[a]	630 (ex 397 nm; PBS)[e]	0.011 (ex 397 nm; PBS)[e]	NA	0.54 (PB + 1% TX100; 630 nm; lysozyme inactivation; RB at 0.75)[f]	NA
Temoporfin (Foscan ™)	650 (EtOH)[g] 652 (H2O)[g]	39000 (EtOH)[g] 23000 (H_2O)[g]	655 nm (PBS)[h]	NA	1.54 x 10^{-5} (PBS + 10% FCS)[i]	0.31 (PBS + 10% FCS; >610 nm; DPBF; hypericin at 0.36)[i]	9.24[j]
Verteporfin (Visudyne ™)	688 (PBS + 2% TX100)[k] 692 (PBS)[k]	31 200 (PBS + 2% TX100)[k] 13 500 (PBS)[k]	694 (PBS + 2% TX100)[k] 695 (PBS)[k]	0.049 (PBS + 2% TX100)[k] 0.002 (PBS)[k]	5.35 x 10^{-5} (PBS + 2% TX100)[k] 2.80 x 10^{-5} (PBS)[k]	0.82 (PB + 1% TX100; 692 nm; lysozyme inactivation; MB at 0.52)[f]	7.76 (calc.)[l]
Talaporfin (Laserphyrin ™)	654 (PBS)[m]	40000 (PBS)[m]	660 (PBS)[m]	NA	8.2 x 10^{-4} (PBS)[m]	0.77 (D_2O, oxygen depletion with FFA)[m]	- 1.92 [n]
Ce6 (Photolon ™)	663 (PBS)[o]	38000 (PBS)[o]	662 (PBS)[o]	0.18 (PBS)[o]	NA	0.75 (PB; 660 nm; lysozyme inactivation; MB at 0.52)[f]	0.78[o]

Ref: [a](Sharman et al. 1999); [b](Spikes 1992); [c](Kimel et al. 1989); [d](Tanaka et al. 2012); [e](Lozovaya et al. 1990); [f](Fernandez et al. 1997); [g](Grahn et al. 1997); [h](Belitchenko et al. 1998); [i](Hadjur et al. 1998); [j](Chen et al. 2011); [k](Aveline et al. 1994); [l](Macalpine et al. 2002); [m](Spikes and Bommer 1993); [n](Kessel 1989a); [o](Isakau et al. 2008)

Abbreviation: λ_{abs} - absorption maxima (Q-band); λ - molar extinction coefficient; λ_{em} - fluorescence emission maxima; Φ_{fl} - fluorescence quantum yield; Φ_{PB} - photobleaching quantum yield; Φ_{Δ} - singlet oxygen generation quantum yield; Log $P_{o/w}$ – log octanol/water partition coefficient; PB – phosphate buffer pH~7.4; EtOH – ethanol; PBS – phosphate buffered saline; TX100 – Triton X100; FFA – furfuryl alcohol; MB – methylene blue; RB – rose bengal; NA – not available

2.3.2.3 Pheophorbide-based chlorins

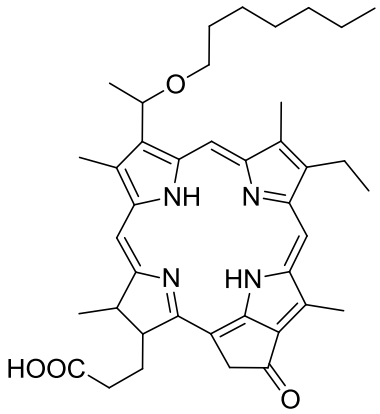

Figure 2.10 Structure of 2-(1-hexyloxyethyl)-2-devinyl pyropheophorbide (HPPH).

Pheophorbide is a chlorin characterised by a reduced exocyclic double bond leading to a further increased absorption to 650–700 nm compared to the chlorins. Perhaps 2-(1-hexyloxyethyl)-2-devinyl pyropheophorbide (HPPH, Photochlor ^{TM}) is currently the most actively investigated photosensitiser for clinical PDT (Figure 2.10). The photosensitiser absorbs at 665 nm with $\varepsilon \sim 47000\ M^{-1}cm^{-1}$ (Lobel et al. 2001). HPPH has been approved for use in clinical trials and has undergone phase I/II trials for obstructive esophageal cancer and Barrett's esophagus, phase I trials involving non-melanomatous basal cell skin cancer and phase I trials for early stage non-small cell lung cancer. Ongoing clinical trials include phase I trials for treating dysplasia or carcinoma of the oral cavity and larynx, phase II trials for precancerous or early stage esophageal cancer, phase I trials involving lung cancer and other peural maglinancies, and phase I trials in patients undergoing surgery for primary or recurrent head and neck cancer (Ormond and Freeman 2013).

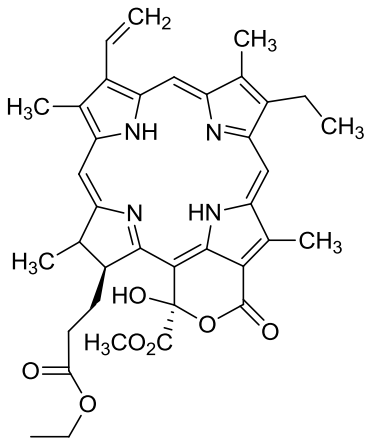

15^1-hydroxypurpurin-7-lactone methyl ethyl ester

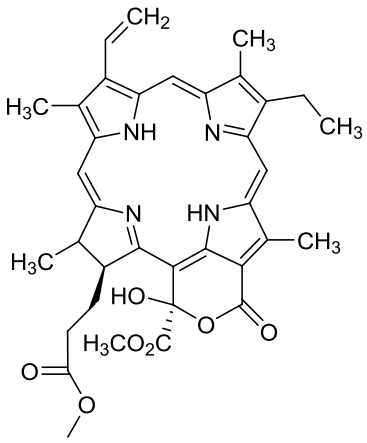

15^1-hydroxypurpurin-7-lactone dimethyl ester (G2)

Figure 2.11 Structure of 15^1-hydroxypurpurin-7-lactone derivatives.

Hydroxypurpurin-7-lactone derivative is another pheophorbide-related photosensitiser characterised by the presence of an exocyclic lactone ring leading to a further increase of absorption to ~ 700 nm. So far, not much has been reported in terms of their photodynamic activity. The only photosensitiser from this group tested for PDT activity is 15^1-hydroxypurpurin-7-lactone methyl ethyl diester, a naturally occurring photosensitiser isolated from plants derived from several distinct families such as *Phaeanthus ophthalmicus* (Annonaceae Family), *Aglaonema simplex* (Araceae Family) *Phyllostachys bambusoides* (Poaceae Family) (Kim et al. 2003; Chee et al. 2005; Tan et al. 2011). The photosensitiser is believed to be a degradation product of chlorophyll-*a*. Our previous studies had shown that 15^1-hydroxypurpurin-7-lactone dimethyl ester (G2), a closely related analogue (Figure 2.11), was found to exhibit potential PDT activity by inducing the closure of capillaries and small neovessels in a chick chorioallantoic membrane (CAM) model (Lim et al. 2010). G2 was also shown to be a promising photosensitiser against head and neck cancer cells by the higher potency of G2 in inducing photocytotoxicity and an ability to evoke a more pronounced apoptosis compared with a known photosensitiser, pheophorbide-*a* (PhA) (Lim et al. 2011). G2

and its analagues will be further evaluated in present study, and more extensive literature review on G2 will be given in the introduction of Chapter 3.

2.3.2.4 Bacteriopheophorbides

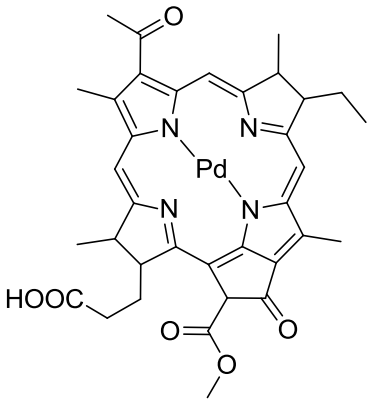

Figure 2.12 Strucuture of palladium-bacteriopheophorbide (Tookad).

Another class of light absorbing chromophore is based on bacteriopheophorbide, which have two reduced double bonds in the pyrroles compared to the porphyrins that further red-shifting the absorbing band. Tookad is a palladium-bacteriopheophorbide derived from bacteriochlorphyll *a*, which is isolated from bacteria (Figure 2.12). The photosensitiser is activated at a relatively long wavelength (763 nm) and acts mainly by shutting down peritumoural vasculature given its lipophilic, anionic nature (Madar-Balakirski et al. 2010). Advantages of Tookad are its deep tissue penetration of light and rapid clearance from the circulation and therefore, cutaneous photosensitisation associated with photosensitisers such as Photofrin or Temoporfin are generally absent (Weersink et al. 2005). A water-soluble derivative of Tookad has been evaluated in phase I and II clinical trials for prostate cancer patients (Davidson et al. 2009; Betrouni et al. 2011).

2.3.2.5 Phthalocyanines

Phthalocyanines are extended porphyrins with each of their pyrrolic ring fused with a benzene ring. This structural change leads to increased aromatic character that resulted in their intense near infra-red (NIR) absorption at λ_{abs} ~ 670-700 nm with $\varepsilon \geq 120000\ M^{-1}cm^{-1}$ (Sekkat et al. 2012). For phthalocyanines to exhibit PDT properties, metal complexation, especially with a transition metal such as aluminium, zinc or silicone, is required to give high yields of singlet oxygen (Ali and van Lier 1999; Wainwright 2009). Besides their NIR absorption, which is crucial for activation in deeper tissular regions, one interesting feature of phthalocyanines is their near absence of absorbance at 400-600 nm that would minimise the chances of skin photosensitisation when exposed to sunlight (Ethirajan et al. 2008). However, the major limitations of most phthalocyanines are their strong tendency to aggregate and low water-solubility (Sekkat et al. 2012).

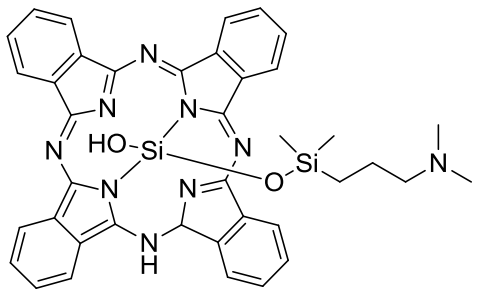

silicon phthalocyanine 4

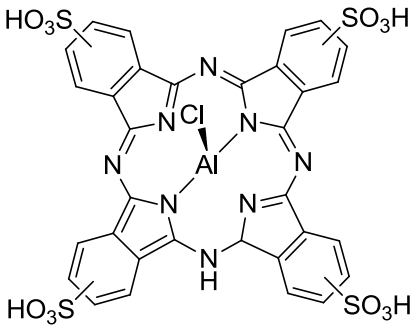

aluminium phthalocyanine tetrasulfonate

Figure 2.13 Structures of silicon phthalocyanine 4 (Pc4) and aluminum phthalocyanine tetrasulfonate (AlPcS4).

Aluminum phthalocyanine tetrasulfonate (AlPcS4, Photosens) and silicon phthalocyanine 4 (Pc4) are two phthalocyanine-based photosensitisers investigated in the clinic to-date (Figure 2.13). Photosens is an isomeric mixture and has been used in Russia to treat various cancers (Wainwright 2009). Meanwhile, Pc4 has completed phase I trial for the treatment of pre-malignant and malignant skin conditions.

2.3.2.6 Texaphyrins

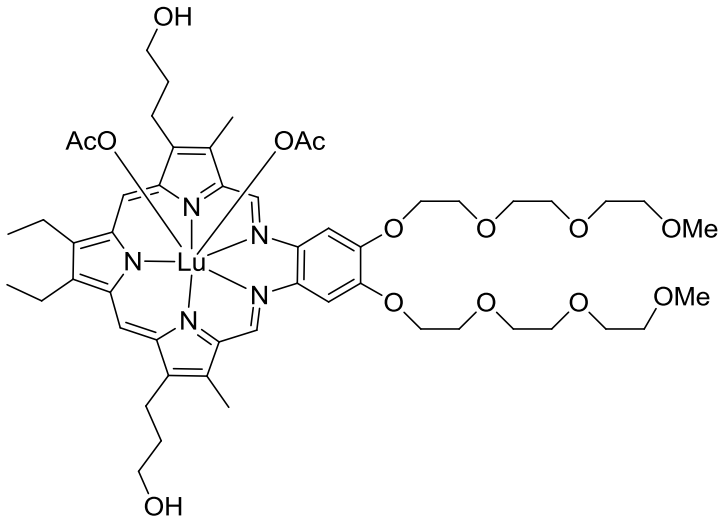

Figure 2.14 Structure of motexafin lutetium.

Texaphyrin is a heterocyclic macrocycles with a five nitrogen atoms core extended with metal complex (Figure 2.14). Motexafin lutetium is a pure, water-soluble texaphyrin with a large broad absorption band centered at 732 nm with $\varepsilon \sim 42000\ M^{-1}cm^{-1}$. The photosensitiser has entered clinical trials for the PDT of recurrent breast cancer, cervical intraepithelial neoplasia and locally recurrent prostate cancer (Dimofte et al. 2002; Patel et al. 2008), as well as for the phototreatment of non-cancerous lesions such as atherosclerosis of peripheral arteries and macular degeneration (Woodburn et al. 2002; Kereiakes et al. 2003).

2.3.3 Non-Tetrapyrrole Photosensitisers

Aside from cyclic-tetrapyrrole structures, a number of naturally occurring as well as synthetic dyes that are non-tetrapyrrole-based have also been evaluated for their photosensitising ability against cancer. In fact, the fundamental of photodynamic action was first described in the early 1900s based on the photo-induced killing effects observed with non-tetrapyrrole photosensitisers namely acridine and eosin (Dolmans et al. 2003). Classes of non-tetrapyrroles that have been investigated for photodynamic activity include perylenequinones, phenothiazines, xanthenes and boron difluoride dipyrromethene.

2.3.3.1 Perylenequinone

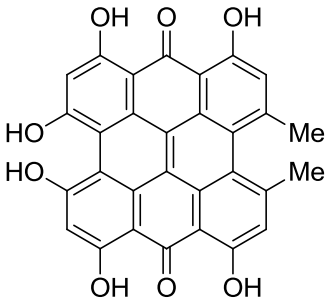

Figure 2.15 Structure of hypericin.

Hypericin (Figure 2.15) is a naturally occurring perylenequinone isolated from St. John's Wort (*Hypericum perforatum*). This photosensitiser is poorly soluble in water but can be dissolved following addition of alcohol (Wirz et al. 2002). Hypericin is one of the most powerful photosensitisers in nature with strong absorbance ($\varepsilon = 44000\ M^{-1}cm^{-1}$) at 590 nm (Ormond and Freeman 2013). Recently, a phase II placebo-control study of PDT with topical hypericin on cutaneous T-cell lymphoma patients has shown significant improvement of the treated skin lesions (Rook et al. 2010).

2.3.3.2 Phenothiazinium

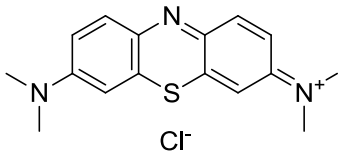

Figure 2.16 Structure of methylene blue.

Phenothiazinium-based structures are a well-known category of non-tetrapyrrole type of PDT agents. During the early period of research in modern PDT, phenothiazinium exemplary by methylene blue (Figure 2.16) was perceived as a standard bioactive photosensitiser, giving a reasonable yield of singlet oxygen (Φ_{Δ} = 0.52 in alcohol) and strong absorption (ε_{max} ~ 82000 $M^{-1}cm^{-1}$) at 666 nm which corresponds with the light therapeutic window for PDT (600-800 nm) (Wainwright 2005). Numerous methylene blue analogues have since been prepared given its ease of synthesis, however this class of compounds has limited therapeutic window due to low light-to-dark toxicity ratio (Wainwright et al. 1997; Wainwright and Giddens 2003; Harris et al. 2005). Nevertheless, methylene blue has found its application in antimicrobial PDT for treatment of chronic periodontitis and pathogen eradication in blood products (Wainwright 2005).

2.3.3.3 Xanthene

Xanthenes are tricyclic systems consisting of two benzene rings joined by a methylene group and an oxygen atom. There are three main series deriving from this chemical skeleton namely the fluoresceins, rhodamines and rosamines (Figure 2.17). The xanthene dyes are excellent singlet oxygen generator and are perhaps the most commonly used compounds where singlet oxygen is required in organic synthesis

(Wainwright 2009). This class of dyes also has a wide-ranging application as fluorescence probes. In terms of photodynamic action, there are only a few examples of xanthene being investigated even though a great range of its derivatives could be easily synthesised.

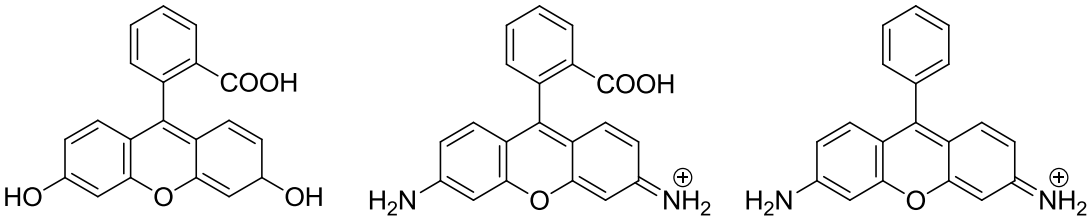

fluorescein-type rhodamine-type rosamine-type

Figure 2.17 Structure of xanthene photosensitisers.

(a) Fluorescein

Fluorescein is widely used as a fluorescent tracker dye for many biomedical applications, especially in fluorescence microscopy due its ease to synthesise, good solubility in aqueous environment and strong fluorescence emission. Fluorescein, namely fluorescein isothiocyanate (FITC), is commonly used as antibody probe in immunohistochemistry staining to allow visualisation of specific target proteins or structures within cells. In cancer PDT, the use of fluorescein was described in the early 1900s, where von Tappeiner and colleagues performed the first PDT trial in patients using eosin (Figure 2.18). In this trial, four out of six patients with facial basal cell carcinoma treated with a 1% eosin solution and a long-term exposure either to sunlight or to arc-lamp light showed total tumour regression and a relapse-free period of 12 months, as quoted by Dolmans et al. (2003).

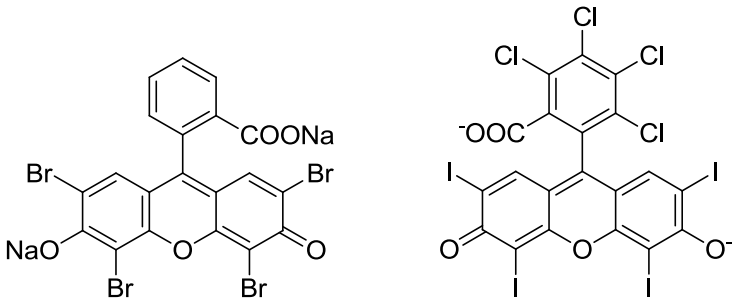

eosin rose Bengal

Figure 2.18 Structures of eosin and rose Bengal.

Another noteworthy fluorescein is the rose Bengal (Figure 2.18), a water-soluble photosensitiser which absorbs strongly at 549 nm with ε = 100000 $M^{-1}cm^{-1}$ (Mousavi et al. 2009). Rose Bengal has high efficiency in singlet oxygen production leading to its application as a reference dye in singlet oxygen quantum yield measurement or in synthetic chemistry where singlet oxygen is required (Wainwright 2009). In PDT, the utility of this photosensitiser is limited to superficial lesions given its shorter absorption wavelength. A formulation of rose Bengal known as PV-10 has been studied in a Phase II clinical trial (NCT00521053) and is currently in preparation for a phase III randomised controlled study for the treatment of metastatic melanoma. Clinical investigation using PV-10 has also been granted to Provectus Pharmaceuticals by the FDA for treatment of cutaneous and subcutaneous tumours under compassionate use in patients whom there is no comparable or satisfactory approved alternative therapies (NCT01260779).

(b) Rhodamines and rosamines

Rhodamines and rosamines belong to the class of dye known as delocalised lipophilic cations (DLCs). In comparison to the fluorescein, both rhodamines and rosamines have their phenolic residues replaced by amino residues where this modification allows the

positive charge of these structures to be permanently delocalised onto the amino nitrogen. The cationic character of these DLCs leads them to be attracted to the negatively charge mitochondrial matrix thereby allowing mitochondrial targeting (Modica-Napolitano and Aprille 2001). For example, DLCs such as rhodamine-123 (Rh123) and tetramethylrosamine (TMR) (Figure 2.19) are extensively used as mitochondrion-selective fluorescence probe (Modica-Napolitano and Aprille 1987; Minamikawa et al. 1999).

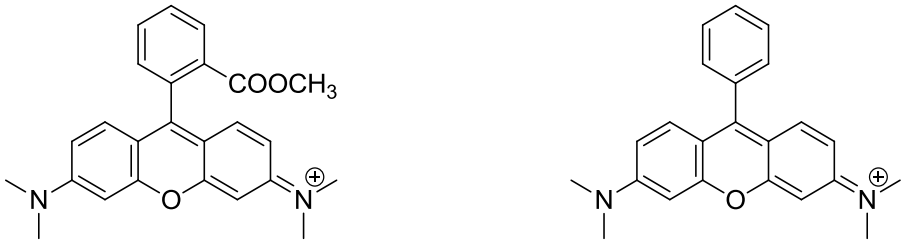

rhodamine-123 tetramethylrosamine

Figure 2.19 Structures of rhodamine-123 and tetramethylrosamine (TMR).

Despite its mitochondrial targeting potential, both Rh123 and TMR are not efficient photosensitisers for PDT due to their relatively short wavelength of absorption and low singlet oxygen quantum yield of 0.01 and 0.08, respectively (Richmond and O'Hara 1993; Detty et al. 2004). Chromophore functionalisation has been carried out to improve absorption wavelength and singlet oxygen yields. For example, addition of alkyl or aryl to the xanthene core has been shown to red-shift the absorption wavelength (David et al. 2008), while halogenation resulted in increased of singlet oxygen yield (Pal et al. 1996). On the other hand, substitution of oxygen with lower chalcogen atoms such as sulfur, selenium or tellurium is associated with increased of both absorption wavelength and singlet oxygen production (Detty et al. 2004; Holt et al. 2006; Calitree et al. 2007). Introduction of heterocyclic ring at the *meso*-position may also altered their spectroscopic properties (Shandura et al. 2007).

2.3.3.4 Boron Difluoride Dipyrromethene

Boron difluoride dipyrromethene (BODIPY) is a class of fluorescent dyes, which is composed of dipyrromethene complexed with a disubstituted boron atom, typically a BF_2 unit. BODIPYs have many ideal photosensitiser characteristics, including high absorption extinction coefficients, high quantum efficiencies of fluorescence, relative insensitivity to environment, resistance to photobleaching (Gorman et al. 2004) and higher light-dark toxicity ratio compared to other non cyclic-tetrapyrole photosensitisers i.e phenothiazinium (Wainwright et al. 1997; Yogo et al. 2005).

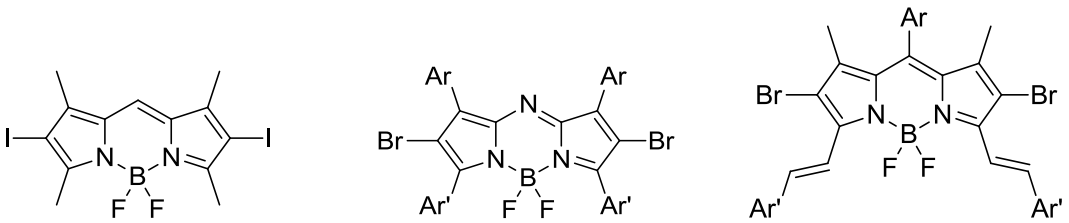

Nagano O'Shea Akkaya

Figure 2.20 Examples of BODIPY photosensitisers for PDT.

Recently, BODIPYs are actively being investigated as an alternative class of non-tetrapyrrole photosensitisers for PDT (Figure 2.20). Nagano and co-workers reported synthesis of a simple diiodo-substituted BODIPY with possible applications that included PDT and fluorescence bio-imaging probes (Yogo et al. 2005). The diiodo-substituted BODIPY at the 4-pyrollic position produces the supposed internal heavy atom effect that enhanced the intersystem crossing efficiency from a singlet to a triplet state which promotes singlet oxygen production. O'Shea and co-workers prepared a series of azadipyrromethenes with high absorption in the far-red wavelengths and demonstrated their efficacy in light-induced toxicity in a panel solid tumour cell line (Gorman et al. 2004). One of the azadipyrromethenes was later shown to effectively eradicate the subcutaneously xenografts MDA-231 breast tumours in nude mice (Byrne

et al. 2009). Atilgan et al. (2006) introduced another class of water-soluble BODIPY dyes with extended conjugation at the 5-pyrollic positions. These photosensitisers were shown to have strong absorptions in the 650-680 nm therapeutic window and good photo-induced cytotoxicity in K562 leukemia cells at sub-micro molar concentration even under low fluence rate LED irradiation.

2.4 Oxygen in PDT

Molecular oxygen occurs in ground triplet state at room temperature and only become reactive in its singlet state. Singlet excited state oxygen is significantly more electrophilic and can react rapidly with unsaturated carbon-carbon bonds, neutral nucleophiles such as sulfides and amines, and as well as with anions (DeRosa and Crutchley 2002). The lifetime of singlet oxygen in organic solvents ranges from 10-l00 μs (MacDonald and Dougherty 2001), but in cellular level, the lifetime of singlet oxygen reduces to approximately 3 μs due to its high reactivity with biological substances (Hatz et al. 2007). Because of the high reactivity and short lifetime of singlet oxygen, PDT-induced oxidative damage is therefore highly localised where only the nearest molecules and structures to singlet oxygen production site are directly affected (Moan and Berg 1991).

In general, the efficacies of PDT critically depend on the concentration of molecular oxygen in the tumour. Several studies have demonstrated that PDT is less effective in hypoxic environment (Moan and Sommer 1985; Henderson and Fingar 1987). This can be a challenge, as most solid tumours have reduced oxygen tensions due to their irregular microcirculation and deteriorating diffusion geometry (Hockel and Vaupel 2001). To overcome this, metronomic PDT where both the photosensitiser and light are delivered at very low dose rates over an extended period has been proposed.

Since oxygen consumption in PDT depends on the fluence of light, the use of lower fluence rates delays oxygen depletion while allowing tissue reoxygenation and has been shown to improve PDT efficacy (Zilberstein et al. 2001; Singh et al. 2010).

2.5 Mechanism for Photodynamic Action

2.5.1 Photophysical and Photochemistry Process of PDT

The interactions between light, photosensitisers and oxygen involve a series of energy transitions in order to generate singlet oxygen as illustrated in a simplified Jablonski diagram (Figure 2.21). Upon light irradiation at wavelengths corresponding to the photosensitiser absorption maxima, ground singlet state photosensitisers will become electronically excited. This excited singlet state photosensitiser is very unstable and may discharge the absorbed energy as fluorescence. Otherwise, it will undergo intersystem crossing to form the more stable triplet state. To return to ground singlet state, photosensitiser in its triplet state may either undergo radiative deactivation by emitting phosphorescence or by non-radiative deactivation processes namely Type I and Type II reactions (Dolmans et al. 2003; Agostinis et al. 2011).

In Type I reaction, the photosensitiser will acquire an electron by reacting directly with an organic molecules within cellular microenvironment to form a free radical. Subsequently, this reduced photosensitiser interacts with oxygen to produce superoxide anion radical (O_2^-). Superoxide is not particularly reactive and does not cause oxidative damage to biological system, but it can be catalysed by superoxide dismutase to hydrogen peroxide, which is in turn rapidly converted to the highly oxidative hydroxyl radical (•OH) by ferrous ion (Fe^{2+}) present in the body (Castano et al. 2004; Agostinis et al. 2011). In the much anticipated Type II reaction, triplet state photosensitiser will transfer its energy to molecular oxygen to form the highly reactive

singlet oxygen ($^1O_2$), which is the key cytotoxic component in PDT. Nevertheless, these energy transfer process between the photosensitiser and oxygen depend on photophysical properties of a photosensitiser and various constant rates such as singlet-to-triplet internal conversion efficiency, intersystem crossing efficiency, triplet state excited energy, triplet state excited lifetime and the efficiency of energy transfer to molecular oxygen that may influence the singlet oxygen production efficiency (Tanaka et al. 2008).

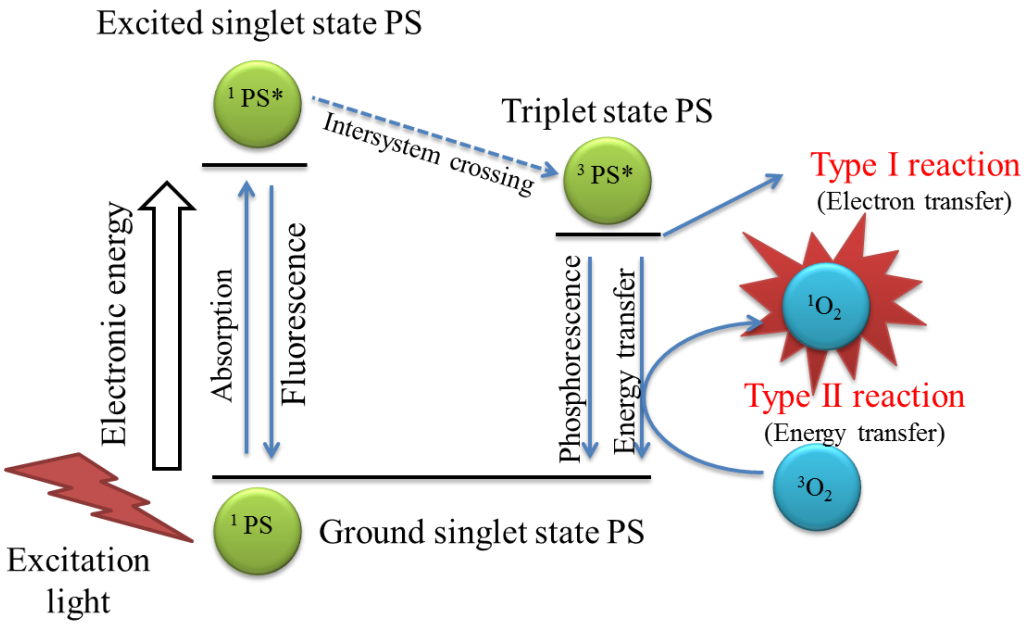

Figure 2.21 A modified Jablonski diagram illustrates the electronic state of photosensitiser and oxygen during the photosensitisation processes. Upon light irradiation, ground singlet state photosensitiser (^{1}PS) absorbed the photon energy to become excited singlet state (^{1}PS*). In a more likely event, the excited photosensitiser will undergo intersystem crossing to form excited triplet state (^{3}PS*) and subsequently transfer its energy to molecular oxygen ($^3O_2$) to form singlet oxygen ($^1O_2$), which is the key cytotoxic component in PDT. The diagram was adapted from Castano et al. (2004).

2.5.2 Mechanisms of PDT-Mediated Tumour Destruction

Tumour ablation in PDT is contributed by three distinct mechanisms. As illustrated in Figure 2.22, singlet oxygen generated during PDT is capable of inducing cellular death of tumour, the shutting down of blood vessels feeding the tumour, and the activation of immunological responses against tumour cells. The latter is an important feature of PDT that is responsible for long-term cure and destruction of metastasised cancer.

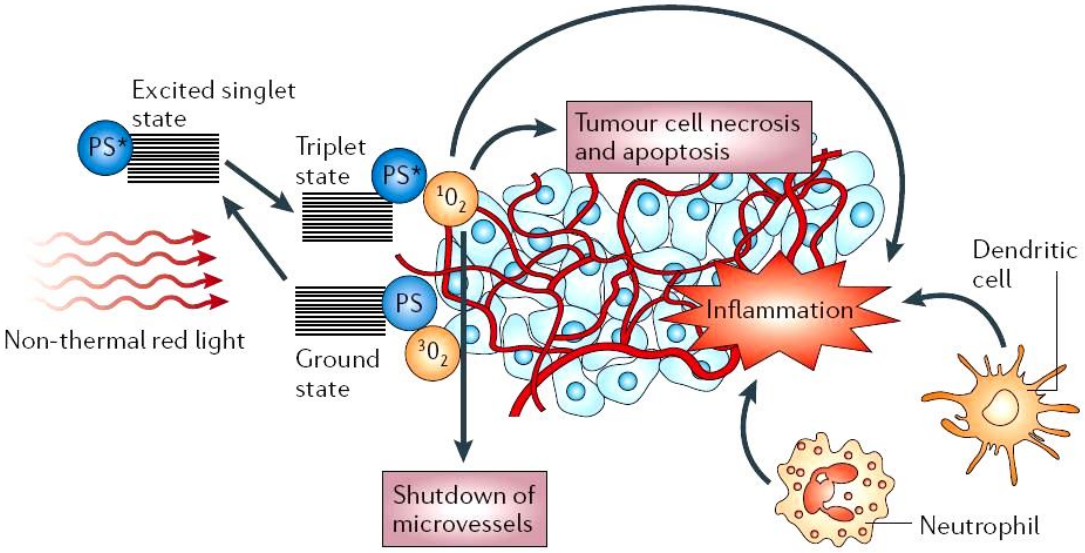

Figure 2.22 Mechanisms of PDT-mediated tumour destruction. Singlet oxygen generated during PDT is capable of inducing cellular death of tumour, shutting down of blood vessels feeding the tumour and activates the immunological responses against tumour cells. The figure was adapted from Castano et al. (2006).

2.5.2.1 PDT-mediated Cytotoxicity

PDT can evoke three cell death pathways i.e. apoptotic, necrotic, and autophagy-associated cell death. The mode of cell death depends on the PDT doses used (both light and photosensitiser doses), subcellular localisation of photosensitiser and cell type (Castano et al. 2005). Due to the high reactivity and short life-time of singlet oxygen,

photodynamic damage is probably confined to targets near to or within a particular subcellular site and affects relatively specific molecular targets (Buytaert et al. 2007).

In general, cell death by apoptosis are more prominent in low doses PDT, while cells exposed to higher PDT doses are more predisposed to necrosis. Studies on several photosensitisers have linked apoptosis induced by PDT is caused by photodamage to membrane bound BCl-2, a regulator for mitochondrial outer membrane permeabilisation, resulting in rapid release of cytochrome c and other pro-apoptotic factors (such as apoptotic-inducing factor-AIF and small mitochondria-derived activator of caspases-Smac) from the mitochondrion to the cytosol (Agarwal et al. 1991; Kim et al. 1999; Usuda et al. 2003; Kessel and Reiners 2007). This results in the activation of the intrinsic apoptotic pathway and initiates activation of the caspase-cascade. Meanwhile, high doses of PDT is thought to inactivate essential enzymes and other components of the apoptotic cascade such as caspases, resulting in a shift of cell death toward necrosis (Mroz et al. 2011). Severe photodamage of inner mitochondria membrane may also cause an increase in mitochondria permeability transition leading to release of Ca^{2+} from the mitochondrion, and subsequent overloading of intracellular with Ca^{2+} could promote activation calcium-dependent proteases such as calpain which contributes to necrotic cell death (Buytaert et al. 2007).

The mode of cell death is also dependent on localisation of photosensitisers in subcellular targets such as mitochondria, plasma membrane, lysosome and endoplasmic reticulum. The mitochondria has been shown to be a primary subcellular target for most photosensitisers used in PDT (Morgan and Oseroff 2001). Given the complex role of mitochondria in regulation of apoptosis, photosensitisers which localise within this organelle usually activate the apoptotic pathway through cytochrome c release. Lysosomal photodamage is also found to induce apoptotic cell death through the release of lysosomal proteolytic enzymes which resulted in cleavage of the pro-apoptotic

protein Bid that subsequently induced the release of cytochrome c from mitochondria (Kessel et al. 2000; Reiners et al. 2002). Meanwhile, photo-oxidation by photosensitiser which localise in plasma membranes can cause loss of plasma membrane integrity, leading to leakage of cytosolic contents and rapid depletion of intracellular ATP, both of which are prominent features of necrosis (Kessel and Poretz 2000).

In certain cell-type, oxidative stress induces by PDT may also lead to the stimulation of autophagic response (Dewaele et al. 2010). Studies have shown that photodamage to cellular organelles such as the mitochondria and endoplasmic reticulum may trigger macroautophagy involving the formation of a double membrane intracytoplasmic vacuole, known as autophagosome, surrounding these damaged organelles (Kessel et al. 2006; Xue et al. 2007). This process can be either pro-survival or pro-death. In cells with intact apoptosis, autophagy promotes cell survival by elimination of damaged organelles from activating the apoptosis pathway. In contrast, pronounced autophagic cell death is observed in apoptosis-deficient cells such as caspase-3-deficient MCF-7 breast cancer cell line (Xue et al. 2010) and Bax-deficient DU-145 prostate cancer cell line (Kessel et al. 2006), suggesting a pro-death function of autophagy. Therefore, autophagy may play a role as alternative death pathway when apoptosis is blocked. Autophagy also appears to play an important part in PDT-mediated antitumour immunity, since the process can result in major histocompatibility class I (MHC-I) presentation of antigens derived from cytosolic proteins (van der Bruggen and van den Eynde 2006).

2.5.2.2 Vascular Destruction

PDT is an efficient modality in disrupting vascular circulation by inducing thrombosis and vasculature occlusion. In fact, PDT has been successfully used for treating vascular

related lesions such as intimal hyperplasia, restenosis, atherosclerotic plaques, corneal and choroidal neovascularisation, and port-wine stains (Krammer 2001). Given their efficient interactions with vascular, a series of experiments have been designed for PDT evaluation purposes, such as the chick chorioallantoic membrane (CAM) model and the murine dorsal window chamber model (Figure 2.23). CAM is a highly vascularised membrane that serves as the respiratory organ for developing chick embryo. It is frequently used in preclinical PDT research for non-invasive study of microvasculature and blood circulation (Lange et al. 2001). Meanwhile, the murine dorsal window chamber model is a chronic preparation that provides access of the interior vasculature surface of the skin. This approach is relevant since all the skin layers from the stratum corneum composed of keratinocytes, stratum granulosum between the stratum corneum and the basal cells, and the facial layers of the dermis are intact in this model (Debefve et al. 2010; Palmer et al. 2011). Both the CAM and the window chamber model have been successfully used to evaluate the PDT vascular occlusion efficacy of a number of photosensitisers that are undergoing clinical trials or already approved for clinical use.

A B

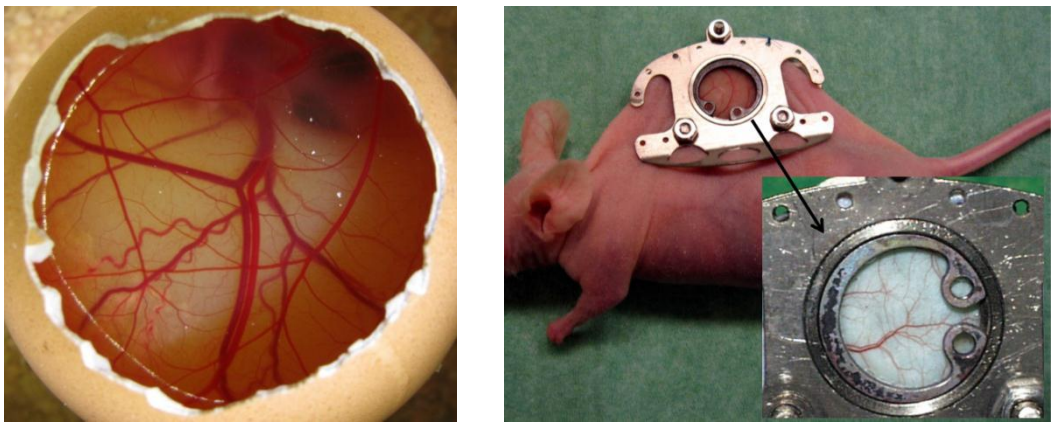

Figure 2.23 Models used to study PDT effects on vasculature**. (A)** Vascularisation of chick's embryo chorioallantoic membrane on egg development day-9. **(B)** An illustration of the dorsal skin fold chamber implanted in a nude mouse. Figure (B) was kindly provided by Dr Patrycja Nowak-Sliwinska of Swiss Federal Institute of Technology (EPFL), Switzerland.

In PDT of cancer, vascular occlusion is essential in disrupting the supply of oxygen and nutrients to lesion tissues in order to achieve long-term cure. The initial vascular effect of PDT begins with light-induced damage of endothelial cells and the subsequent exposure of vascular basement membrane led to the formation of thrombogenic sites within the vessel lumen. This process promotes platelet binding and aggregation, and release of thromboxane that causes vessel constriction as well as further increases the platelet aggregation. The blood vessel is therefore shut down and the ensuing hypoxia and nutrient deprivation induces extensive tumour cell-death (Krammer 2001). The vasculature targeting of PDT largely depends on the photosensitiser pharmacokinetics. For most exogenous photosensitiser, peak plasma concentration of the photosensitiser is usually achieved immediately after intravenous administration, and is followed by a rapid exponential decay in plasma concentration. The period of time when photosensitiser is still largely confined in the blood vessels provides a temporal therapeutic window for vascular targeting, and light irradiation during this period leads to a potent vascular damage (Chen et al. 2006a).

2.5.2.3 Immunoactivation

PDT is known to provoke both the innate and adaptive immune response. PDT-mediated innate immunity is initiated immediately following tumour tissue damage by singlet oxygen, that results in the release of pro-inflammatory endogenous damage-associated molecular patterns molecules (DAMPs) such as intracellular proteins and nuclear DNA (Korbelik 2006). This prompts the host to activate inflammatory response in order to protect and maintain tissue homeostasis at the affected site by removing damaged cells and promoting local tissue healing. The inflammatory response is led by the infiltration of phagocytic cells such as neutrophils, macrophages and dendritic cells aimed to neutralise the source of DAMPs by eliminating debris containing

compromised tissue elements, including injured and dead cells (Krosl et al. 1995; Agostinis et al. 2011).

The induction of the earlier innate immune system is required for the subsequent activation of adaptive antitumour immunity. *In vivo* mechanistic studies revealed that the incubation of immature dendritic cells with PDT-treated tumour cells lysate activates the dendritic cells to express interleukin-12 (IL-12), which is critical to the development of cellular immune response. These cells will migrate to tumour-draining lymph nodes where they differentiate into professional antigen-presenting cells and stimulate the activation of tumour-specific $CD8^+$ T cells that home into the tumour and eliminate the remaining tumour cells (Gollnick et al. 2002; Jalili et al. 2004).

Studies have examined the ability of PDT to enhance antitumour immunity in a clinical setting. A study on the use of ALA-PDT to treat vulval intraepithelial neoplasia resulted in higher $CD8^+$ T cell tumour-infiltration in patients with MHC-I positive tumours than non-responding patient with MHC-I negative tumours (Abdel-Hady et al. 2001). Subsequently, a case report shows that PDT treatment of multifocal angiosarcoma of the head and neck resulted in spontaneous regression of distant untreated tumours that correlated to increase $CD8^+$ T cell tumour-infiltration (Thong et al. 2007). In a more recent study, PDT treatment of basal cell carcinoma (BCC) was shown to enhance systemic immune reactivity to a BCC-associated tumour antigen, which may provide micro-metastatic control and long-term tumour cure (Kabingu et al. 2009). Although, it is clear that induction of antitumour immunity after PDT may act as effective antitumour vaccines, this favourable result is not always observed. The variations may be due to the difference in tumour cells immunogenicity, the presence of immune suppression by regulatory T cells or the presence of dendritic cells dysfunction caused by the tumour (Mroz et al. 2010).

CHAPTER 3

Evaluation of 15[1]-Hydroxypurpurin-7-Lactone Dimethyl Ester (G2) and Its Analogues as Photosensitiser for Photodynamic Therapy

3.1 Introduction

In the course of the screening program conducted at Cancer Research Initiatives Foundation, Malaysia on Malaysia's Biodiversity for potential photosensitisers for use in PDT of cancer (Kamal et al. 2009; Ong et al. 2009; Kamarulzaman et al. 2011), five pheophorbide-related photosensitisers from an ethanol soluble extract of the leaves and stems of *Aglaonema simplex* were isolated (Chee et al. 2005). While four of the compounds were commonly reported degradation products of chlorophylls, the fifth compound, 15[1]-hydroxypurpurin-7-lactone methyl ethyl diester, was isolated for the first time from the Araceae plant family. The latter showed strong photo-killing potency against human promyelocytic leukemia cells HL-60 and human oral squamous cell carcinomas HSC2 and HSC3 with IC_{50} values ranging from 0.30-0.41 μM. The only one other report of the compound as a naturally derived photosensitiser was by Kim et al. (2003), isolated from the leaves of bamboo plant *Phyllostachys bambusoides* where they reported rapid onset of apoptosis in the CMK-7 human leukemia cells upon light activation.

The initial *in vitro* studies involving 15-hydroxypurpurin-7-lactone methyl ethyl diester were conducted using the small quantities of naturally derived materials (Chee et al. 2005). Therefore, to generate sufficient quantities for further preclinical assessment, a closely related analogue, 15[1]-hydroxypurpurin-7-lactone dimethyl ester, termed G2, was prepared through semi-synthesis from chlorophyll-*a* containing extracts of

Spirulina platensis (Figure 3.1). G2 was found to exhibit potential PDT activity by inducing the closure of capillaries and small neovessels in a chick chorioallantoic membrane (CAM) model (Lim et al. 2010). G2 was also shown to be a promising photosensitiser against head and neck cancer cells by the higher potency of G2 in inducing photocytotoxicity and an ability to evoke a more pronounced apoptosis compared with a known photosensitiser, pheophorbide-a (PhA) (Lim et al. 2011). Even though the potency data for G2 was promising, solubilisation of G2 was challenging throughout because of its hydrophobic nature. Precipitation of the compound was a major problem and formulation of G2 for intravenous injection in the CAM experiments was only successful with the addition of a small amount of Cremophor@ EL as an emulsifier.

One of the strategies to improve aqueous solubility of photosensitiser is by attaching them to hydrophilic moieties such as amino acids (Roberts et al. 1988; Pandey et al. 1994; Wang et al. 2008). The conjugation of amino acids to tetrapyrrolic photosensitiser has been shown to improve their solubility and facilitates its entry into the cells (Kwitniewski et al. 2005). It has also been reported that photosensitisers conjugated with amino acids showed improved biological activity both *in vitro* and *in vivo* (Kwitniewski et al. 2005; Kwitniewski et al. 2009). With this notion, analogues of G2 conjugated with ionisable aspartyl (G2-Asp) and lysyl (G2-Lys) groups were synthesised, with the aim to optimise the drug-like properties of G2 as a quality candidate for clinical PDT.

The G2 analogues evaluated in this study was synthesised and provided by Dr Lee Hong Boon's group from Cancer Research Initiatives Foundation, Malaysia. G2-Asp and G2-Lys were prepared (Figure 3.1) by dicyclohexylcarbodiimide (DCC)/ dimethylaminopyridine (DMAP) mediated esterification of G2 in its acid form (G2 acid) with Boc-amino acids as previously described (Sternberg et al. 1998). In this

study, these G2 analogues were compared for their photophysical properties, *in vitro* photo-killing efficacy, single oxygen generation quantum yield, photobleaching, intracellular uptake and subcellular localisation. G2 and G2 acid were also evaluated in the present study with G2 used as a positive control since previous studies have demonstrated its efficacies (Chee et al. 2005; Lim et al. 2010; Lim et al. 2011). The most promising candidate compounds were further evaluated in mouse tumour allograft model to establish their *in vivo* efficacies. Even though many photosensitisers have been developed or are being developed for PDT center around the cyclic-tetrapyrrolic pharmacophore, the hydroxypurpurin structure described in this work has never been tested for its PDT efficacy beyond cell-based assays.

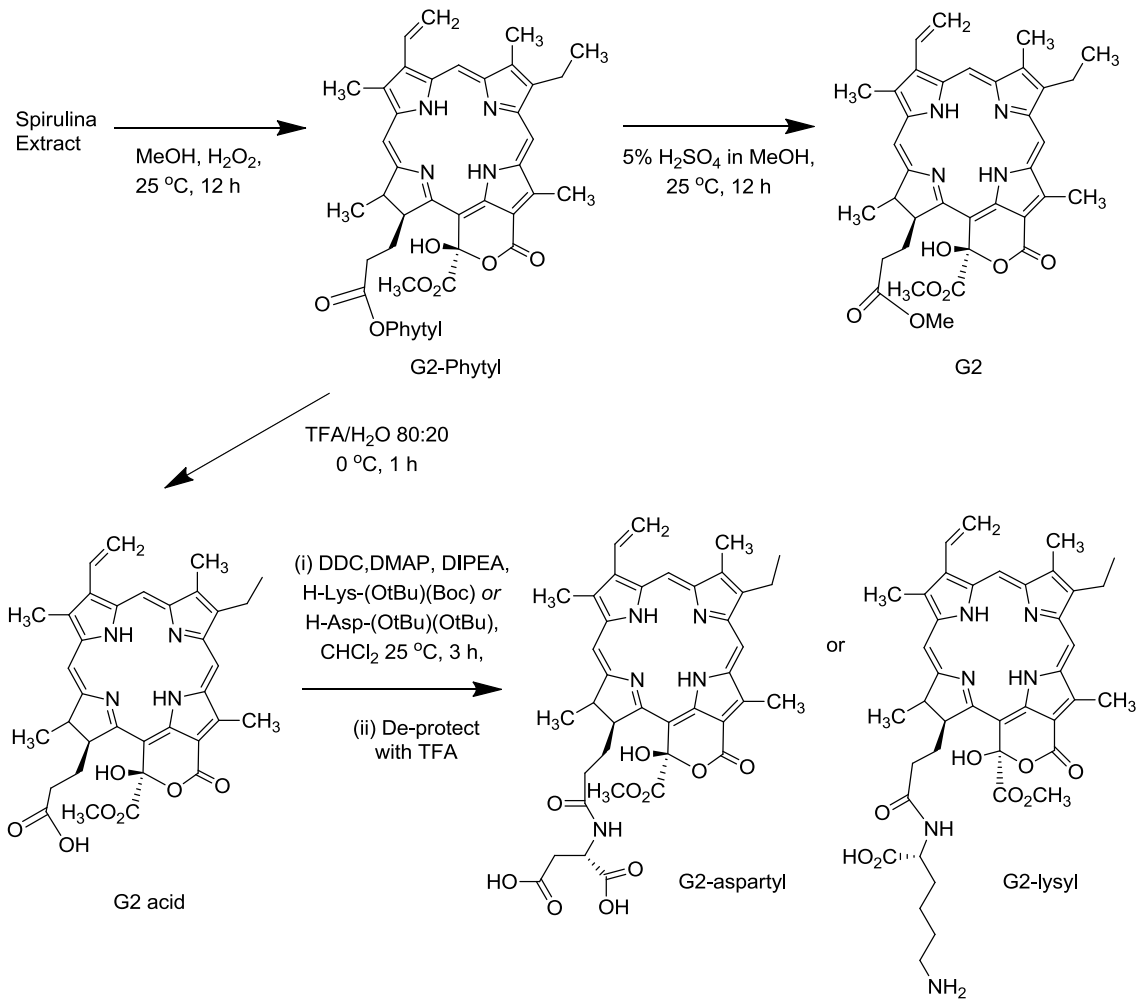

Figure 3.1 Schematic diagram for the synthesis of G2 and its derivatives.

3.2 Materials and Methods

3.2.1 Materials

3.2.1.1 Chemicals and Reagents

Cell culture reagents including Minimum Essential Media (MEM), RPMI 1640 medium with L-glutamine, Pen-Strep (10000 U/ml penicillin, 10 mg/ml streptomycin), trypsin 10× and foetal bovine serum (FBS) were purchased from Gibco, Invitrogen (Auckland, New Zealand). 1,3-diphenylisobenzofuran (DPBF) fluorescein isothiocyanate dextran (FITC-dextran, 20 kD) and dimethyl sulfoxide (DMSO) were purchased from Sigma-Aldrich (MO, USA) while thiazoyl blue tetrazolium bromide (MTT) was purchased from Amresco (OH, USA). Ethanol, isopropanol, octanol-1, and acetonitrile were purchased from Fisher Scientific (Leics, UK). Tiletamine-zolazepam (Zoletil) was purchased from Virbac (Carros, France). Ketamine (Ketamil) and xylazine (Xylazil-100) were obtained from Troy Laboratories (NSW, Australia). Pheophorbide-*a* (PhA) was purchased from Frontier Scientific (UT, USA). ER-Tracker Blue-white DPX, LysoTracker Blue DND-22 and rhodamine-123 (Rh123) were purchased from Molecular Probes, Invitrogen (OR, USA). Saline (0.9% sodium chloride) was obtained from Duopharma Sdn. Bhd. (Selangor, Malaysia).

3.2.1.2 Instrumentations

All cell culture works were carried out with aseptic technique in an Airstream class II biological safety cabinet (ESCO, Singapore). Cultured cells were incubated in a Forma direct heat CO_2 incubator (Thermo Fisher Scientific, OH, USA). UV-visible absorption and fluorescence emission spectra were recorded with the cuvette platform of SpectraMax M4 (Molecular Devices, CA, USA) using 1 cm pathlength quartz cuvettes. Meanwhile, the absorbance and fluorescence intensity of samples in a 96-well plate was

measured with the microplate platform of SpectraMax M4. Photoirradiation for *in vitro* experiments was performed with a light source consisting of a Halotone 300 W halogen lamp (Philips Electronic, Netherlands). A water column was used to filter off the infrared radiation and a Roscolux #26 Light Red (>580 nm) (Rosco, NY) filter were placed in the irradiation path before the sample. The irradiation intensity was measured with a calibrated Nova-Oriel power meter (Newport Corp, CA, USA). Other equipments used only for specific experiment are listed under their respective methodology sections.

3.2.1.3 Animal Model

Fertilised Lohmann Brown chicken eggs were supplied by Hing Hong Sdn. Bhd. (Selangor, Malaysia). Female BALB/c mice aged between 4-6 weeks were obtained from Monash University Sunway Campus (Selangor, Malaysia) and were allowed to acclimatise for two weeks in the animal holding facilities in Department of Pharmacology, Faculty of Medicine, University of Malaya. All animal experiments were conducted in accordance with the protocols reviewed and approved by Dr. Haji Azizuddin Bin Haji Kamaruddin, Laboratory Animal Centre (LAC) Animal Care and Use Committee (ACUC), Faculty of Medicine, University of Malaya (reference number FAR/14/07/2010/LSH). Mice were maintained in individually ventilated cages rodent housing system (Allentown Inc., NJ, USA) in a controlled environment of 12 h light-dark cycles with free access to food (standard pellet diet purchased from Altromin International, Lage, Germany) and water. Female mice were used because the hormonal environment essential for development of implanted 4TI mouse mammary carcinoma would be present.

3.2.2 Preparation of Compound

G2 and its analogues were prepared and supplied by Dr Lee Hong Boon's group from Cancer Research Initiatives Foundation, Malaysia. Their syntheses, purification and NMR characterisation are included in Appendix C. All the compounds used for *in vitro* experiments were dissolved in DMSO to make stock solutions of 10 mM, aliquoted into appropriate volume and stored at -20 ºC prior to use.

3.2.3 Photophysical properties

Compounds were dissolved in ethanol at 10 μM for the measurements of UV-visible and fluorescence emission spectra. The UV-visible spectral data was collected from 300 to 800 nm wavelengths. The compounds were excited at their respective maximal absorption (λ_{abs}) for the measurement of fluorescence emission spectrum, which was recorded from 600 to 800 nm. Extinction coefficient (ε) for each compounds were determined and the fluorescence quantum efficiency (Φ_{fl}) was calculated using PhA in ethanol ($\Phi_{fl} = 0.28$) as a reference (Röder et al. 2000).

3.2.4 Cell Culture

HSC2 was obtained from Health Science Research Resources Bank (Japan Health Sciences Foundation, Japan). The cell line was grown in MEM medium supplemented with 10% FBS and 1% of penicillin-streptomycin and maintained in a 25 cm^2 tissue culture flask in a humidified atmosphere containing 5% CO_2 and 37 ºC. When the culture reaches confluency of 80%, cells were washed twice with sterile PBS to remove all traces of serum which contains trypsin inhibitors before 1.0 ml of trypsin-EDTA 1× was added for 5-10 min at 37 ºC to disperse the monolayer cells. Then, 3 ml of

complete culture medium was added to the dispersed cells followed by repeated gentle pipetting to split apart the cell clumps. An aliquot of the cell suspension was transferred to a new 25 cm^2 tissue culture flask containing 5 ml of fresh medium at a subculture ratio of 1:4 to 1:8 and incubated at 37 ºC.

3.2.5 Photo-induced Cytotoxicity Assay

Approximately 3000 cells/well in a phenol-red-free culture medium containing 10% fetal bovine serum were seeded in a 96-well plate. Cells were allowed to adhere overnight before test compounds were introduced. Photosensitiser stock solutions (10 mM in DMSO) were diluted with medium, and concentrations varying from 0.001 to 100.0 μM were tested on the cells. The control wells received 0.01% of DMSO, equivalent to the highest amount of DMSO used as vehicle in the compound-treated wells. Following 2 h of treatment, cells were irradiated at a fluence rate of 8.9 mW/cm^2 for 10 min to obtained irradiation light dose of 5.3 J/cm^2 (as calculated using Equation 1) using a custom-made broad spectrum irradiation light source filtered with a Roscolux #26 Light red (>580 nm) (Rosco, NY, USA) interference filter (Figure 3.2).

Equation 1

$$\text{Light dose } (J/cm^2) = \frac{\text{light power (W)} \times \text{irradiation time (s)}}{\text{area of irradiation } (cm^2)}$$

After irradiation, the cells were further incubated for 24 h before cell viability was assessed using the MTT assay (Marshall et al. 1995). Following incubation, 15 μl of MTT solution (5 mg/ml) was added into each well and incubated for 4 h at 37 ºC. The medium was then removed and 100 μl of DMSO was added to dissolve the formazan crystal formed. Absorbance, as a measurement of viable cell number, was read at 570

nm with a microplate spectrophotometer and the percentage of cell viability was determined using Equation 2.

Equation 2

$$\% \text{ of cell viability} = \frac{\text{average absorbance of treated cells}}{\text{average absorbance of control cells}} \times 100$$

A dose response curve was constructed and the IC_{50} value (the concentration of compound that inhibits the proliferation rate by 50% compared with the control untreated cells) was interpolated from the curve. An equivalent experiment without light exposure was carried out concurrently to determine the dark toxicity of each compound.

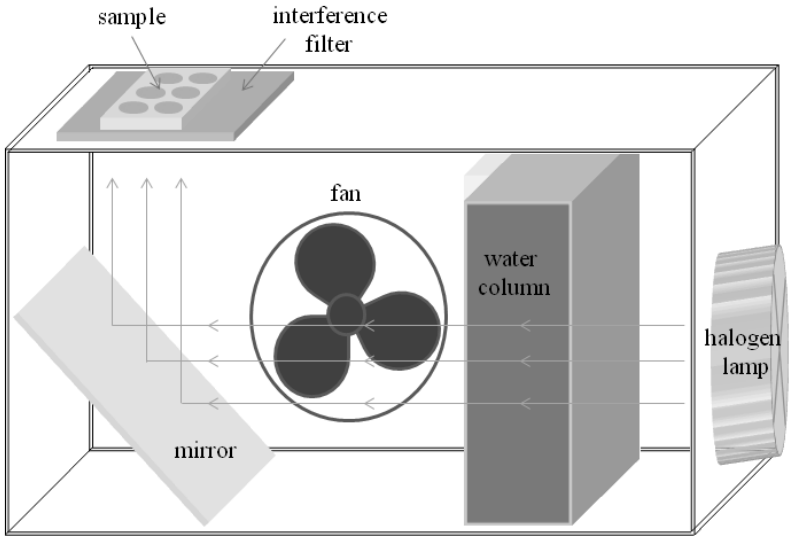

Figure 3.2 Schematic illustration of a custom-made irradiation light box setup which consists of a) an intensity-controlled halogen lamp as illumination light source; b) a water column to filter off the ultraviolet and infrared radiation; c) a 45° mirror to direct light path to the sample; d) an interference filter was placed in the irradiation path before the sample to attain desired irradiation wavelength and; e) a fan for system cooling. The irradiation intensity is measured with a calibrated power meter.

3.2.6 Relative Rate of Singlet Oxygen Generation

The singlet oxygen generation of the photosensitiser was measured by monitoring the bleaching of DPBF, a known singlet oxygen acceptor (Kochevar and Redmond 2000). Photosensitisers at 0.5 μM prepared in 8 ml of 50 μM DPBF in aerated isopropanol in a 6-well plate was irradiated at 5.3 mW/cm^2. A 200 μl of the solution was sampled into a covered 96-well plate in duplicates at fixed intervals over 1 h and the absorbance was read at 410 nm using a microplate reader. An irradiated well without photosensitiser was also performed as a negative control. The singlet oxygen generation rate was deduced from the reduction of DPBF absorbance over time and the quantum yield was determined by using PhA ($\Phi_\Delta = 0.52$) as a reference (Hackbarth et al. 2001).

3.2.7 Distribution Coefficient (Log D)

Distribution coefficient was determined by the shake flask method (Berthod and Carda-Broch 2004). Octanol-1 and phosphate buffered saline (PBS) (pH 7.4) were pre-saturated with each other by shaking vigorously a mixture of both in separate bottles and the mixtures were allowed to settle down overnight. A stock solution of compounds in known concentrations (5 to 20 μM) in octanol-1 was prepared. This solution was shaken vigorously with a same volume of PBS (pH 7.4) in a 2 ml microcentrifuge tube. Another set of experiment was prepared by diluting the octanol-1 stock solution by half its concentration and shaking a same volume of this diluted stock solution with a second volume of PBS. To facilitate equilibration, tubes were centrifuged at 400 *g* for 10 min. Both the octanol-1 and aqueous phases were carefully sampled for absorbance measurement and the compound concentrations in both phases were interpolated from a standard curve of the compound determined at 400 nm. The distribution coefficient or Log D was then calculated using Equation 3.

Equation 3

$$\text{Log D} = \text{Log} \frac{\text{Concentration}_{\text{octanol-1}}}{\text{Concentration}_{\text{PBS pH 7.4}}}$$

3.2.8 Intracellular Localisation

Intracellular localisation of photosensitiser was analysed by confocal microscopy using dual staining techniques (Marchal et al. 2007). Cells grown on round glass coverslips in 12-well plates were co-incubated with 100 nM of photosensitser together with organelle-specific fluorescence probes. The endoplasmic reticulum was labeled with 100 nM of ER-Tracker Blue-White DPX, the lysosomes were stained with 500 nM of LysoTracker Blue DND-22, and the mitochrondria were tracked with 100 nM of Rh123, each for 15-30 min of incubation at room temperature. After incubation, cells were gently rinsed in PBS to remove free dyes, and the stained cells were observed using Olympus DSU spinning disk confocal microscope configured with a PlanApo 60× oil objective (Olympus Optical Corp. Ltd., Tokyo, Japan) and iXon EM+ digital camera (Andor Technology, CT, USA). Fluorescence images of Z sections at 0.2 μm were collected sequentially using Olympus Cell software. Organelle-specific fluorescence probes were respectively excited at 330-385 nm wavelengths to illuminate ER-tracker and LysoTracker, at 460-490 nm for Rh123 and at 400-440 nm for the G2 derivatives. The intracellular localisation of the photosensitiser was determined by comparing its fluorescence topographic profile with the topographic profile of each organelle-probe generated from a longitudinal transcellular axis.

3.2.9 Intracellular Uptake of Photosensitiser

HSC2 cells were seeded into 96-well plate at 4000 cells/well and incubated overnight. Cells were treated with compounds at 10 μM for indicated periods. Following incubation, the content of each well was removed and the wells were washed twice with PBS. Each well was then incubated with 200 μl of acetonitrile:water (4:1) for 30 min at room temperature to lyse the cells and extract the photosensitisers. Subsequently, 100 μl of the extract was transferred to a black 96-well plate and their fluorescence intensity (excitation/emission at 400/675 nm) was measured. The concentrations of the photosensitiser were determined from a calibration curve.

3.2.10 Photostability Studies

Photosensitiser photostability was studied by monitoring the photobleaching of the phototosensitiser following light irradiation (Rotomskis et al. 1996). Briefly, 10 μM of compounds in 100 μl of PBS (pH 7.4) were irradiated at 8.9 mW/cm^2 for various durations. Following irradiation, the samples absorbance was recorded at 400 nm.

3.2.1 PDT on the CAM Vasculature (*in ovo*)

3.2.11.1 CAM Model Development

The CAM experiment was performed as previously described (Lange et al. 2001). Freshly fertilised chicken eggs were incubated at 37.6 ºC with 65% relative humidity (Savimat MG 200, Chauffry, France) with the narrow apex down in a swinging incubator. On embryo development day (EDD) three, an eggshell opening of ~4 mm in diameter was bored at the narrow apex with a sharp curved point forceps. The purpose of boring a hole on the eggshell at early days of incubation is to ensure that the growing

CAM will not encounter a continuous surface to be attached to and will detach from the eggshell. The hole was then sealed with adhesive tape to avoid contamination and desiccation of the egg contents. The eggs were further incubated in stationary position with the narrow apex upright until EDD-9. At the time of the assay, the CAM was accessible without damage by carefully opened the eggshell around the window made.

Critical steps

- *Continuous use of eggs source from one supplier decreases the variability in development of embryos and the degree of vascularisation (Ribatti et al. 2006).*
- *The use of fertilised eggs obtained from facilities where hens do not receive any antibiotic, artificial hormone or nutritional supplements is recommended to avoid interference of such substances with the assays.*
- *Eggs are best incubated soon after laying or must be maintained at 15-20 ºC prior to incubation. Long periods (more than 5 days) between egg laying and incubation decrease embryos' survival.*
- *Falling of chipped eggshell onto the CAM should be avoided since eggshell pieces induce inflammation.*
- *Work performed on the embryos must be done under aseptic conditions as the chick embryo is susceptible to infections especially from Aspergillus fumigatus, Staphylococcus aureus and Pseudomonas aeruginosa (Ribatti et al. 2006).*

3.2.11.2 Microscope Setup for Photo-irradiation and Imaging

Microscopic observation of CAM vasculature and the light irradiation during PDT were performed with a MVX10 macro zoom fluorescence microscope equipped with a MV PLAPO 2XC lens (Olympus, Japan). Illumination was provided by a 75 W Xenon lamp burner (Olympus, Japan). Light doses were adjusted with neutral density filters and measured with Nova-Oriel power meter (Newport Corp, CA, USA). For exciting and detecting G2 analogues, a 400-440 nm excitation filter set (U-FBVW; Olympus, Japan) was used. For detecting FITC, a 460-480 nm excitation filter set (U-MGFPHQ; Olympus, Japan) was used. Fluorescence angiograms were acquired with a XM10

monochrome cooled CCD camera driven with Cell^{M} Software from Olympus Soft Imaging Solution (Münster, Germany).

3.2.11.3 PDT on the CAM Vasculature (*in ovo*)

On EDD-9, the egg opening was extended to ~30 mm in diameter. Embryos were intravenously administered with a single bolus of photosensitiser in a dosing vehicle (CrEL 5%, EtOH 5% in saline). For control group, embryos were injected with the dosing vehicle only. Dosing was performed at the CAM main vasculature using microliter syringe affixed with a 12º beveled point 33g needle (Hamilton Company, NV, USA). The needle was inserted at < 20º angle to avoid vascular damage and hemorrhage. One minute after injection, a site with vessels of diameter between 5-100 µm was irradiated with light dose of 20-40 J/cm^2. Irradiation was performed with light at 400-440 nm at a fluence rate of 130 mW/cm^2 over an area of 0.02 cm^2. The duration of irradiation was determined as described in Equation 1. Subsequently, the egg opening was sealed with parafilm and was further incubated for 24 h before assessing the PDT-induced damage.

Fluorescence angiograms were performed in order to assess the PDT-induced vasculature damage. Blood vessels were perfused with 10 µl of 25 mg/ml FITC-dextran followed by injection of Indian ink into the allantoic cavity to decrease the embryo's interfering fluorescence from deeper located vessels. The vasculature network at the site of irradiation was illuminated by exciting the FITC at 465-495 nm wavelengths on the fluorescence microscope. The vasculature network was imaged and the extent of damage induced by PDT was scored using a previously defined arbitrary damage scale from 1 to 5 as listed in Table 3.1 (Lange et al. 2001). At least 10 embryos were assessed for each treatment group.

Table 3.1 The damage score of PDT-induced vasculature network occlusion.

Occlusion score	Findings	Pre-irradiation	Post-irradiation
0	No occlusion	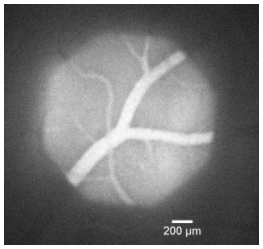	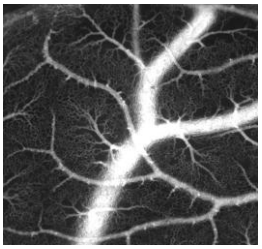
1	Partial closure of capillaries of diameter < 10 µm	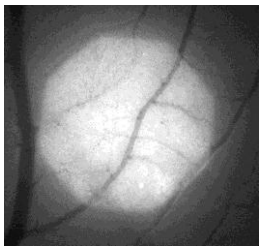	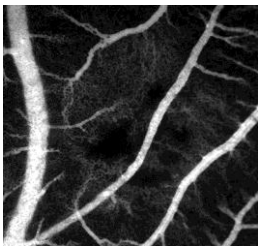
2	Closure of capillary system, partial closure of blood vessel of diameter < 30 µm and size reduction of larger blood vessels	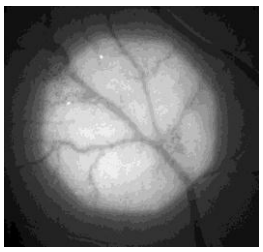	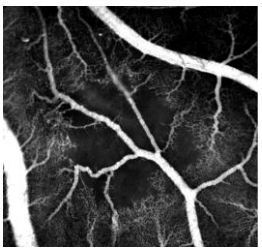
3	Closure of vessels of diameter < 30 µm and partial closure of larger blood vessels	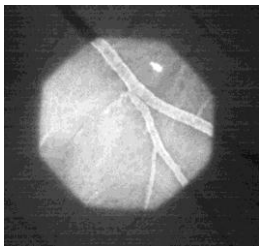	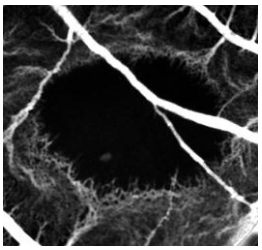
4	Total closure of vessels of diameter < 70 µm and partial closure of larger vessels	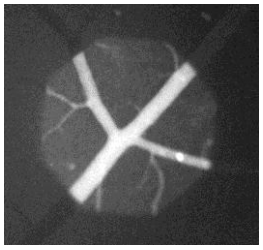	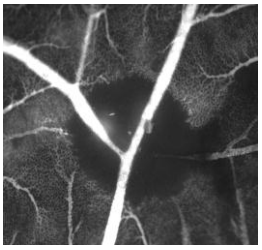
5	Total occlusion of vessels in the irradiated area	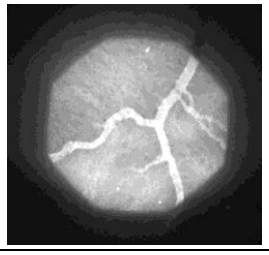	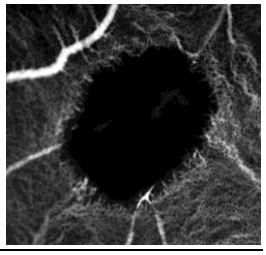

Critical steps

- *Embryo tolerability to the injection solution should be determined in advance.*
- *Care should be taken to inject only inside the vessel and not in surrounding tissue.*
- *PDT on CAM must always be performed using embryo at matching EDD. This is because body weight, blood volume and CAM features change during embryo development (Ribatti et al. 2001; Vargas et al. 2007).*
- *The evaluation of PDT effects must be at exactly the same period of time post PDT, because the initial occlusion of vessels observed 24-h post-PDT can induce angiogenic stimuli, resulting in reperfusion of occluded vessels and neovascularisation (Zuluaga et al. 2007).*

3.2.12 *In Vivo* PDT Efficacy Studies

Tumour allografts were initiated by injecting 5×10^5 of 4T1 mouse mammary carcinoma cell in 0.1 ml RPMI 1640 media into the mammary fat-pad at the lower left quadrant of the mice's abdomen (Jin et al. 2010). Treatments were initiated when tumours reached a volume range of 100-200 mm^3. Mice were administered respectively with 15 mg/kg G2 or G2-Asp dissolved in a mixture of 10% cremophor, 10% ethanol in saline as dosing vehicle via the lateral tail vein at 10 ml/kg. For solvent control group and unirradiated control group, dosing vehicle and 15 mg/kg of G2 or G2-Asp only was given, respectively. Following dosing at various intervals, mice were anesthetised by intraperitoneal injection of an anesthetic cocktail (25 mg/ml tiletamine-zolazepam, 80 mg/ml ketamine, 20 mg/ml xylazine) and PDT was performed after the onset of anaesthesia. The tumour area was focally illuminated using the Lumacare LC-122A fiber optic light delivery system (Lumacare, Newport Beach, CA) fitted with 665/32 bandpass filter. The total fluence delivered was 100-200 J/cm^2 with a fluence rate of 130 mW/cm^2 over a 12 mm diameter irradiation spot. Following illumination, animals were allowed to recover from anesthesia in a warm chamber. Animal weights and tumour volume were measured thrice weekly for a month or earlier when the mice were

deemed necessary to be sacrificed owing to excessive tumour burden (tumour volume >2000 mm^3). At least six mice were assessed for each treatment group.

Growth of the solid tumours was monitored using *in situ* caliper measurement of two perpendicular dimensions (length and width) and tumour volume was calculated using the formula for a prolate ellipsoid using Equation 4. (Plowman et al. 1997; Hollingshead 2008).

Equation 4

$$\text{Tumour volume } (mm^3) = \frac{\text{length (mm)} \times \text{width}^2 \text{ (mm)}}{2}$$

The median tumour volume – time profile for each group was plotted and results were expressed as median ± 95% confidence interval. To determine the antitumour activity, terminal % T/C was calculated from the growth curve (Equation 5).

Equation 5

$$\text{Terminal \% T/C} = \frac{\Delta T}{\Delta C} \times 100, \text{ if } \Delta T > 0$$

or

$$\frac{\Delta T}{T_1} \times 100, \text{ if } \Delta T < 0$$

Where ΔT and ΔC are the changes in the median tumour volume for each treated and control group after the treatment had ended.

3.2.13 Statistical Analysis

Statistical significance was performed using one-way ANOVA followed by Bonferroni's post-hoc test (SPSS 16.0, IBM Corporation, Armonk, NY) and differences were considered significant when $p<0.05$.

3.3 Results and Discussion

3.3.1 Photophysical Properties

Figure 3.2 showed the absorption and fluorescence emission spectra for G2 analogues assessed at 10 μM in ethanol. Their photophysical parameters are summarised in Table 3.2. The conjugation of G2 with aspartyl or lysyl as well as G2 in acid form did not result in a shift in the absorption and emission peaks. All the analogues have similar absorption spectra shape with a B-band at approximately 400 nm and a major Q-band at 667 nm. However, the Q-band molar extinction coefficient of G2 acid (ε = 8400) and G2-Lys (ε = 6500) were appreciably lower compared to G2 (ε = 34100) and G2-Asp (ε =31800). Meanwhile, the fluorescence emission wavelength among the G2 analogues is very similar at ~ 675 nm and their fluorescence quantum yield (Φ_{fl}) in ethanol were ranging from 0.14-0.19 as calculated using PhA (Φ_{fl} = 0.28 in ethanol) as a reference.

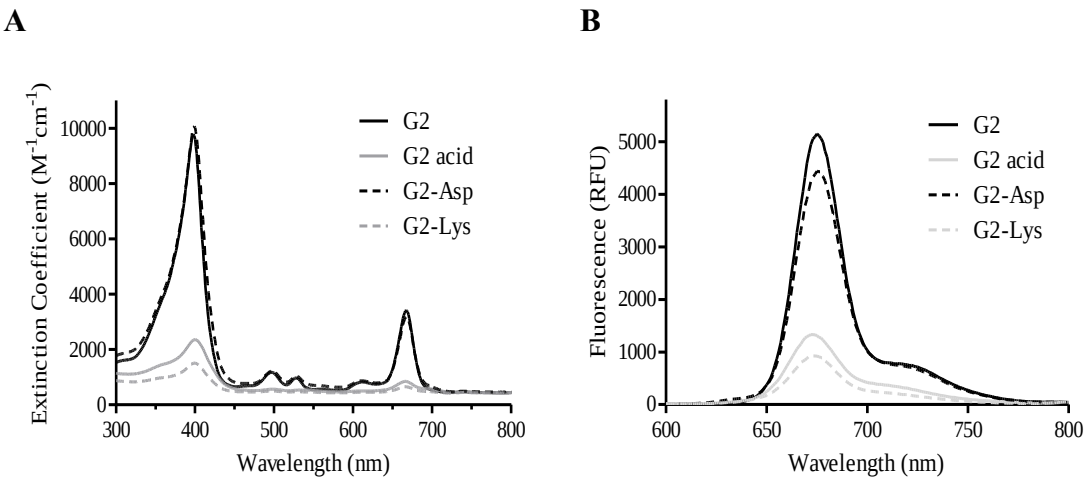

Figure 3.2 Photophysical properties of G2 analogues at 10 μM in ethanol. A) UV-visible spectrum for G2 analogues. B) Fluorescence emission spectra for G2 analogues when excited at B-band λmax.

Table 3.2 Photophysical parameters of G2 analogues in ethanol.

Compounds	B-band λ_{abs} (nm)	Q-band λ_{abs} (nm)	λ_{em} (nm)	Q-band ε ($M^{-1}cm^{-1}$)	Φ_{fl}
G2	398	667	675	34 100	0.16
G2 acid	400	666	672	8 400	0.18
G2-Asp	397	667	675	31 800	0.14
G2-Lys	399	667	672	6 500	0.19

Φ_{fl} : Quantum efficiency of fluorescence was calculated using pheophorbide-*a* in ethanol (Φ_{fl} = 0.28) as a reference

This observation is consistent with previous reports that also observed lower extinction coefficients with the conjugation of hydrophilic amino acids to porphyrins. (Roberts et al. 1988; Serra et al. 2010). This reduction is undesirable because in order to receive sufficient excitation energy especially in deep-seeded tissues, a photosensitiser should have a relatively high absorption bands (>20000-30000 $M^{-1}cm^{-1}$) at wavelengths between 600-800 nm where light can penetrate effectively (Castano et al. 2004).

3.3.2 Distribution Coefficient Log D

Distribution coefficient (Log D) is defined as the equilibrium concentrations ratio of a compound (ionised plus unionised) dissolved in each phase of a mixture of two immiscible solvents, namely an aqueous buffer and n-octanol. The measurements of Log D values of G2 analogues were determined using the shake flask method. From the experiment, G2-Lys and G2-Asp had Log D values of 0.3 and -0.4 respectively, which were significantly lower (p<0.05) compared to the unconjugated G2 with a value of 1.3 (Table 3.3). The lower Log D values indicated that the conjugation of G2 with aspartyl or lysyl amino acids had increased its solubility in the aqueous phase. The negative Log D value of G2-Asp reflects its preferential solubilisation in the aqueous compared to the

octanol phase. Meanwhile, the Log D value for G2-acid at 1.2 was similar to that for G2 (p>0.05).

Data from the observation showed that the attachment of aspartyl or lysyl amino acids was able to improve the aqueous solubility of G2 as represented by the lower or negative Log D values. This is expected as Asp and Lys are highly polar, in which the acidic aspartyl moiety is set to lose an H^+ (proton) at its carboxylic side chain to become negatively charged and engages in ionic bonding, whereas the amine side chain of the lysyl moiety accepts an H^+ to become positively charged and engages in hydrogen bonding.

3.3.3 Singlet Oxygen Generation Quantum Yields

The ability of a photosensitiser to generate singlet oxygen determines their efficiency as a PDT agent. This event is essential because the singlet oxygen produced is the key cytotoxic agent that can directly oxidise many biological molecules. The singlet oxygen quantum yield of G2 analogues were quantified by monitoring the bleaching of the singlet oxygen scavenger DPBF at an initial concentration of 50 μM in isopropanol over a period of 1 h light irradiation. The irradiation was performed at 5.3 mW/cm^2 of light dose at room temperature. The singlet oxygen quantum yield was determined using PhA as a reference. Under this experimental condition, G2 exhibited significantly higher Φ_Δ value (p<0.05) at 0.66 which is at least 2-fold higher compared to G2 acid, G2-Asp and G2-Lys (Table 3.3). In the meantime, reduction of DPBF was not observed in the negative control well indicating that its reduction was not caused by photobleaching of the DPBF reagent.

Table 3.3 Singlet oxygen quantum yield, Log D, and photocytotoxicity of G2 analogues

Compounds	Log D[a]	Φ_Δ[b]	IC_{50} (μM)[c]
G2	1.3 ± 0.2[§]	0.66 ± 0.03[§]	0.48 ± 0.02[§]
G2 acid	1.2 ± 0.1[§]	0.32 ± 0.01[†]	2.8 ± 0.1[†]
G2-Asp	-0.4 ± 0.1[‡]	0.32 ± 0.03[†]	0.91 ± 0.07[§]
G2-Lys	0.3 ± 0.1[†]	0.29 ± 0.02[†]	3.3 ± 0.4[†]

[a] Distribution coefficient determined using a modified shake flask method in n-octanol and PBS (pH 7.4).

[b] Singlet oxygen quantum yield in isopropanol with pheophorbide-a (ΦΔ = 0.52 in EtOH) as reference.

[c] IC50 (half maximal inhibitory concentration) in HSC2 cells determined using MTT assay following 24 h incubation with compounds (light dose 5.3 J/cm^2). No dark cytotoxicity was observed up to 10 μM.

Values represent mean ± SD of three independent replicates. Means with different symbols are significantly different from each other (p<0.05) within each parameter.

3.3.4 *In Vitro* PDT Activity

To determine the photocytotoxicity of G2 analogues, HSC2 cells treated with the photosensitisers were irradiated with a light dose 5.3 J/cm^2. The cell viability following treatment was determined 24 h later using MTT assay. The MTT assay is based on the conversion of tetrazolium salt to purple formazan by the mitochondrial dehyrogenase activity of viable cells (Mosmann 1983). In this study, G2 was the most potent photosensitiser with an IC_{50} value of 0.48 μM followed by G2-Asp, G2 acid and G2-Lys with IC_{50} values of 0.91, 2.8 and 3.3 μM, respectively (Table 3.3). The reduction of G2-Asp PDT potency was not significant (p>0.05), while the potency for G2-Lys and G2 acid were significantly reduced (p<0.05) when compared to G2. Photosensitisers treatment up to 10 μM without irradiation did not cause significant loss in cell viability.

The results in this study showed that the conjugation of aspartyl or lysyl amino acids to G2 reduces its *in vitro* PDT potency. When analysed according to singlet oxygen generation ability, the phototoxicity of the G2 analogues decreased in accordance with decreasing singlet oxygen production following conjugation to aspartyl or lysyl group. Since the light-absorbing chromophore in the G2 analogues remained the

same, the decrease in the singlet oxygen generation could be linked to the lower molar absorption coefficient of the more polar analogues, which would in turn affect the amount of light energy absorbable to generate singlet oxygen.

3.3.5 Cellular Uptake

The cellular uptake of a photosensitiser may also influence cellular susceptibility to PDT, whereby higher level of cellular uptake is often correlated with greater photocytotoxicity. In the present study, the kinetic of G2 analogues cellular accumulation was studied in HSC2 cells by measuring the molar amount of photosensitisers taken up by cells following 10 μM incubation of photosensitiser in the dark. From the study (Figure 3.4), G2 exhibited the highest uptake, whereby the accumulation of G2 increased significantly within the first 0.5 h (p<0.05) and continued to rise to 150 nmol/mg protein at 24 h (p<0.05). Meanwhile, the uptake rates and amounts for G2-acid, G2-Asp and G2-Lys within the first 24 h were low with concentrations detected at approximately 18 nmol/mg protein.

When analysed together with *in vitro* PDT potency, greater photocytotoxicity was observed in analogues that showed higher level of cellular uptake. The greater cellular uptake by G2 compared to G2-Asp and G2-Lys is probably due to the greater lipophilicity of the former as lipophilic compounds can cross the membrane lipid bilayers more easily. While it is generally true that the uptake of compounds into cells is largely governed by their relative lipophilicity, several studies have shown that uptake of certain tetrapyrroles demonstrated non-linear correlation with their lipophilicity parameter (Margaron et al. 1996; Huang et al. 2010). An example is that extremely lipophilic tetrapyrrole tends to form aggregate in the media and thus prevent plasma membranes diffusion.

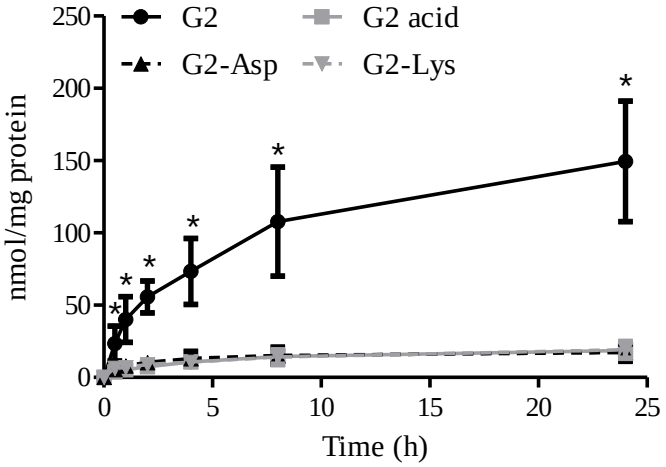

Figure 3.4 Intracellular uptake profiles of G2 analogues at 10 μM in HSC2 cells. Intracellular accumulation of G2 increased rapidly within the first four hours and continued to rise to 150 nmol/mg protein at 24 h. Meanwhile, the uptakes for G2 acid, G2-Asp and G2-Lys within 24 h were approximately 18 nmol/mg protein. *Statistically significant differences compared to each group at their respective time point with $p<0.05$.

3.3.6 Photostability

Degradation of photosensitiser following irradiation reduces their availability to perform PDT due to photobleaching. Photostability study was performed by irradiating 10 μM of photosensitisers in PBS (pH 7.4) at 8.9 mW/cm^2 in order to mimic the *in vitro* assay settings. From Figure 3.5, G2 and G2-Asp were relatively stable to irradiation at wavelength between 600-800 nm. Meanwhile, G2 acid and G2-Lys were found to be photodegraded within the first 20 min of irradiation by 8% and 15% from their initial concentration, respectively. However, their degradations were minimal within the first 10 min which corresponds with the irradiation duration used for *in vitro* study. Therefore, photostability has minimal effects in modulating the potency patterns exhibited by these photosensitisers.

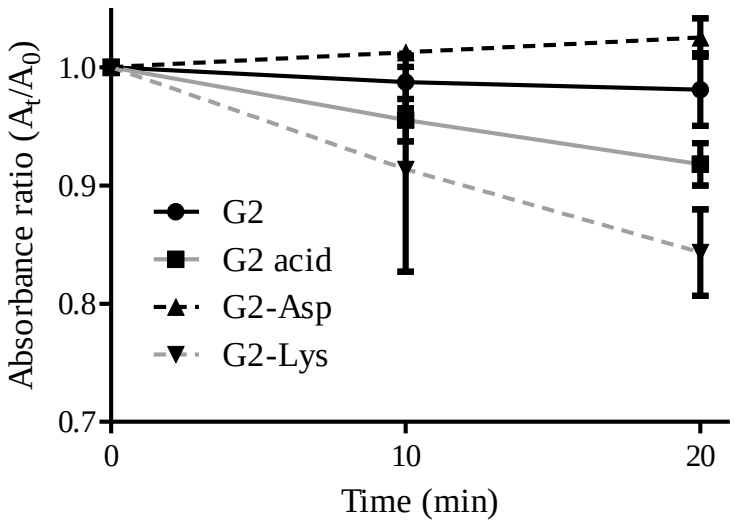

Figure 3.5 Photostability assessment through UV-visible spectra of 10 μM of G2 analogues in PBS (pH7.4) upon irradiation with light of 600-800 wavelengths at 8.9 mW/cm^2.

3.3.7 Intracellular Localisation

The singlet oxygen generated immediately after PDT has a short half-life and limited diffusion in the biological environment (Moan and Berg 1991). Therefore, different subcellular organelle localisation of a photosensitiser is known to produce different mechanisms of PDT-mediated cell toxicity and this affects its potency. The accumulation of a photosensitiser in the mitochondria and reticulum endoplasm is found to be more efficient in triggering cell death following PDT as compared to their accumulation in lysosomes. The mitochondrial damage by PDT has been shown to correlate with several cellular events associated with apoptosis i.e. rapid loss of mitochondrial membrane potential, cytochrome c release and the activation of cytotoxic caspases (Morgan and Oseroff 2001). Meanwhile in endoplasmic reticulum, PDT is observed to induce carbonylation of cellular proteins that leads to stress in that organelle and could trigger cell death (Szokalska et al. 2009). The photosensitisation of lysosomes

is reported to initiate autophagy response which can either promote survival or facilitate the death of the photodamaged cells. It is observed that lysosomal proteases were photoinactivated by certain photosensitisers and this had led to impaired autophagic processes leading to cell survival (Reiners et al. 2010).

The intracellular localisation of the two G2 analogues namely G2 and G2-Asp was analysed by confocal microscopy using dual staining techniques. Only G2 and G2-Asp were included in this study because these photosensitisers have fluorescence intensities high enough for live cell imaging. Co-staining images of the photosensitisers with organelle-specific probes namely Rh123 (for mitochondria), Lyso-tracker (for lysosome) and ER-tracker (for endoplasmic reticulum) were photographed and their localisation topographic profiles were compared (Figure 3.6).

In our study, the lipophilic G2 was shown to localise predominantly in the endoplasmic reticulum while only colocalised partially in the endoplasmic reticulum and lysosomes. Meanwhile, the localisation of hydrophilic photosensitiser especially G2-Asp shifted to the lysosomes. No staining of the nucleus or plasma membrane was observed for both G2 and G2-Asp. Similar preferential for lysosomes localisation was also reported for chlorin-e6 with aspartyl conjugation at the similar carbon-position (Roberts et al. 1988). The explanation for the observed subcellular localization may be attributed to the lipophilicity and the anionicity of the compounds. Photosensitisers which are more lipophilic (e.g. G2) tend to accumulate in cellular compartment with high lipid bilayer content such as mitochondria and endoplasmic reticulum where PDT-induced damage to these organelles is likely to amplify cell toxicity. In contrast, anionic photosensitisers such as G2-Asp may be too polar to diffuse across the plasma membrane are instead taken up by cell lysosomes through endocytosis. As lysosomes are less sensitive organelles than the mitochondrial, this might explain our observation on the better *in vitro* PDT activity of G2 compared to G2-Asp.

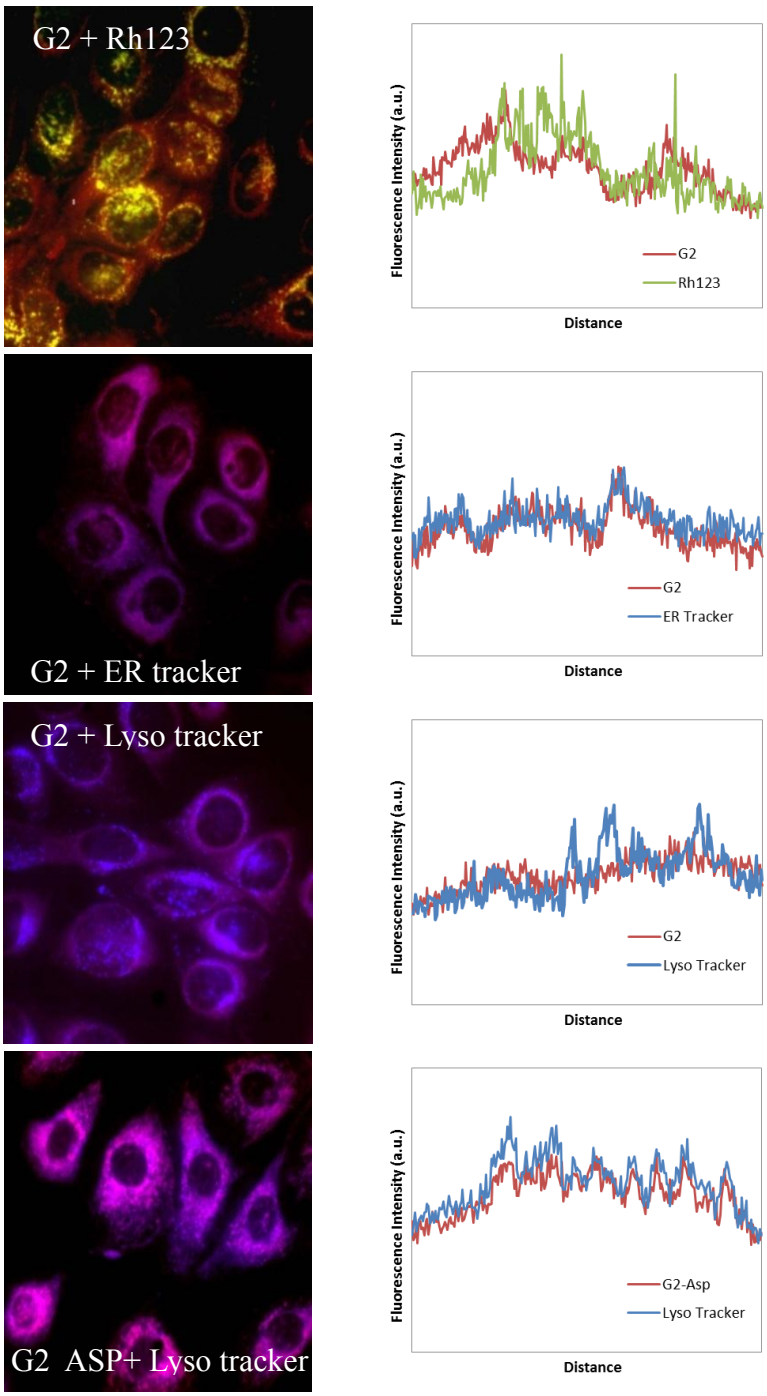

Figure 3.6 Intracellular localisation of G2 and G2-Asp in HSC2 cells. Spinning disk confocal fluorescence images and their respective fluorescence topographic profiles of HSC2 cells double-stained with 100 nM of G2/G2-Asp and organelle probes. Mitochondria were labeled with 100 nM of Rh123 and excited at 494 nm. Endoplasmic reticulum were labeled with 100 nM ER-Tracker and excited at 365 nm. Lysosomes were labeled with 500 nM of LysoTracker and excited at 365 nm. Both G2 and G2-Asp was excited at 420 nm. Topographic profiles revealed that **G2** localised predominantly in the endoplasmic reticulum, while G2-Asp localised in the lysosomes. Objective magnification × 60.

3.3.8 PDT-induced Vascular Occlusion

One method to evaluate the PDT efficacy of a photosensitiser is by determining the ability of the agent to induce vasculature occlusion. Only G2 or G2-Asp were selected to be evaluated for their vascular occlusion efficiency in CAM model given their better *in vitro* potency. In Figure 3.7, G2 at 6 nmol/embryo was shown to induce closure of vessels < 30 μm in diameter with an average occlusion score of 2.5 when irradiated with a light dose of 20 J/cm^2. At similar drug and light doses, G2-Asp only induced partial closures of capillaries of diameter below 10 μm with a damage score of 1. When the light dose was increased to 40 J/cm^2, G2 at 6 nmol/embryo was able to induce complete closure of vessels with diameter < 30 μm with an occlusion score of 3.3, while G2-Asp induced an occlusion score of 4,0 with total occlusion of vasculature observed for vessels with diameter < 70 μm. Meanwhile, the control eggs that received 20 μl of vehicle (2.5% CrEL, 2.5% EtOH in saline) and exposed to similar light dose showed no detectable vascular alteration in the treated area. This indicated that the vascular occlusion observed in embryos treated with G2 or G2-Asp was neither caused by the vehicle components nor was it a result of heat generated by the light irradiation.

CAM is a viable model that has been successfully used to evaluate the PDT-induced vascular occlusion efficacy of photosensitisers, some of which are currently in clinical trials or are already clinically approved (Hammer-Wilson *et al.*, 2002). Data from the study showed that both G2 and G2-Asp were able to occlude CAM blood vessels following PDT, with G2-Asp achieving similar photodamage (p>0.05) compared to G2 when higher light dose was used. This observation could be due to the longer circulating half-life of the more hydrophilic G2-Asp compare to G2 because lipophilic photosensitiser tend to leak out of the circulatory system faster. As the irradiation time to achieve 40 J/cm^2 is twice longer than 20 J/cm^2 at a fixed fluence of 130 W/cm^2, there may be lesser circulating G2 by the later stage of the irradiation.

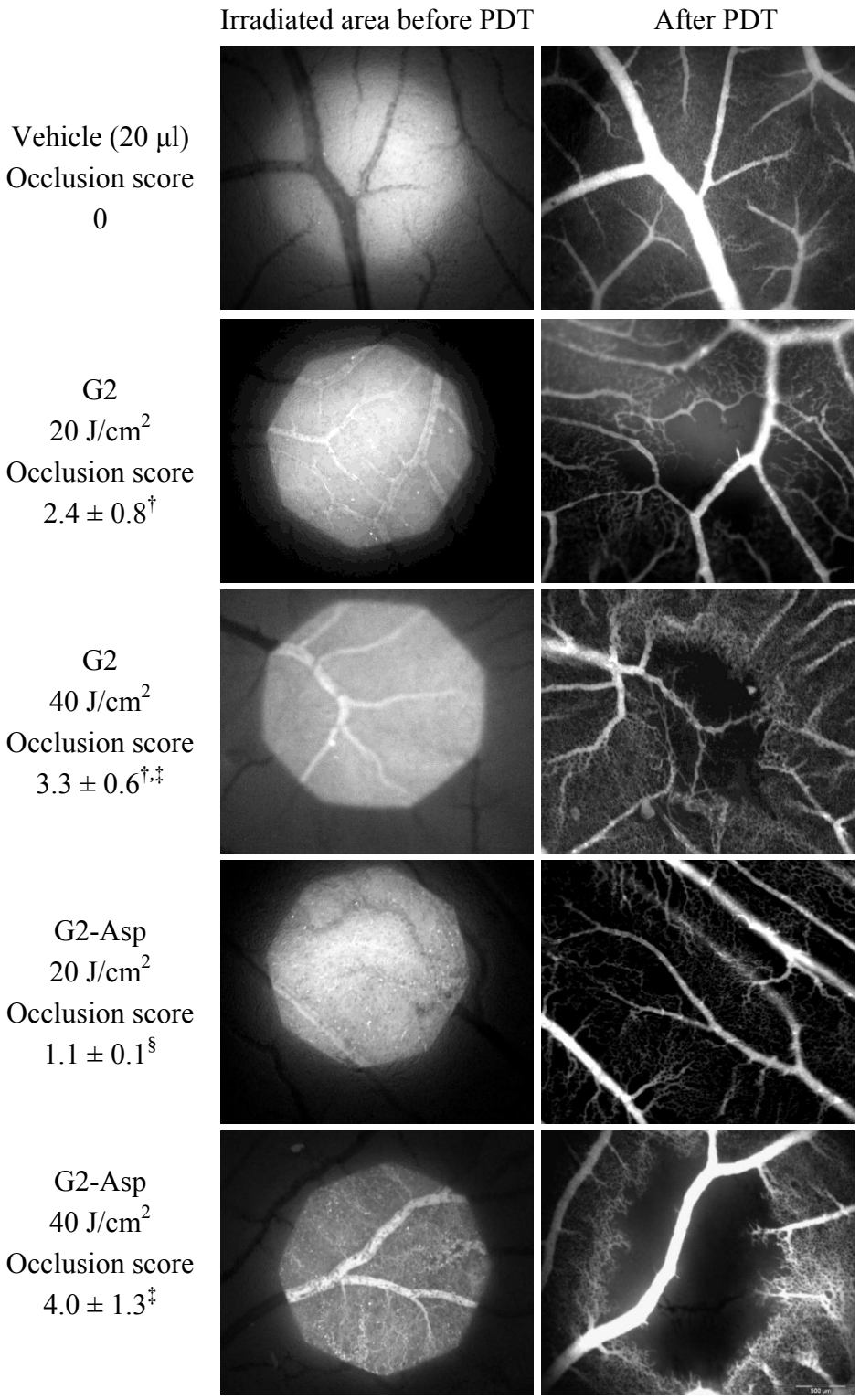

Figure 3.7 Representative angiographies of CAM vasculature before and 24 h after PDT, illustrating the vascular occlusion efficacy induced by G2 and G2-Asp at 6 nmol/embryo. Irradiation was performed at 400-440 nm of excitation wavelength with 20-40 J/cm^2 of light dose. Occlusion score represents mean values from at least ten embryos. Score with different symbols are significantly difference from each other (p<0.05). Objective magnification ×4.

3.3.9 PDT-mediated Tumour Response *In Vivo*

A dose finding experiment was first conducted to determine the potential therapeutic and tolerable dose levels using the typical two mice per dose level with a doubling dose increase or dose-halving decrease design (Workman et al. 2010). BALB/c mice implanted with 4T1 tumour were administered with 15 mg/kg of G2 or G2-Asp and PDT was performed with at fluence of 100 or 200 J/cm^2 at drug-light intervals of 1 h and 24 h respectively. Observations were summarised in Table 3.4 where each treatment group consisted of two mice. Both mice in the group that received PDT with 200 J/cm^2 of light 1 hr following drug dosing resulted in functional loss of the lower limb close to the irradiation site, which is an unacceptable adverse effect. In contrast, no clear evidence of PDT-induced antitumour response was detected for mice in the group with 24 h drug-light interval when irradiated with 200 J/cm^2 of light. Subsequently, the light dose was reduced to 100 J/cm^2 with the drug-light interval of 1 h and the treated mice presented evidence of antitumour response with the observation of tumour cyanosis within 24 h after PDT. This was followed by the typical development of inflammation and eschars within day 2-3 (Figure 3.8).

Table 3.4 Effects of different route of administration, light dose and drug-light interval on the PDT efficacy and toxicity of G2 on 4T1 murine tumour implanted BALB/c mice.

Route	G2 Dose (mg/kg)	Light dose (J/cm^2)	Drug-light interval (h)	Observable PDT effect	Toxicity
Intraperitoneal	15	100	20	No	No
Intraperitoneal	15	200	20	No	No
Intravenous	15	200	20	No	No
Intravenous	15	200	20	No	No
Intravenous	15	200	1	Yes	Yes
Intravenous	15	100	1	Yes	No
Intravenous	15	50	1	Yes	No

Each treatment group consists of two mice.

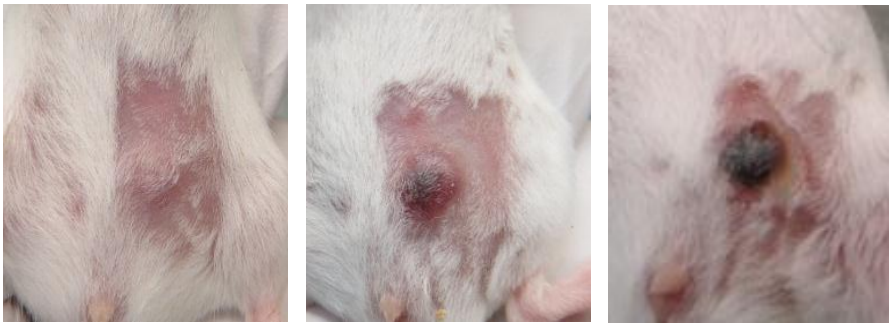

Pre-treatment 24 h post-PDT 72 h post-PDT

Figure 3.8 Photographs of 4T1 syngeneic murine tumour implanted at the inguinal mammary fat-pad of BALB/c mice before, 24 h and 72 h after PDT (15 mg/kg of G2 + 100 J/cm^2 light). Evidence of antitumour response was observed with the development of tumour cyanosis within 24 h after PDT and followed by the typical development of inflammation and eschars within day 2-3.

In our tumour model, both G2 and G2-Asp at a dose of 15 mg/kg are effective to inhibit the growth of 4T1 when the mice were irradiated with 100 J/cm^2 of light 1 h post drug injection (Figure 3.9). At the end of 14-days observation period, the tumour growth in mice receiving G2 + 100 J/cm^2 and G2-Asp + 100 J/cm^2 was inhibited with % T/C of 41% (p<0.05) and 43%% (p<0.05), respectively compared to the vehicle control group. There were no statistically significant differences in tumour growth between the two treatment groups. However, complete tumour regression was observed in two out of eight mice receiving 15 mg/kg G2-Asp + 100 J/cm^2 of light but not in the G2 + 100 J/cm^2 group. No tumour growth inhibition was observed in animals receiving 15 mg/kg of G2 or G2-Asp only.

There was no treatment-related toxicity or significant loss of animal body weight observed in all treatment groups exposed to 100 J/cm^2 of light 1 h post drug injection. Tumour growth was only monitored for two weeks before the experiments were terminated given the high risk of tumour metastasis of 4T1 tumours grown in mammary fat pad of Balb/C mice. A previous study conducted using the same murine tumor

model has shown that no metastasis was detected up to 18 days following tumour cell inoculation (Wenzel et al. 2010).

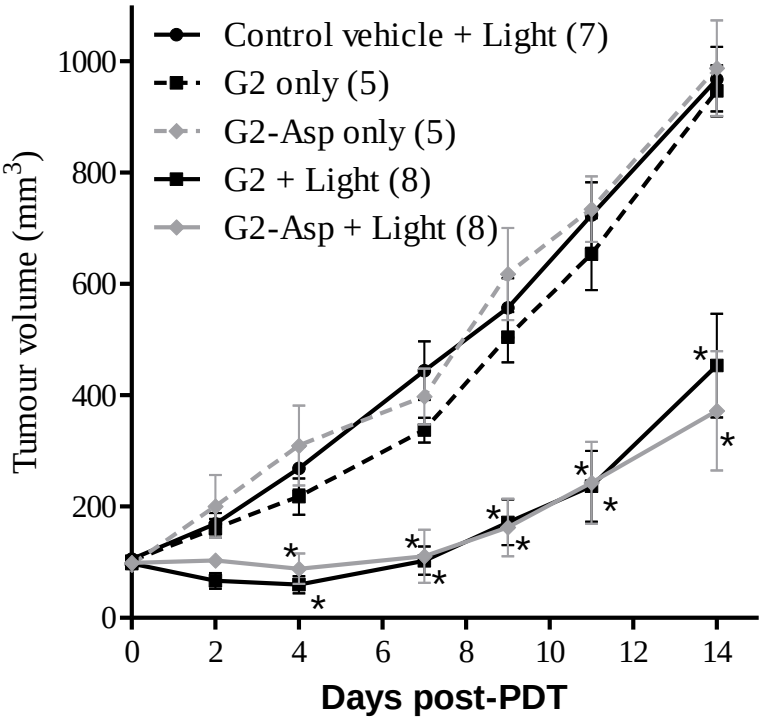

Figure 3.9 Effects of G2 and G2-Asp on tumour growth of 4T1 *in vivo*. Treatment was initiated when tumours reach volume of ~ 100 mm^3. For PDT, tumour site was irradiation 1 h after drug dosing with 665/32 bandpass filtered light with a light dose of 100 J/cm^2 and at a fluence rate of 130 mW/cm^2. At day 14, the tumour growth in mice receiving G2 + 100 J/cm^2 and G2-Asp + 100 J/cm^2 was inhibited with % T/C of 41% and 43%, respectively compared to the vehicle control group. Mixture of 10% CrEL, 10% EtOH in saline was used as dosing vehicle and number in parenthesis indicates number of mice in each treatment group. * Statistically significant differences compared to control group at each time point with $p<0.05$.

Data from the study indicates that G2 and G2-Asp showed similar effectiveness in inhibiting tumour growth although the former is two-fold more potent *in vitro*. A possible explanation for this observation is that other than direct cell-killing which may

dominate in the G2 treated mice, the observed tumour shrinkage was probably also caused by shutting down of blood vessel supplying the tumour which would be more prominent in the hydrophilic G2-Asp.

3.4 Conclusion

From the study, conjugation of tetrapyrrole with hydrophilic amino acids was able to alter their photosensitising potencies and efficacies by modifying multiple parameters, including absorption coefficient, singlet oxygen quantum yield, cellular uptake and intracellular localisation. However, these conjugates (i.e G2-Asp and G2-Lys) exhibited a reduced *in vitro* PDT potency. Further evaluation showed that G2-Asp was able to achieve similar potency in inducing vasculature occlusion of the CAM and in inhibiting tumour growth in a syngeneic mouse model compared to G2. In conclusion, the conjugated G2-Asp is a promising candidate to develop as a PDT agent because it has more ideal photophysical properties such absorption maxima at far-red wavelength (675 nm) and molar extinction coefficient and its ability to inhibit tumour growth in the preclinical mouse model. Given the hydrophilic nature of G2-Asp, the photosensitiser is a pharmaceutically advantageous candidate as it can be formulated easily for administration thereby reducing the risk of vascular aggregation.

CHAPTER 4

Evaluation of Boron Difluoride Dipyrromethene (BODIPY) as Photosensitiser for Photodynamic Therapy

4.1 Introduction

Boron difluoride dipyrromethene (BODIPY) chromophore is an alternative class of non-tetrapyrrole photosensitisers that has recently emerged. BODIPYs have many characteristics of an ideal photosensitiser including high extinction coefficients, relative insensitivity to environment and resistance to photobleaching. However, unconjugated BODIPYs also have high quantum efficiencies of fluorescence. Since fluorescence occurs through relaxation from singlet excited states, high quantum yields for fluorescence are undesirable since this means that much of the energy absorbed on excitation does not cross to the much desirable triplet states for singlet oxygen generation. Consequently, BODIPYs for PDT have to be modified to depress fluorescence and enhance singlet-to-triplet intersystem crossing. Such modifications include attachment of electron donating groups such as akyl, phenyl and distyryl as well as heavy-atom like bromine and iodine at the periphery of the BODIPY in order to optimise their photophysical and therapeutic properties (Gorman et al. 2004; Yogo et al. 2005; Atilgan et al. 2006).

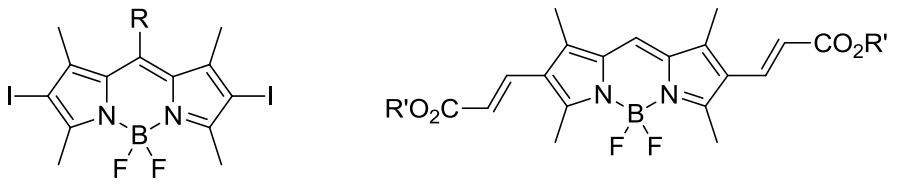

Structural variation 1 Structural variation 2

Figure 4.1 Structure variations of BODIPY evaluated.

This study investigates the effects of two structural variations of BODIPY (Figure 4.1) on their photocytotoxicity in terms of photophysical properties, *in vitro* and *in vivo* efficacies. In the first variation, functionalisations such as *meso*-substitution as well as sulphonation to improve hydrophilicity were tested to fine-tune the activity of iodinated BODIPY-based structures such as **B6** (see Figure 4.2). As photosensitisers that absorb in the longer wavelengths may be activated deeper in the tissues and may therefore be clinically favoured, a second variation consisting of compounds with extended conjugation at the 4-pyrollic position, which is a structural variation that has not been studied prior to this, were included in this study. First, the PDT efficacy of these BODIPY-based photosensitisers on a panel of leukemia and solid tumour cell lines, with particular attention on their structure-activity relationship was evaluated. The most active derivative was further investigated for intracellular localisation, cell cycle arrest and onset of apoptosis experiments, as well as in a preclinical model using the chick chorioallantoic membrane (CAM) for PDT efficacy in terms of vascular occlusion. Compound **B6** which has been shown to be a highly efficient and photostable photosensitiser (Yogo et al. 2005) was used as positive control.

The BODIPYs evaluated in this study were provided by Prof Kevin Burgess's group from the Department of Chemistry, Texas A&M University, Texas, USA. BODIPY series with structural variation 1 can be prepared with ease (Scheme 1) by condensation of acyl chlorides with pyrroles. The resulted dipyrromethene hydrochloride salt intermediates were then reacted with boron trifluride etherate in the presence of triethylamine to yield the desired BODIPY structures. BODIPYs with structural variation 2 were prepared by direct conjugation of electron withdrawing groups (EWG) at the pyrrroles through palladium mediated C-H functionalisation (Scheme 2) (Loudet and Burgess 2007). The preparation of BODIPY series is feasible given the easy access to various substituted pyrroles commercially.

Scheme 1

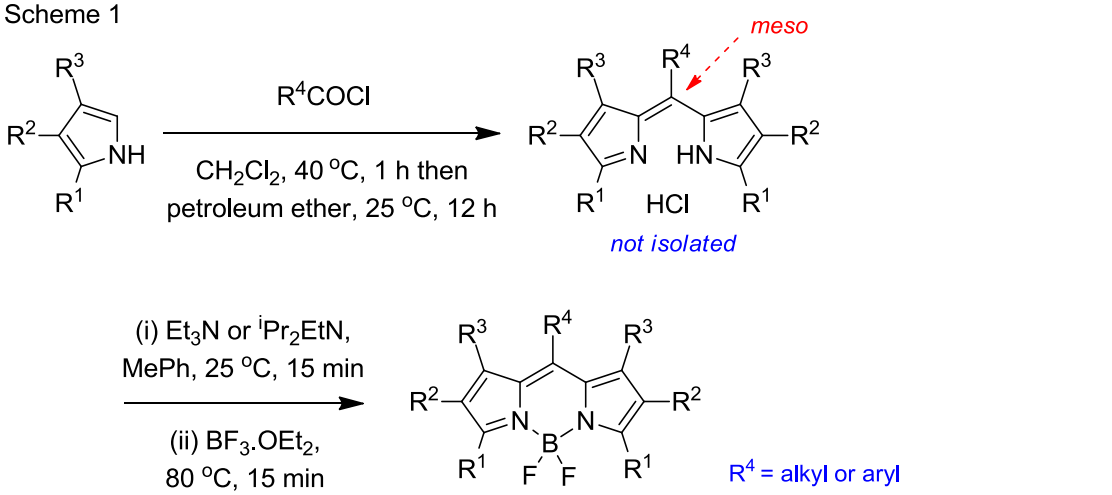

Scheme 2

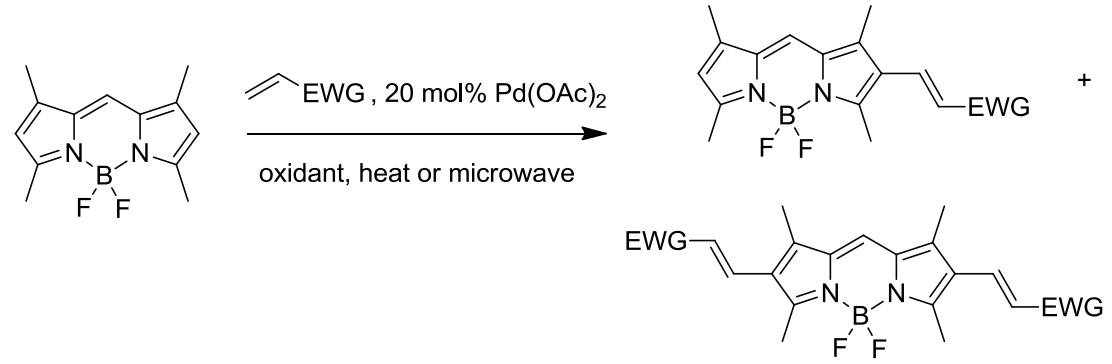

4.2 Materials and Methods

4.2.1 Materials

4.2.1.1 Chemicals and Reagents

SYTOX Green was purchased from Molecular Probes, Invitrogen (OR, USA). Methylene blue and ribonuclease A (RNase A) were purchased from Sigma (MO, USA). Annexin V-FITC Apoptosis Detection Kit 1 was purchased from BD Biosciences (CA, USA). Other chemicals and reagents used were as described in Section 3.2.1.1.

4.2.1.2 Instrumentations

Flow cytometry analyses were performed using FACSCalibur flow cytometer with 488 nm argon laser (Becton Dickinson, CA, USA) and data were acquired on CellQuest software. Other equipment used were as described in Section 3.2.1.2.

4.2.2 Preparation of Compounds

A total of fifteen BODIPYs used in this study were prepared and supplied by Prof Kevin Burgess's group from the Department of Chemistry, Texas A&M University, Texas, USA. Their syntheses, purification and NMR characterisation were previously described by Loudet and Burgess (2007); Li et al. (2008); and Wu and Burgess (2008a). All the compounds used for *in vitro* experiments were dissolved in DMSO to make stock solutions of 10 mM, aliquoted into appropriate volume and stored at -20 ºC prior to use.

4.2.3 Photophysical Properties

Absorbance spectra were obtained on a Varian 100 Bio UV-Vis spectrophotometer at room temperature. Extinction coefficients were determined from Beer's Law plots using three data points.

4.2.4 Cell Culture and Photo-induced Cytotoxicity Assay

HL-60, HSC2 and HK1 cell lines were used to evaluate the photocytotoxicity of BODIPY *in vitro*. HL-60 human promyelocytic leukemia cells were obtained from American Type Culture Collection (VA, USA) and maintained in RPMI 1640 medium supplemented with 10% heat inactivated FBS and 1% of penicillin-streptomycin. A

confluent HL-60 culture was subcultured by transferring an aliquot of 0.5 ml cells to a new 25 cm^2 tissue culture flask containing 5 ml of fresh medium. HK1 nasopharyngeal epithelial carcinoma cell line was a gift from University of Hong Kong Culture Collection (University of Hong Kong, Hong Kong) and grown in MEM medium supplemented with 10% FBS and 1% of penicillin-streptomycin. HK1 cells were maintained similarly to HSC2 (refer Section 3.2.3). The photocytotoxicity experimental procedure and conditions were similar as described in Section 3.2.4, unless specified. For HL-60 cells, approximately 15000 cells/well in a phenol-red-free culture medium containing 10% fetal bovine serum were seeded in a 96-well plate. PDT was performed with 4.1 J/cm^2 of fluence with light with a fluence rate of 6.8 mW/cm^2 for 10 min.

4.2.5 Comparative Singlet Oxygen Generation Measurements

8 ml of aerated 2-propanol containing 50 μM of DPBF and the photosensitiser (0.5 μM or 5 μM) in a 6-well plate was irradiated at 6.8 mW/cm^2 of filtered light of >510 nm wavelength with a Roscolux medium yellow no. 10 filter (Rosco, NY) at room temperature for 1 h. Aliquots of 200 μl were removed from the mixture at various fixed intervals, and the absorbance of DPBF was measured at 410 nm. Irradiation of DPBF-isopropanol solution in the absence of photosensitiser as a negative control and solution containing methylene blue as a comparative control was also carried. The singlet oxygen production rate for each photosensitiser was determined from the reduction DPBF absorbance recorded over time. in relative to methylene blue.

4.2.6 Intracellular Localisation

As described in Section 3.2.8. BODIPY were excited at 520-550 nm wavelength.

4.2.7 Annexin V-FITC Apoptosis Analysis

The event of apoptosis was determined using Annexin V-FITC Apoptosis Detection Kit 1 according to manufacturer's protocol. Briefly, cells grown in 60 mm dishes at 50% confluency were treated with test compounds. For PDT active compound, cells were irradiated with 4.1 J/cm^2 of broad spectrum light following 2 h of incubation. At various treatment intervals, floating cells in the medium were pooled together with the adherent cells after trypsinisation and were washed twice with cold phosphate buffered saline PBS). The cells were resuspended with 1× binding buffer at 1×10^6 cells/ml. A 100 µl of cell suspension was transferred to a flow cytometry tube followed by addition of 5 µl of annexin V-FITC. The cells were gently mixed and incubated for 15 min at room temperature in the dark before analysed on a flow cytometer. The fluorescence data of 1×10^4 cells were collected with the FL1 detector containing 530/30 band-pass filter to collect annexin-FITC fluorescence.

4.2.8 Cell Cycle Analysis

Cells grown in 60 mm dishes at 50% confluency were treated with test compounds. Cells were then irradiated with 4.1 J/cm^2 of broad spectrum light following 2 h of incubation. At various treatment intervals, floating cells in the medium were pooled together with the adherent cells after trypsinisation and were washed twice with cold PBS. Cells were then fixed in 70% ice-cold ethanol (v/v in PBS) overnight at 4 ºC. Following fixation, the cells were washed twice in cold PBS. The pellet was then resuspended in PBS solution containing 20 µg/ml RNase A and 1 µM SYTOX Green for and incubated for 30 min at room temperature before analysed on a flow cytometer. The DNA-SYTOX Green fluorescence of 1×10^4 cells were collected with the FL1 detector containing 530/30 band-pass filter.

4.2.9 *In Ovo* CAM Model

As described in Section 3.2.10. For exciting and detecting BODIPY, a 520-530 nm excitation filter set (U-MNG; Olympus, Japan) was used. Irradiation was performed with light dose of 20 or 40 J/cm^2 at 520-550 nm wavelength achieved at an irradiation fluence rate of 130 mW/cm^2 over a 0.02 cm^2 of irradiation area.

4.2.10 Stastical Analysis

Statistical significance was performed using one-way ANOVA followed by Bonferroni's post-hoc test (SPSS 16.0, IBM Corporation, Armonk, NY) and differences were considered significant when $p<0.05$.

4.3 Results and Discussion

4.3.1 Structural Variations and Photophysical Properties

Two structural variations around the BODIPY core of compound **B1** were investigated in this study (Figure 4.2). The first (compounds **B2**-**6**) investigated the effectiveness of various iodinated derivatives in order to maximise the 'heavy atom effect'. To fine-tune the activity of iodinated BODIPY-based structures, additional functionalisations such as *meso*-substitution with alkyl or aryl groups as well as sulphonation to improve hydrophilicity were tested. Compound **B5** contains a carboxylic acid handle and could be easily attached to other molecules later if required. For the second variation (compounds **B7**-**15**), the effect of extended conjugation at the 4-pyrollic position was examined. Extended conjugation at the 4-pyrrolic positions increases the absorption wavelength of the compounds to the red, permitting the use of longer excitation wavelength that penetrates deeper into biological tissues for effective treatment.

Table 4.1 summarises the photophysical data of compounds **B1-15**. The absorption and emission wavelengths of compounds **B1-15** range from 500 nm to 600 nm. As expected for compounds **B8-15**, extending the conjugation with an acrylate shifts the λ_{abs} to the red by 20-30 nm while attaching two acrylates red-shifts the λ_{abs} by 50-60 nm, compared to compound **B1**. The λ_{abs} values for iodinated compounds **B3**, **B5** and **B6** are also red-shifted compared to compound **B1** but not for compounds **B2** and **B4** which are aryl-iodinated at the *meso* position. In addition, all compounds have high extinction coefficients and high quantum efficiencies of fluorescence except for a few structures. Among the exceptions, compounds **B3**, **B5** and **B6** have much lower quantum efficiency of fluorescence and a correspondingly higher singlet oxygen generation rate (Table 4.2) compared to the other BODIPY's studied here, probably as a result of the enhanced intersystem crossing efficiency from the lowest singlet excited state to the triplet state contributed by the internal heavy-atom effect. As in the case of λ_{abs} values above, compounds **B2** and **B4** which contain a para-iodo-aryl group at the *meso* position did not demonstrate the same loss in fluorescence yields or the same increase in singlet oxygen generation rate as compound **B3**, **B5** and **B6** probably because the iodo-aryl group is twisted relative to the BODIPY plane (Burghart et al. 1999), overall causing the aryl iodine atom to only, at most, elicit an intramolecular external heavy-atom effect (Gorman et al. 2004).

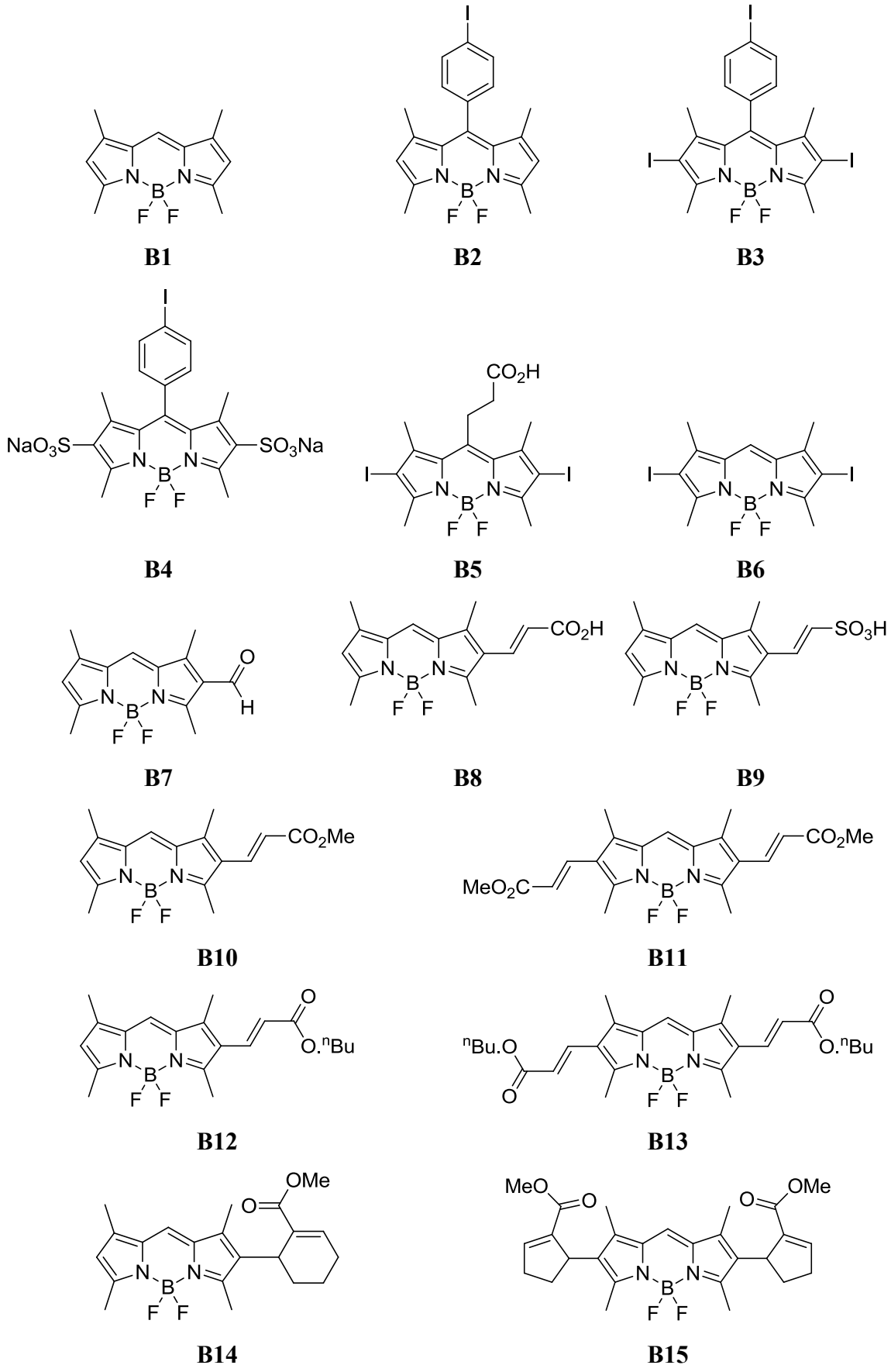

Figure 4.2 Structures of BODIPY.

Table 4.1 Photophysical properties of BODIPY derivatives

Compd.	λ_{abs} (nm)	ε ($M^{-1}cm^{-1}$)	λ_{em} (nm)	Φ_{fl} [a]	Ref. dye [b]	Solvent
B1	505	83000	516	0.80	1	EtOH
B2	504	82000	510	0.64	1	$CHCl_3$
B3	537	89000	552	0.05	2	CH_2Cl_2
B4	498	100000	509	0.34	1	H_2O
B5	525	93000	540	0.03	2	EtOH
B6	534	110000	548	0.02	1	MeOH
B7	494	81000	504	0.95	1	EtOH
B8	531	27000	570	0.42	2	EtOH
B9	529	-[c]	560	0.25	2	EtOH
B10	527	63000	549	0.73	2	EtOH
B11	559	13000	580	0.51	3	EtOH
B12	528	62000	551	0.73	2	EtOH
B13	560	30000	580	0.52	3	EtOH
B14	517	63000	527	0.78	2	EtOH
B15	530	72000	539	0.92	2	EtOH

[a] Φ_{fl} represents quantum efficiency of fluorescence.

[b] Reference dyes used for quantum yield determination (solvent, Φ_{fl}): 1. fluorescein (0.1 M NaOH, 0.92), 2. rhodamine 6G (EtOH, 0.94), 3. rhodamine B (EtOH, 0.97).

[c] Value not determined.

4.3.2 *In Vitro* Photocytotoxic and Comparative Singlet-oxygen Generation

The *in vitro* photocytotoxic activity of compounds **B1-15** against a promyelocytic leukemia cell line (HL-60), an oral squamous carcinoma cell line (HSC2) and a nasopharyngeal carcinoma cell line (HK1) following irradiation with 4.1 J/cm^2 of a broad spectrum light was determined using a modified MTT assay. Parallel assays without light irradiation were also carried out to determine cytotoxicity in the dark. Results were expressed as IC_{50} – the concentration of compound (in μM), that inhibits proliferation rate by 50% as compared to control untreated cells (Table 4.2). The parent compound, denoted as **B1**, was also prepared and tested for comparison. From the

assay, all compounds had negligible or undeterminable unirradiated cytotoxicity up 100 μM. Upon irradiation with 4.1 J/cm^2 of light, compounds **B1-6**, **B10-15** demonstrated photosensitised cytotoxicity with IC_{50} values in the sub-micromolar to tens of micromolar range. Compounds **B5** and **B6**, which had two iodine atoms directly attached to the BODIPY core showed the highest activity among the analogues, with IC_{50} values that are up to 100 times lower than that of compound **B1** (0.045 μM *vs* 4.4 μM in HL-60). In contrast, compounds **B7-9** displayed poor activity with undeterminable IC_{50} up to 100 μM.

The influence of the iodine atom on the photocytotoxic activity of the compounds was evident from studying compounds **B1-6**. *Meso*-substitution with an para-iodo aryl group in compound **B2** does not alter the photocytotoxicity significantly compared to compound **B1**, while further substitution with iodine atoms on the two pyrrolic 4-carbon to yield either compound **B3** from **B2** or compound **B6** from **B1**, improved the activity by ten-and hundred-fold respectively in all three cell lines, alluding to the importance of iodine atom substitution on the pyrrollic carbons rather than on the *meso*-aryl position. Compound **B5**, which has an additional carboxylic acid tether at the *meso* position has similar to marginally better activity than compound **6** in all three cell lines. An attempt to improve the water-solubility of compound **B2** by substituting with sodium sulphonate to yield compound **B4** resulted in ten times loss in activity.

For the effect of extended conjugation at 4-pyrrolic positions on photocytotoxic activity of BODIPYs, compounds **B7-15** were studied. Extending the 4-pyrollic carbon with a single aldehyde (**B7**) or the hydrophilic allylic carboxylic (**B8**) and allylic suphonic acid (**B9**) resulted in loss of activity to greater 100 μM IC_{50} values. Single extensions at the 4-pyrrolic position with acrylate esters affected the activity differently depending on the length of the alkyl ester group, where the methyl compound **B10**

showed no change in activity while n-butyl compound **B12** demonstrated ten-fold improvement in activity compared to compound **B1**. For compounds with double extension with the same groups at the 4-pyrollic positions, the methyl compound **B11** remained unaltered in its activity compared to compound **B1** but interestingly, the n-butyl compound **B13** showed ten-fold loss in activity compared to **B1** or hundred-fold loss compared to the singly-extended counterpart **B12**. The explanation for structure-activity relationship of the n-butyl acrylate esters compared with the methyl acrylate esters is not obvious. Compounds **B14** and **B15** which failed attempts to prepare the analogous ring-constrained conjugated structures were also tested and showed similar activities compared to compound **B1**, further indicating the minor role that 4-pyrrolic extended conjugation or the lack of it plays in modulating the photocytotoxicity of the BODIPY structures.

Subsequently, the relative rate of singlet oxygen generation was measured for compounds **B1**-**15** by monitoring the reaction of known singlet oxygen acceptor DPBF with photosensitisers generated singlet oxygen . This was achieved by following the loss of DPBF absorbance at 410 nm at initial concentration of 50 μM over a time period of 1 h. A light source filtered at 510 nm wavelength was used to minimise the photobleaching of DPBF. As a result, this would have caused an under-estimation of singlet oxygen generation rate of the compounds with λ_{abs} lower than 510 nm as the light transmission through the filter begins to drop below 510 nm. Each of the compounds was tested at an equivalent concentration of reference sensitiser methylene blue. The results from this study ranged from 0.01- to over 24-fold of singlet oxygen generation rate compared to that of methylene blue. Importantly, the rate of reactive oxygen generation measured generally correlated to the potency of these compounds and may then be the main factor affecting the photocytotoxicity of these BODIPY compounds.

Table 4.2 Comparative singlet oxygen generation and i*n vitro* photo cytotoxicity induced by BODIPY

BODIPY	Φ_Δ [a]	Activity IC_{50} (μM) [b]					
		HL-60		HSC2		HK1	
		0 J/cm^2	9.6 J/cm^2	0 J/cm^2	9.6 J/cm^2	0 J/cm^2	9.6 J/cm^2
B1	0.48	>100	4.4±0.4	>100	8.7±2.0	76.8±10.6	6.2±1.2
B2	0.15	>100	2.7±1.2	>100	5.1±0.8	>100	5.7±0.1
B3	13.9	10	0.42±0.06	10	0.5±0.1	95.5±7.9	0.69±0.08
B4	0.07	>100	54±8	>100	59±6	>100	59.0±7.1
B5	24.6	>100	0.045±0.004	>100	0.10±0.06	55.8±0.8	0.57±0.1
B6	23.9	>100	0.062±0.011	>100	0.64±0.06	>100	0.57±0.06
B7	0.07	>100	>100	>100	>100	>100	>100
B8	0.01	>100	>100	>100	>100	>100	>100
B9	0.00	>100	>100	>100	>100	>100	>100
B10	0.57	>100	4.8±0.7	>100	5.4±0.6	>100	5.3±0.6
B11	0.41	>100	5.2±0.6	>100	11.1±7.4	>100	8.5±0.5
B12	0.73	>100	0.49±0.07	>100	0.6±0.1	99.6±0.6	1.1±0.6
B13	0.17	>100	58±7	>100	38±16	>100	>100
B14	0.24	>100	4.9±0.6	>100	4.1±0.2	>100	5.0±0.6
B15	0.29	>100	3.8±0.7	-	-	>100	4.8±0.9

[a] Φ_Δ - Comparative singlet oxygen generation rate of photosensitisers in relative to methylene blue.

[b] IC_{50}, the concentration of compound, which inhibits the proliferation rate by 50% as compared with control untreated cells. Values represent the mean ± SD of three determinations assessed 24 h using standard MTT assay. Cells were incubated with compound for 2 h prior to irradiation with 9.6 J/cm^2.

4.3.3 Photosensitiser Cellular Localisation

To ascertain the intracellular localisation of the BODIPYs, compound **B5**, owing to its good potency data, were chosen and examined by spinning disk confocal microscopy using dual staining techniques. Co-staining images and topographic profiles of HSC2 cell line loaded with compound **B5** and a mitochondria-specific dye Rh123 revealed an

almost identical overlap, suggesting that compound **B5** localised particularly well in mitochondria (Figure 4.3 A and B). In comparison, compound **B5** displayed only partial co-localisation with endoplasmic reticulum and lysosomes, according to the confocal images and topographic profiles of compound **B5** with ER-Tracker (Figure 4.3 C and D) and with LysoTracker (Figure 4.3 E and F) respectively. Staining of the cytoplasmic or nuclear membrane by compound **B5** was not detected, indicating that it does not react non-specifically with biological membranes. Furthermore, the nucleus remained free of compound **B5** (dark nuclear area) signifying that this class of compounds would not be expected to directly damage DNA.

Mitochondria perform vital cellular functions and are involved in multiple signaling cascades in regulation of metabolism, cell cycle control development and cell death (McBride et al. 2006). In PDT, the mitochondrion is an important target. During mitochondria-photosensitisation in PDT, cytochrome c is released from mitochondria to directly affect rapid cell death through downstream effector pathways of apoptosis, bypassing other upstream apoptotic signaling pathways that require synthesis of new proteins. This mechanism of action is particularly useful in the treatment of cancer types which are chemo-resistant due to mutations in upstream pro-apoptotic signaling pathways (Morgan and Oseroff 2001).

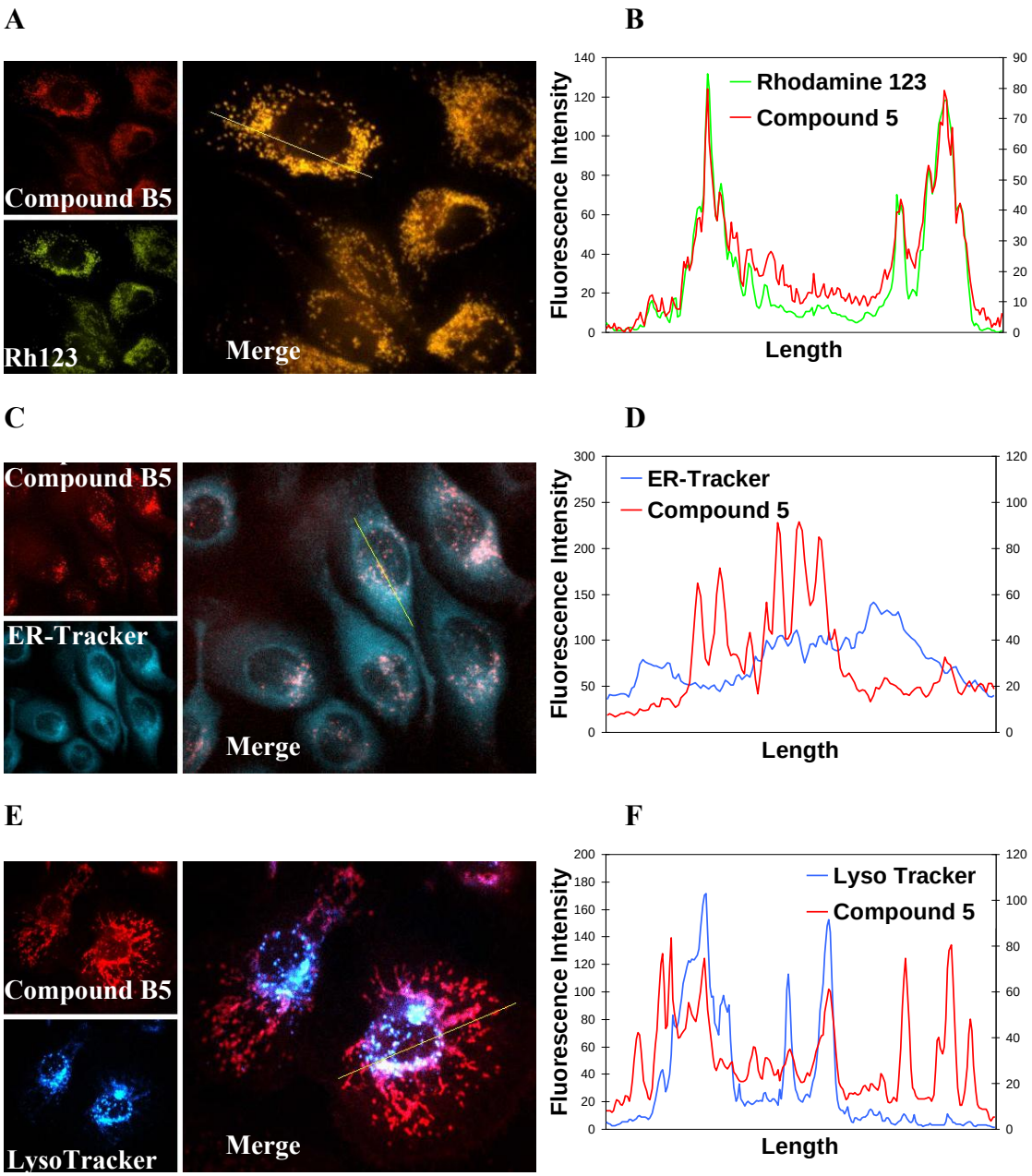

Figure 4.3 Intracellular localisation of **B5** in HSC2 cells. Spinning disk confocal images (**A**, **C**, **E**) and fluorescence topographic profiles (**B**, **D**, **F**) of HSC2 cells double-stained with 100 nM of compound **B5** and respective organelle probes. (**A**, **B**) Mitochondria were labeled with 100 nM of Rh123 and excited at 494 nm. (**C**, **D**) Endoplasmic reticulum were labeled with 100 nM ER-Tracker and excited at 365 nm. (**E**, **F**) Lysosomes were labeled with 500 nM of LysoTracker and excited at 365 nm. Compound **B5** was excited at 575 nm. From the fluorescence profiles, **B5** localised almost exclusively in the mitochondria and partially in the endoplasmic reticulum and lysosomes. Line indicates the longitudinal transcellular axis analysed to generate the topography fluorescence profiles. Objective magnification × 60.

4.3.4 Cell Cycle Arrest and Apoptosis

To study the mechanism of action of compound **B5** that contributed to its photocytoxicity, the effect of compound **B5** on cell cycle and apoptosis of HSC2 cell line were investigated using flow cytometric method. The cell cycle profile of HSC2 cells treated with compound **B5** was analysed in a time course experiment. At the concentration of 0.25 μM, compound **B5** was found to induce G_2/M arrest in HSC2 cells as early as 2 h following light irradiation (Figure 4.4). HSC2 cells in G_2/M phase gradually increased significantly (p<0.05) from 26.1% in the control group to 39.8%, 48.4%, 55.5%, respectively, at 2, 4 and 6 h after light irradiation. Concomitant with the increased of G_2/M phase cells proportion, HSC2 cell in G_1 phase reduced significantly (p<0.05) from 57.7% to 46.3%, 33.8% and 26.4%, while the proportion of HSC2 cells in S phase remained fairly constant. At 8 and 12 h, the proportion of cells arresting in G_2/M phase was reduced to 48.8% and 26.0%, respectively after light irradiation. Following the reduction of proportion of cells arresting in G_2/M phase, an increase of sub-G_1 cells population from 8 h to 12 h (4.4% (p>0.05) to 10.6% (p<0.05)) was observed. The cells proportion treated with compound **B5** without irradiation remains unchanged compared to control.

In the present study, the maximal level of G_2/M cell-cycle arrest was observed at 6 h after PDT. Thereafter the recovery of the cell cycle profile to one with a reduced G_2/M peak may be due to the redistribution of cells to sub-G_1, indicating the onset of apoptosis of arrested cells. A similar G_2/M arrest was also observed in hypericin-based PDT, a naturally occurring photosensitiser currently undergoing research (Vantieghem et al. 2002; Lee et al. 2006). Photosensitisation of HeLa cervical cancer cells with hypericin resulted in phosphorylation of mitochondria Bcl-2 that correlated with G_2/M cell cycle arrest, followed by the onset of apoptosis (Vantieghem et al. 2002).

A

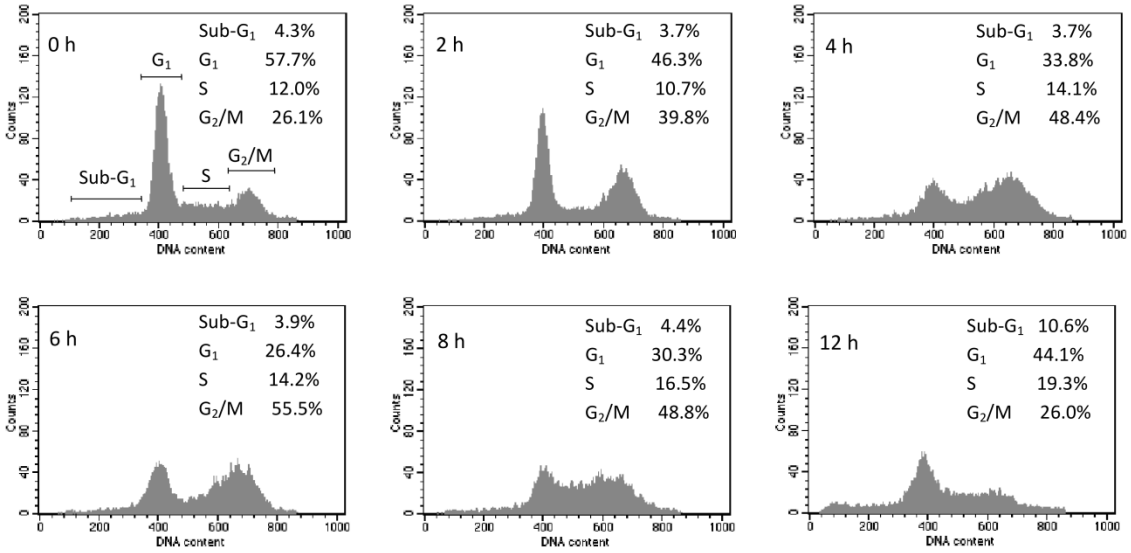

B

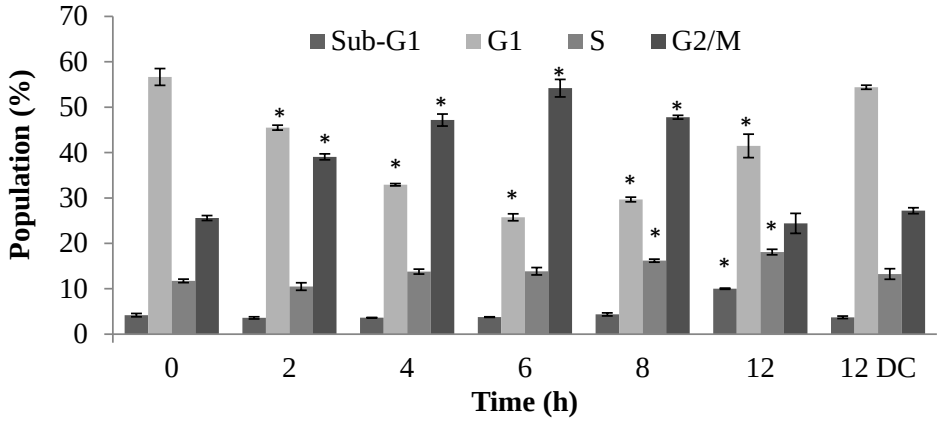

Figure 4.4 Cell cycle arrest induced by **B5. A)** A representative histograms of event of HSC2 cell cycle phase at various intervals post-irradiation analysed using flow cytometry after treatment with 0.25 µM of compound **B5** and irradiated with a light dose of 9.6 J/cm^2. **B**) Mean percentage of proportion of cell population in pre-G1, G_1, S and G_2/M phases, an increased of cell population arrested in G_2/M phase cell cycle was observed from 2-6 h following light irradiation. Thereafter, from 8-12 h the G_2/M population decreased with a redistribution of cells to sub-G_1 phase. *Difference with p<0.05 compared to 0 h control at each cell cycle phase.

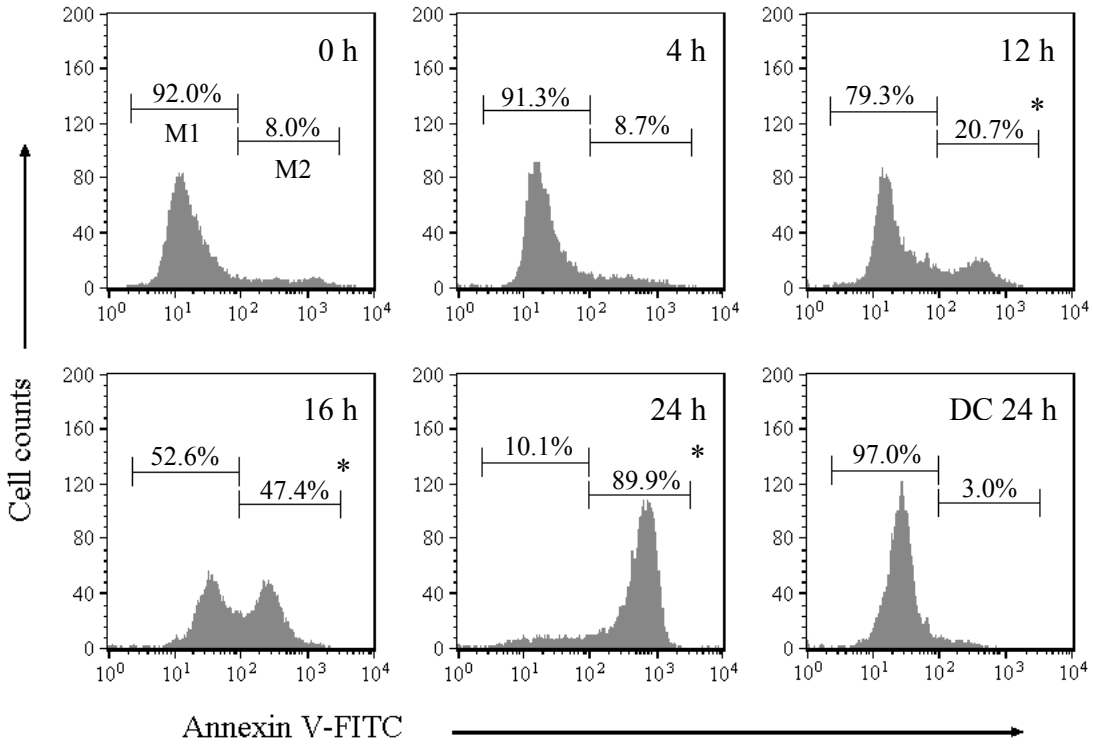

Figure 4.5 Apoptotic cell death induced by **B5.** Representative histograms of the event of annexin V- fluorescein isothiocyanate (FITC) binding to phosphatidylserine as an indicator of apoptosis in HSC2 cells treated with 0.5 μM of compound **B5** and irradiated with a light dose of 9.6 J/cm^2. Onset of apoptosis was observed at 12 h following PDT. M1 represents viable cell population, M2 represents apoptotic cell population and DC represents unirradiated dark control. *Difference with $p<0.05$ compared to 0 h control .

In addition to cell cycle analysis, the onset of apoptosis was also quantified in flow cytometry experiments by measuring the externalisation of membrane phosphatidylserine through annexin V-FITC staining, an event which is considered characteristic of cells undergoing apoptosis (Figure 4.5). Flow cytometric analysis of HSC2 cells treated with 0.5 μM of compound **B5** showed the onset of apoptosis by 12 h following irradiation with 20.7% of the cells stained positive for annexin V compared to less than 10% at 0 h or 4 h time-points ($p<0.05$). The proportion of cells undergoing apoptosis continued to increase rapidly to 47.4% by 16 h ($p<0.05$) and at 24 h the apoptotic cell proportion was at 89.9% ($p<0.05$). The induction of apoptotic cell death

by BODIPY was probably due to their mitochondria localisation characteristic. This is consistent with other photosensitisers which localised in the mitochondria, where photosensitisation of the organelle induces permeabilisation of mitochondrial outer membrane that subsequently leads to prominent increase apoptotic cell population (Agarwal et al. 1991; Kim et al. 1999; Usuda et al. 2003; Kessel and Reiners 2007).

4.3.5 PDT-induced Vascular Occlusion

One of the ways PDT causes damage during cancer treatment is by shutdown of blood vessels feeding the tumour (Chen et al. 2006a). Hence, the ability of compound **B5** to exert vasculature disruption was investigated using *in ovo* chick embryo chorioallantoic membrane (CAM) as a model. In the present study, the ability of compound **B5** to induce occlusion of blood vessels in the CAM by PDT was performed at 2-4 μg/embryo with a light dose of 20-40 J/cm^2. The degree of vascular occlusion was scored 24 h after treatment according to Table 3.1. The score for photosensitiser-mediated PDT-induced vascular occlusion is shown in Figure 4.6 and the angiograms representing the vascular occlusion score are shown in Figure 4.7. As expected, the degree of vascular occlusion increased with drug and light dose. The average CAM vasculature damage score when irradiated at 20 J/cm^2 on embryos treated with 2 and 4 μg/embryo of compound **B5** were at approximately 2 and 3 respectively. When the light dose increased to 40 J/cm^2, the damage score increased accordingly to 3.5 and 5. Meanwhile, the control eggs that received 20 μl of vehicle (CrEL 2.5%, EtOH 2.5% in saline) and exposed to a similar light dose showed no detectable vascular alteration in the treated area. This indicated that the vascular occlusion observed in embryos treated with compound **B5** was neither caused by the vehicle components nor was it thermally-

induced. On the other hand, treatment with compound **B5** alone without irradiation did not induce any vascular occlusion as non-irradiated areas remained perfused after 24 h.

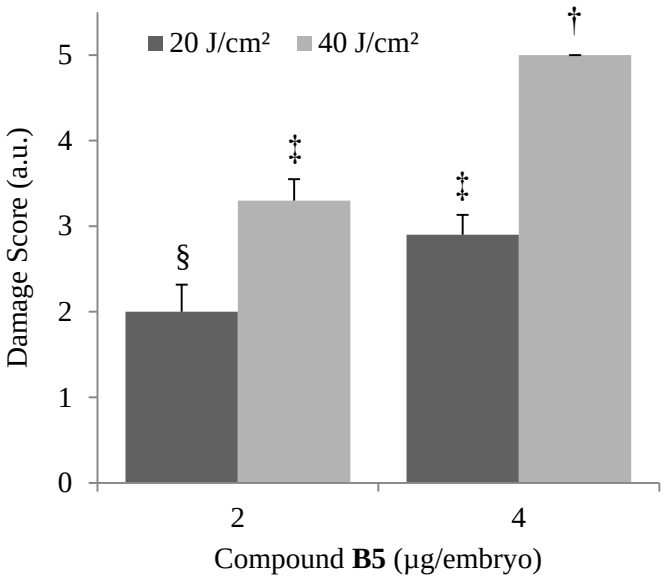

Figure 4.6 Effects of drug concentration and light dose on vascular occlusion efficacy of **B5** in the CAM model. The average of vasculature damage score was drug and light dose dependent, where the damage scores when irradiated at 20 J/cm^2 on embryos treated with 2 and 4 µg/embryo of **B5** were at approximately 2 and 3 respectively. When the light dose increased to 40 J/cm^2, the damage scores increased accordingly to 3.5 and 5. Occlusion score represents mean values from at least ten embryos. Damage score with different symbols are significantly different from each other (p<0.05).

In this study, **B5** was formulated in CrEL based on earlier experiences on other similar lipophilic photosensitisers. CrEL consists of a complex mixture of hydrophobic and hydrophilic molecules for effective solubilisation of lipophilic drugs, and it has been used in combination with EtOH to solubilise lipophilic antineoplastic drug such as paclitaxel (Strickley 2004) and photosensitisers such as TOOKAD, phthalocyanine- and purpurin-based photosensitisers (Kessel 1989b; Whitacre et al. 2000; Rück et al. 2005). Although the use of CrEL is associated with anaphylactic hypersensitivity reaction and

neurotoxicity in patients (Gelderblom et al. 2001), it is still accepted in early formulations for preclinical studies given its efficiency in solubilising lipophilic entities and its ease of preparation. Our earlier study also demonstrated that administration of 20 µl per embryo of 2.5% CrEL, 2.5% of EtOH in saline as a dosing excipient is well tolerated by chick embryos (Lim et al. 2010). This formulation is therefore used to deliver the photosensitiser evaluated in the present study.

CAM as the main respiratory organ of the chick embryo is a well-vascularised membrane that is suitable as a model for PDT. It is easily accessible, inexpensive and relatively easy to handle for photosensitiser administration, light irradiation, fluorescence analysis of administered photosensitiser, and microscopy examination of PDT-induced vascular damage (Lange et al. 2001; Vargas et al. 2007). CAM is a viable model which has been successfully used to evaluate the photodynamic-induced vascular occlusion efficacy of some photosensitisers that are either in clinical trials as well as those that are already clinically approved such as Tookad, Photofrin, lutetium texaphyrin, 5-aminolevulinic acid and verteporfin (Hammer-Wilson et al. 2002; Rück et al. 2005). For example, a PDT experiment in the CAM model using verteporfin at a dose that is similar to the recommended clinical dosage has been shown to cause complete occlusion of the large neovessels, an observation that correlates well with clinical setting (Lange et al. 2001). In addition, in a BALB/c mouse model where PDT treatment by verteporfin resulted in suppression of tumour growth, antivascular effects were also observed, whereby a decrease in the blood volume at the tumour site was noted (Kurohane et al. 2001; Ichikawa et al. 2004). In the PDT treatment of cancer, complete closure of larger vessels is desirable as to disrupt the delivery of oxygen and nutrients to the fast-growing tumour tissues. The results from the study demonstrated these effects can be achieved with compound **B5** at 7.0 nmol/embryo and 40 J/cm^2 of light dose.

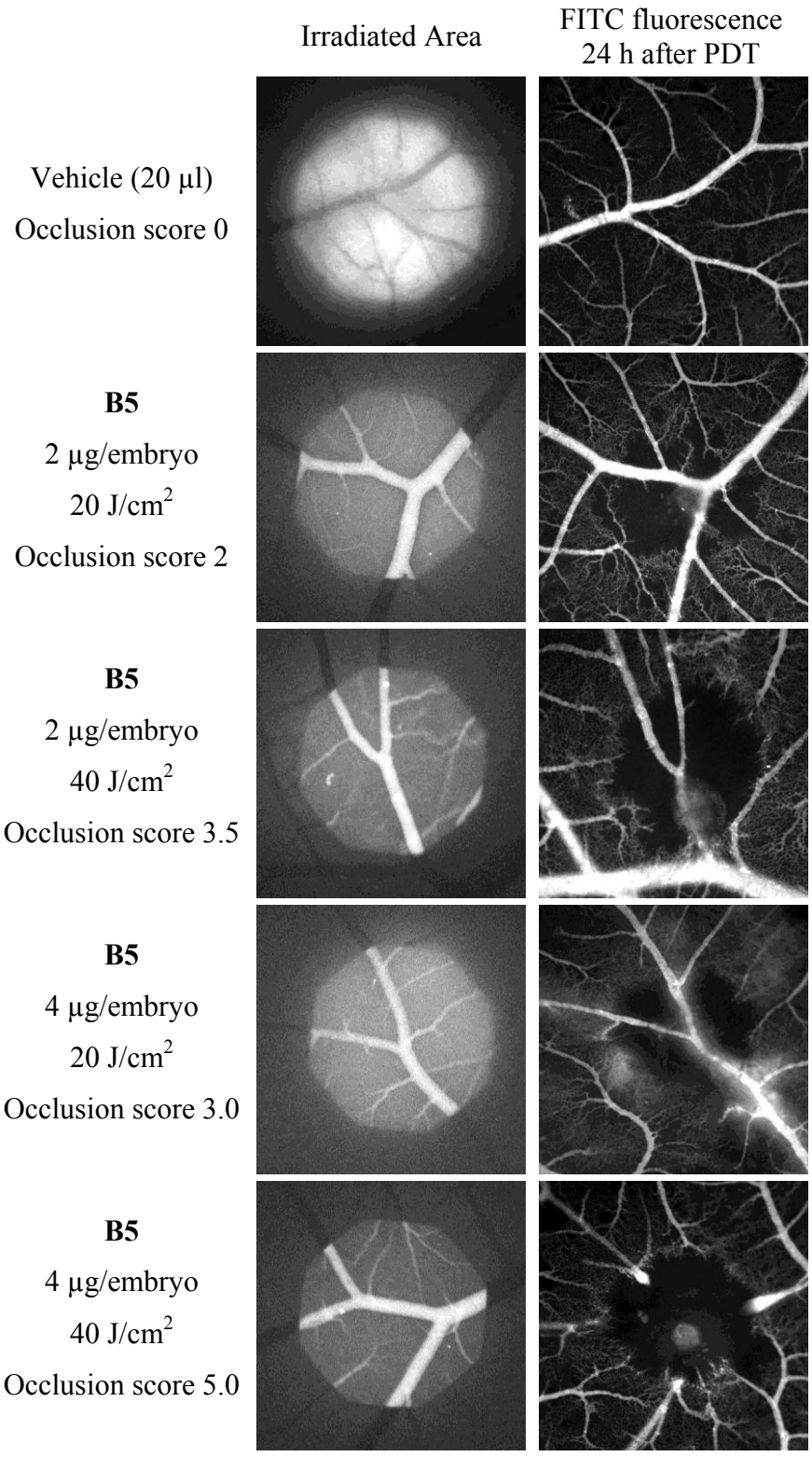

Figure 4.7 Representative angiographies of blood vessels supplying the CAM at beginning and 24 h after PDT illustrating the vascular occlusion efficacy induced by compound **B5** at 2 µg/embryo and 4 µg/embryo. Irradiation was performed at 510-560 nm of excitation with 20-40 J/cm^2 light dose. CrEL 2.5%, EtOH 2.5% in saline was used as a control vehicle. Objective magnification is ×4.

4.4 Conclusions

We have demonstrated the *in vitro* photocytotoxic activity of BODIPY derivatives against cell lines from leukemia and two types of solid tumour. Structure-activity relationship study indicated the importance of having iodine atoms directly substituted on the BODIPY pyrollic carbon-4 position rather than at the *meso*-aryl position, in accordance with the high singlet oxygen generation rate of these compounds. Extended conjugation at the 4-pyrollic positions shifts the λ_{abs} to the red but did not confer extra potency except for the compound with a single n-butyl acrylate ester (**B12**). Hydrophilic analogues substituted with groups such as carboxylic acid, sulphonic acid or sodium sulphonate generally drastically diminished the activity. An exception here was the doubly-iodinated compound **B5** with an aliphatic carboxylic acid which showed up to 100-fold lower IC_{50} value in HL-60 compared to the parent compound **B1**, perhaps due to the structural difference where the carboxylic acid group is not directly conjugated with the BODIPY core. Fluorescence microscopy studies showed that compound **B5** localised exclusively within the mitochondria. This, together with data from cell cycle analysis and onset of apoptosis studies, suggests that compound **B5** probably induced cell death through mitochondria-dependent apoptosis rather than through damage to nucleic materials. In addition, an emulsion of compound **5** was able to occlude the vasculature network in the CAM model, further showing its potential as an effective PDT agent. Overall, our results showed that BODIPY structures especially compound **B5** have potential to be explored as a clinically useful agent for PDT of cancer.

CHAPTER 5

Evaluation of Rosamines as Photosensitiser for Photodynamic Therapy and as Anticancer Agents

5.1 Introduction

Rosamines belong to the class of dyes known as delocalised lipophilic cations (DLCs). In comparison to fluorescein, both rhodamines and rosamines have their phenolic residues replaced by amino residues where this modification allows the positive charge of these structures to be permanently delocalised onto the amino nitrogen. The cationic character of these DLCs leads them to be attracted to the negatively charge mitochondrial matrix thereby allowing mitochondrial targeting (Modica-Napolitano and Aprille 2001). For example, DLCs such as Rh123 and tetramethylrosamine (TMR) are extensively used as a mitochondrion-selective fluorescence probe (Modica-Napolitano and Aprille 1987; Minamikawa et al. 1999).

Despite its mitochondrial targeting potential, TMR with its relatively short absorption wavelength λ_{abs} of 552 nm and low singlet quantum yield of 0.08 low are not an efficient photosensitiser for PDT (Detty et al. 2004). Therefore, chromophore functionalisation has been carried out to increase absorption to the red wavelength and singlet oxygen yields, for example, alkylation or halogenation to the core; substitution of oxygen with heavier chalcogen atoms; and heterocyclic substitution at *meso* position. (Pal et al. 1996; Detty et al. 2004; Holt et al. 2006; Calitree et al. 2007).

The series of rosamine evaluated in this study consists of cyclic-amine substituents and represents a new class of rosamines not reported prior to this. Like the BODIPY, the synthesis of simple rosamine analogues is relatively straightforward

(three main steps), thus facilitating compound series preparation. The starting material of xanthone ditriflate was prepared in solution by triflation of the phenols, followed by animation of the triflate with piperidine to give symmetrical cyclic-amines substitution (*Scheme 1*) or by stepwise addition of piperidine and morpholine to give unsymmetrical cyclic-amines substitution (*Scheme 2*) (Wu and Burgess 2008b). The resulted 3,6-diamino-xanthen-9-one was reacted with organolithium or Grignard reagents to yield the desired rosamine structures. These compounds were synthesised and provided by Prof Kevin Burgess's group from the Department of Chemistry, Texas A&M University, Texas, USA.

Scheme 1

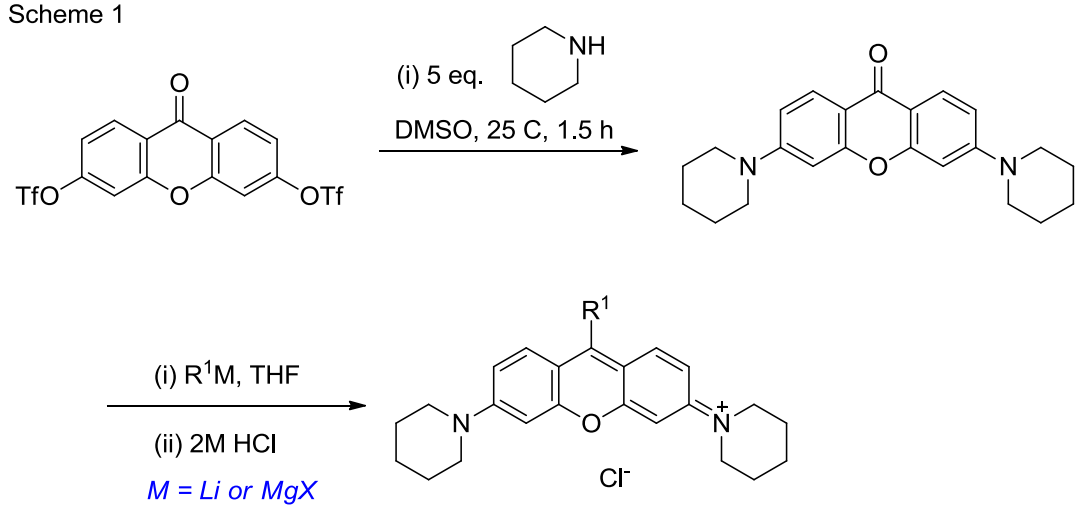

Scheme 2

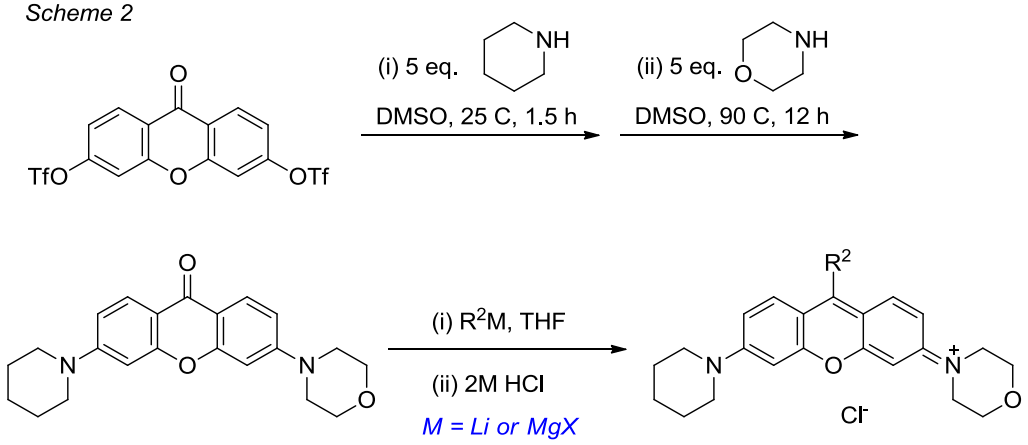

The research reported here was first undertaken to probe how substitution of rosamine with various peripheral cyclic-amines and various groups at the *meso* position

would affect their photodynamic efficiency in terms of photophysical properties and *in vitro* efficacy. However, preliminary *in vitro* data showed that the rosamines evaluated here have poor photodynamic activity but several of these derivatives displayed potent antiproliferative activity with IC_{50} values in the nanomolar range. Despite their low PDT efficacy, this class of compounds has not been further reported for its anticancer potency and given their structural novelty, we subsequently evaluated their potential utility as a mitochondrial targeting anticancer agent.

The reprogramming of energy metabolism has recently been listed as one of the emerging hallmarks of cancer and mitochondria are recognised as a potential targets for anticancer therapy (Hanahan and Weinberg 2011; Hainaut and Plymoth 2013). Mitochondria are the energy generators that maintain cell life and essential cell functions, including multiple signaling cascades that regulate cells, for instance, metabolism, cell cycle control, development, and cell death (McBride et al. 2006). Therefore, shutting down the mitochondria will disrupt essential cellular functions and will subsequently lead to cell death. In cancer chemotherapy, mitochondria-targeting drugs are known to interfere with cancer cell metabolisms by pertubing the mitochondrial transmembrane potential, inhibiting the electron redox chain complexes, interfering the mitochondria transmembrane permeability, and targeting mitochondrial-DNA (Biasutto et al. 2010; Wang et al. 2010). The most common types of mitochondria-targeting drugs are lipophilic, cationic drugs; these are selective for cancer cells because they tend to have higher mitochondrial membrane potentials than normal epithelial cells (Lampidis et al. 1985; Modica-Napolitano and Aprille 2001).

Consequently, we examined the cytotoxicities of rosamines with particular attention to structure-activity relationship. Rh123 which is a well-studied delocalised lipophilic cation was included as a positive control. Selected rosamines were further

investigated for their intracellular localisation, induction of cell cycle arrest and cell death and their effect on the cellular redox systems. The *in vivo* antitumour activity of the most potent rosamine was then evaluated in a syngeneic mouse tumor model. Selected rosamines were also evaluated in the NCI-60 human tumour cell lines screen for cancer cell type selectivity, activity correlation with specific genes mutations, and comparison of the mode of action by COMPARE analyses.

5.2 Materials and Methods

5.2.1 Materials

5.2.1.1 Chemicals and Reagents

Complex I, Complex II, Complex IV and ATP Synthase Enzyme Activity Microplate Assay Kit were purchased from MitoSciences (OR, USA).). JC-1 was purchased from Molecular Probes, Invitrogen (OR, USA). Protein assay dye reagent concentrate was obtained from Bio-Rad Laboratories (CA, USA). Ethylene glycolbis(aminoethylether)-tetra-acetic acid (EGTA), 3-(N-morpholino)propanesulfonic acid (MOPS), sucrose and Tris were purchased from Fisher Scientific (Leicestershire, UK). Other chemicals and reagents used were as described in Section 3.2.1.1 and 4.2.1.1.

5.2.1.2 Instrumentations

As described in Section 4.2.1.2

5.2.1.3 Animal Model

Mouse model used was as described in Section 3.2.1.3

5.2.2 Preparation of Compound

A total of 21 rosamines were prepared and supplied by Prof Kevin Burgess's group from the Department of Chemistry, Texas A&M University, Texas, USA. Their syntheses and NMR characterisation were previously described by Wu and Burgess (2008b). All the compounds used for *in vitro* experiments were dissolved in DMSO to make stock solutions of 10 mM, aliqouted into appropriate volume and stored at -20 ºC prior to use.

5.2.3 Photophysical Properties

Absorbance spectra were obtained on a Varian 100 Bio UV-Vis spectrophotometer at room temperature. Extinction coefficients were determined from Beer's Law plots using three data points.

5.2.4 Cell Culture and Cytotoxicity Assay

MCF-7, HCT116, HL60, HSC2 and HK1 cell lines were used to evaluate the photocytotoxicity/cytotoxicity of rosamine *in vitro*. The experimental procedure and conditions were similar as described in Section 4.2.4, unless specified. Both MCF-7 breast carcinoma and HCT-116 colon carcinoma cell lines were obtained from American Tissue Culture Collection (VA, USA) and maintained in RPMI 1640 medium supplemented with 10% heat inactivated FBS and 1% of penicillin-streptomycin.

5.2.5 Intracellular Localisation

As described in Section 3.2.8. Rosamine was excited at 520-550 nm wavelength.

5.2.6 Analysis of Cell Cycle and Annexin V-FITC Apoptosis

As described in Section 4.2.7 and 4.2.8.

5.2.7 Mitochondria Isolation and Detergent Solubilisation

Functional mitochondria were isolated from mouse liver by differential centrifugation method (Frezza et al. 2007). Briefly, a mouse (~30 g) was starved overnight before sacrificed by cervical dislocation. The liver was harvested promptly and rinsed with ice-cold mitochondria isolation buffer (10 mM Tris-MOPS, 1 mM EGTA/Tris, 0.2 M sucrose, pH 7.4) until blood-free. The liver was then cut into small pieces in a beaker using scissors while keeping in an ice-bath. The buffer was replaced with 5 ml of fresh isolation buffer and the liver was homogenised with a Polytron probe (Ultra-Turrax T8, Ika-Werke, Germany) until smooth. The homogenate was centrifuged at 1000 g for 15 min at 4 ºC. The pellet was discarded and the supernatant was centrifuged at 12000 g for 15 min at 4 ºC to pellet the mitochondria. The mitochondria were washed twice with 4 volumes of isolation buffer containing 1× protease cocktail inhibitor. The concentration of the mitochondrial protein was determined using the Bradford (Biorad protein assay) method. The mitochondria were frozen in 10 mg/ml aliquots at -80 ºC.

Detergent solubilisation of the mitochondria proteins was done prior to measurement of the oxidative phosphorylation complexes activity. Mitochondria were diluted to 5.5 mg/ml with PBS and solubilised by addition of a 1/10th volume of detergent provided to give the final protein concentration of 5 mg/ml. The mixture was incubated on ice for 30 min and centrifuged at 17000 g at 4 ºC for 20 min. The supernatant was collected and diluted to the appropriate concentrations for each oxidative phosphorylation complexes activity.

5.2.8 Measurement of Oxidative Phosphorylation Complexes Activity

The measurement of mitochondria oxidative phosphorylation activities for Complex I, II, IV and ATP-synthase were carried out using the microplate immunocapture ELISA assay kit according to their respective manufacturer's protocols (Nadanaciva et al. 2007). Briefly, the plate pre-coated with appropriate immunocapture antibody was incubated with mitochondria extract at recommended concentration to allow immobilisation of their respective complexes. Complex activity was measured by addition of substrates solution mix provided by the kit and compound was added at concentration ranging from 0.01-10 μM in triplicate. Control wells treated with only 0.1% DMSO (v/v) and wells without mitochondria extract incubation were included as background reference. The kinetic of the complexes activity was recorded with SpectraMax M4 microplate spectrophotometer reader using the suggested measurement parameters.

5.2.9 JC-1 Analysis of Mitochondrial Membrane Potential

The mitochondrial membrane potential was measured based on the potential-dependent accumulation of the cationic JC-1 dye which results in a shift of fluorescence emission from green (~525 nm) to red (~590 nm) due to the formation of J-aggregates (Reers et al. 1991). Therefore, mitochondrial depolarisation is indicated by a decrease in the red/green fluorescence intensity ratio. Briefly, cells were collected and suspended in 1 ml warm media at approximately 1×10^6 cell/ml. In a control tube, 1 μl of 50 mM carbonyl cyanide 3-chlorophenylhydrazone was added and incubated at 37 ºC for 5 min. Then, 10 μl of 200 μM JC-1 was added into the cells and incubated at 37 ºC for 30 min. Cells were washed twice with warm PBS, resuspended in 500 μl of PBS and analysed

on a FACSCalibur flow cytometer using 488 nm excitation with 530/30 nm and 585/42 nm bandpass emission filters.

5.2.10 NCI-60 Human Tumour Cell Line Screen

NCI-60 cell-lines panel screening was performed by the National Cancer Institute's Developmental Therapeutics Program. Sulforhodamine B assay was used to assess the cytotoxicity of test agents in a panel of 60 cell lines (Boyd and Paull 1995). Briefly, the human tumour cell lines of the cancer screening panel were grown in RPMI 1640 medium containing 5% FBS and 2 mM L-glutamine. For a typical screening experiment, cells were inoculated into 96 well microtiter plates in 100 µl at plating densities depending on the doubling time of individual cell lines. After cell inoculation, the microtiter plates are incubated at 37° C, 5% CO_2 and 100% relative humidity for 24 h. Following incubation, aliquots of 100 µl of compound at different dilutions were added to the appropriate microtiter wells and were further incubated for 48 h. At the assay end-point, cells were fixed with trichloroacetic acid followed by Sulforhodamine B staining for cellular protein content. Sulforhodamine B absorbance was read at 515 nm of wavelength as a measurement of cell density.

5.2.11 *In Vivo* Antitumour Efficacy

Female BALB/c mice aged 6-8 weeks with a minimum weight of 17 g were used in the experiment. Tumour allografts were initiated by subcutaneous injection of 5×10^5 4T1 mouse mammary carcinoma in 0.1 ml RPMI 1640 media into the inguinal mammary fat-pads of mice (Jin et al. 2010). Tumour growth was monitored and treatments were initiated when tumours reached volume of approximately 200 mm^3. To assess the tumour growth inhibition, 4T1 tumour bearing mice were randomised into groups with

at least eight animals per group. Compound was prepared at 0.3 mg/ml in normal saline and treatment was administered intravenously at 5 mg/kg on staging day or 3 mg/kg every other day for six treatments (q2dx6). For control group, normal saline was given.. Animal weights and tumour volume were measured three times weekly for 14 d. At least eight mice were assessed for each treatment group.

Growth of the solid tumours was monitored using *in situ* caliper measurement of two perpendicular dimensions (length and width) and tumour volume was calculated using the formula for a prolate ellipsoid using Equation 4 (Section 3.2.12). Relative tumour volume (RTV) was calculated for every tumour volume using Equation 6 (Plowman et al. 1997).

Equation 6

$$\text{Relative tumour volume, RTV} = \frac{\text{tumour volume at any given time, } V_t}{\text{tumour volume at staging day, } V_0}$$

The median RTV – time profile for each group was plotted and results were expressed as median ± 95% confidence interval. To determine the antitumour activity, terminal % T/C was calculated from the growth curve (Equation 5, Section 3.2.12) and tumour growth delay to attain a specified number of doublings compared to control group (Equation 7).

Equation 7

$$\text{Tumour growth delay} = \frac{T - C}{C} \times 100$$

Where T and C are the median days for the treated and control groups respectively, to attain a specified number of doublings from its staging day tumour volume

5.2.12 Stastical Analysis

Statistical significance was performed using one-way ANOVA followed by Bonferroni's post-hoc test and differences were considered significant when $p<0.05$. Statistical analysis for mean data obtained from NCI screen were performed using one-sample t-test and Student's t-test (SPSS 16.0, IBM Corporation, Armonk, NY).

5.3 Results and Discussion

5.3.1 Structural Variations and Photophysical Properties

The rosamines investigated in present study were cyclic-amines substituted around the compound TMR core which represent a new structural variation not reported before (Table 5.1). Rosamines **R1-R6** were functionalised with various heterocylic amine substitution patterns aimed to increase the chomophore aromaticity which is postulated to red-shift the absorption wavelength. Meanwhile, rosamines **R7-R21** were prepared to examine the effects of *meso*-substitution with alkyl (**R7**), aryl (**R8-R9**), heterocyclic (**R10-R12**), aryl-halide (**R13-R16**), methoxy-aryl (**R17-R19**) and of hydrophilic substituents such as the phenolic **R20** and the carboxylic **R21** moieties on the spectroscopic properties of rosamine.

The photophysical data of the rosamines were summarised in Table 5.1. As expected, heterocylic amine substitutions (**R1-R6)** resulted in a red-shift of λ_{abs} and higher molar extinction coefficient compared to TMR (ε = 83000 $M^{-1}cm^{-1}$ at 552 nm). Rosamine substituted with hydrophobic cyclic-amines such as pyrrolidine (**R1**), piperidine (**R2**) and Boc-piperazine (**R5**) exhibited higher far-red absorbance than rosamine substituted with hydrophilic cyclic-amines that contain exposed oxygen or NH isosteres (**R3**, **R4** and **R6**). For the effect of *meso*-substitution, conjugation with heterocyclic (**R10-R12**) or phenyl halide (**R13-R16**) moieties further red-shifted the

λ_{abs}, while varying substitution with alkyl (**R7**), unsubstituted-aryl (**R8-9**), methoxy-aryl (**R17-19**) or hydrophilic substituents such as the phenolic **R20** and the carboxylic **R21** moieties had little effect on the λ_{abs} value when compared to **R2**. Substitution of hydrophilic moieties such as furan **R11**, di-2-methoxy aryl **R19**, phenolic **R20** and the aryl carboxylic **R21** resulted in decreased molar extinction coefficient.

5.3.2 *In Vitro* Antiproliferative Assay

The *in vitro* antiproliferative activity of compounds **R1-R21** against a promyelocytic leukemia cell line, HL-60 was determined using a 24 h endpoint MTT assay. Results were expressed as IC_{50} in μM, concentration of compound that inhibits proliferation rate by 50% as compared to control untreated cells. From the assay, compounds **R1-R3**, **R5**, **R8-R19** demonstrated their antitumour activity with IC_{50} values in the sub-micromolar range. In contrast, compounds **R4**, **R6**, **R7**, **R20** and **R21** displayed moderate to poor activity from single-digit micro-molar IC_{50} values to undeterminable IC_{50} up to 100 μM. Meanwhile, there were no significant decreases in IC_{50} values when HL60 cells were irradiated with 5.3 J/cm^2 of broad spectrum light after 2 h of rosamine treatment compared to unirradiated cells, except for **R9** which demonstrated 6-fold decreased in IC_{50} value following irradiation. However, this effect was negligible compared to strong photosensitisers such as BODIPYs that demonstrated up to 1000-fold increase in photo-induced cytotoxicity. Therefore, the rosamines evaluated here were considered poorly photo-active, but given their potent cytotoxicity and structural novelty, their potential utility as an anticancer agent was evaluated instead. We thereby examined their cytotoxicities with particular attention to structure-activity relationship.

Table 5.1 The structure-activity relationship and *in vitro* antiproliferative activities of rosamine analogues in HL-60 cells

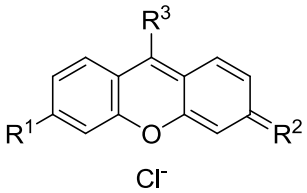

Cmpd	R^1	R^2	R^3	λ_{abs} (nm)	ε ($M^{-1}cm^{-1}$)	[a] IC_{50} (μM)	
						0 J/cm^2	5.3 J/cm^2
R1	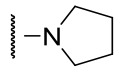	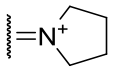	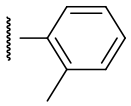	558	127400	0.72±0.09	0.49±0.19
R2	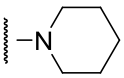	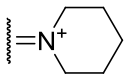	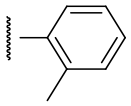	565	123600	0.76±0.03	0.40±0.04
R3	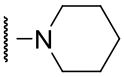	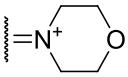	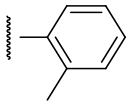	559	111000	0.35±0.01	0.56±0.08
R4	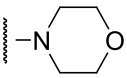	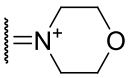	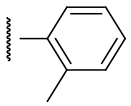	554	106900	8.3±2.2	7.2±1.9
R5	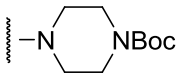	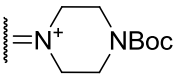	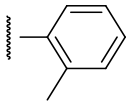	555	120800	0.62±0.07	0.52±0.09
R6	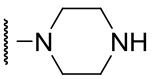	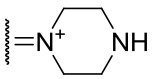	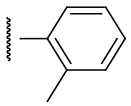	558	-	53.3±0.3	75.6±7.8
R7	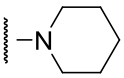	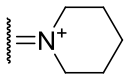		555	101900	3.9±1.5	4.7±1.5
R8	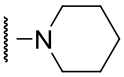	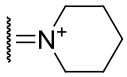		566	95900	0.82±0.04	0.63±0.13
R9	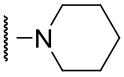	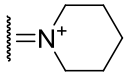	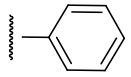	565	106000	0.47±0.13	0.08±0.01
R10	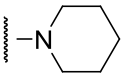	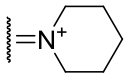	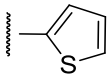	582	107600	0.10±0.04	0.07±0.02
R11	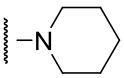	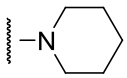	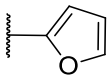	592	86900	0.13±0.01	0.15±0.02
R12	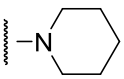	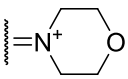	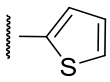	576	87600	0.23±0.02	0.27±0.02
R13	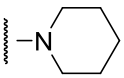	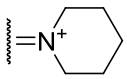	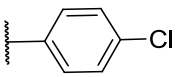	570	119100	0.17±0.01	0.14±0.01
R14				570	110800	0.50±0.04	0.49±0.04
R15				570	115400	0.09±0.01	0.06±0.01

Table 5.1, continued

R16	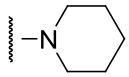	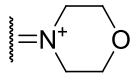	565	80 900	0.17±0.05	0.18±0.03
R17	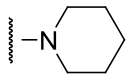	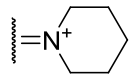	562	116700	0.66±0.17	0.57±0.08
R18	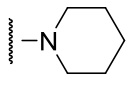	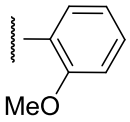	566	118000	0.95±0.01	0.25±0.11
R19	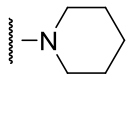	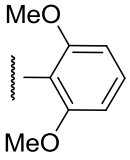	565	87300	0.25±0.22	0.06±0.01
R20	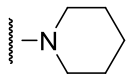	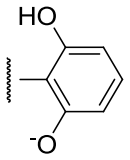	557	71000 (EtOH)	2.9±1.9	4.3±1.8
R21	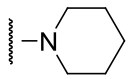	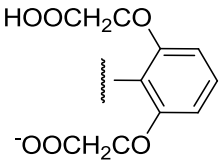	557	84800 (EtOH)	>100	>100
Rh123		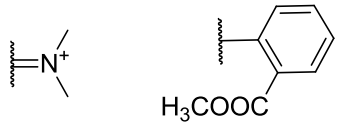	508	111000 (EtOH)	7.8±06	7.8±0.2
TMR			[b] 552	[b] 83000 (MeOH)	ND	ND

[a] Values represent the means ± SD of three determination assessed 24 h post-treatment using MTT assay.
[b] Data obtained from literature (Detty et al. 2004)

The influence of the cyclic-amine substituents on the antiproliferative activity of the compounds was evident from studying compounds **R1-R6**. Regardless of the size of the ring, the derivatives containing hydrophobic cyclic-amines from pyrrolidine (**R1**), piperidine (**R2**) to Boc-piperazine (**R5**) exhibited moderate antiproliferative activity with IC_{50} values of 0.62-0.76 μM. On the other hand, the derivatives with cyclic-amines that contain exposed oxygen or NH isosteres as in the case of compounds **R4** and **R6** had 10- to 70-fold higher IC_{50} of 8.3 or 53.3 μM respectively. The unsymmetrical rosamine **R3**, which had a combination of piperidine and morpholine substituents interestingly, had the lowest IC_{50} value among compounds **R1-6**, alluding

to the possible importance of an amphilic structure with contrasting hydrophobic and hydrophilic halves.

For the effect of *meso*-substitution on antiproliferative activity of rosamines, compounds **R7-21** were studied. Similar to compounds **R4** and **R6** above, the derivatives with hydrophilic substituents such as the phenolic **R20** and the carboxylic **R21** had higher IC_{50} values than the unsubstituted *meso*-aryl **R9**. Having an aryl subtituent at the *meso* position, whether directly (**R9-19**) or through an alkyl spacer (**R8**), was important for antiproliferative activity and was convincingly demonstrated in the lower activity observed in compound **R7** which had only a simple methyl substituent at the *meso* position. Among the aryl substituted compounds, the heterocyclic (**R10-R12**) and the phenyl-halide (**R13-R16**) structures had the lowest IC_{50} values compared to a simple phenyl-substituted compound **R9**, while 4-methoxy aryl (**R17)**, mono-2-methoxy (**R18**) and di-2-methoxy (**R19**) aryl substitutions did not confer additional activity.

Subsequently, the *in vitro* antiproliferative activity of the most active compounds, **R9-16**, were assessed against a panel of cell lines derived from human solid tumours including breast carcinoma (MCF-7), colon carcinoma (HCT-116), oral squamous cell carcinoma (HSC2) and nasopharyngeal carcinoma (HK1). A 48 h endpoint MTT assay which is more typical of cytotoxicity studies was used. The antiproliferative activity of Rh123 was also simultaneously determined for comparison.

The IC_{50} values for these rosamines across the panel of cancer cell lines tested ranged from 0.07-1.2 μM and on average were at least 10-folds more potent than Rh123 (Table 5.2). From this study, compound **R10** which had a thiofuran showed the highest activity among the analogues with average IC_{50} of 0.11 μM. SAR study revealed that rosamines bearing phenyl halide or heterocyclic moieties were significantly (p<0.05)

more potent than phenyl substituted rosamine **R9**. Halide substitution resulted in improvement of cytotoxicity; this was expected because substitution of *H* by halide is commonly used to increase compound lipophilicity that improves lipid-bilayer membrane permeability (Gerebtzoff et al. 2004). Within the halide series, cytotoxicities increased in the following order **R13** > **R14** > **R15** (Cl > Br > I), although not statistically significant (p>0.05). The compounds with *meso*-heterocyclic substituents **R10** and **R11** were more potent than the aromatic halides **R13-R15**. Of the two compounds with *meso*-heterocycles the thiofuran-substituted **R10** was slightly more active than **R11**, the furan-substituted one.

Table 5.2 Antiproliferative activities of rosamine analogs against a panel of cancer cell lines.

Rosamine	Activity IC_{50} (μM)[a]				
	MCF-7	HCT-116	HSC2	HK1	Mean[b]
R9	1.2 ± 0.7	0.60 ± 0.41	0.09 ± 0.00	0.61 ± 0.07	0.63†
R10	0.18 ± 0.02	0.07 ± 0.02	0.09 ± 0.01	0.10 ± 0.00	0.11§
R11	0.31 ± 0.14	0.10 ± 0.03	0.09 ± 0.00	0.31 ± 0.08	0.20‡,§
R12	0.17 ± 0.10	0.07 ± 0.02	0.22 ± 0.11	0.53 ± 0.00	0.25‡,§
R13	0.15 ±0.04	0.22 ± 0.14	0.09 ± 0.01	0.25 ± 0.01	0.18‡,§
R14	0.29 ± 0.04	0.30 ± 0.08	0.19 ± 0.11	0.34 ± 0.00	0.28‡,§
R15	0.59 ± 0.12	0.39 ± 0.07	0.35 ± 0.05	0.29 ± 0.03	0.41‡
R16	0.26 ± 0.07	0.24 ± 0.07	0.22 ± 0.10	0.44 ± 0.01	0.29‡,§
Rh123	5.6 ± 0.6	7.9 ± 1.0	4.5 ± 2.2	5.9 ± 0.2	6.0$^{\Psi}$

[a] IC_{50}, the concentration of compound, which inhibits the viability by 50% as compared with control untreated cells. Values represent the mean ± SD of three determination assessed 48 h post-treatment using methylthiazolyldiphenyl-tetrazolium bromide assay. [b] Values with different symbols are significantly different from each other (p<0.05).

Compound **R16** has a more polar combination of amine substituents than the symmetrical *bis*piperidine **R15**, and was proved to be more cytotoxic (Table 5.2). This is consistent with our earlier data for **R3** unsymmetrically substituted with piperidine

and morpholine which showed nearly 2-fold lower IC_{50} values compared with the symmetrical hydrophobic structure containing only piperidine **R2** (Table 5.1). Meanwhile for the *meso*-thiofuran **R10**, substitution of one of the piperidine groups with morpholine gives **R12**, which has a slightly decreased activity, contrary to our expectations.

5.3.3 Intracellular Localisation

TMR with its cationic characteristic is known to be attracted to the negatively charge mitochondrial matrix leading to its localisation in the mitochondria. We would like to investigate whether the rosamines investigated in this study would retain their mitochondrial targeting properties following cyclic-amine substitutions. Therefore, the intracellular localisation of **R15** in HSC2 cells was examined by confocal microscopy using dual staining techniques (Figure 5.1). **R15** was chosen as a representative compound given its higher fluorescence quantum yield to allow better visualisation.

Co-staining images and topographic profiles of cells containing **R15** and a mitochondria-specific dye Rh123 revealed an almost identical overlap, suggesting that **R15** localised particularly well in mitochondria (Figure 5.1 A and B). In comparison, **R15** displayed only partial co-localisation with endoplasmic reticulum and lysosomes, according to the confocal images and topographic profiles of **R15** with ER-Tracker (Figure 5.1 C and D) and with LysoTracker (Figure 5.1 E and F) respectively. Staining of the cytoplasmic or nuclear membrane by **R15** was not detected, indicating that it did not react non-specifically with biological membranes. Furthermore, the nucleus remained free of **R15** (dark nuclear area) signifying that this class of compounds would not be expected to directly damage DNA.

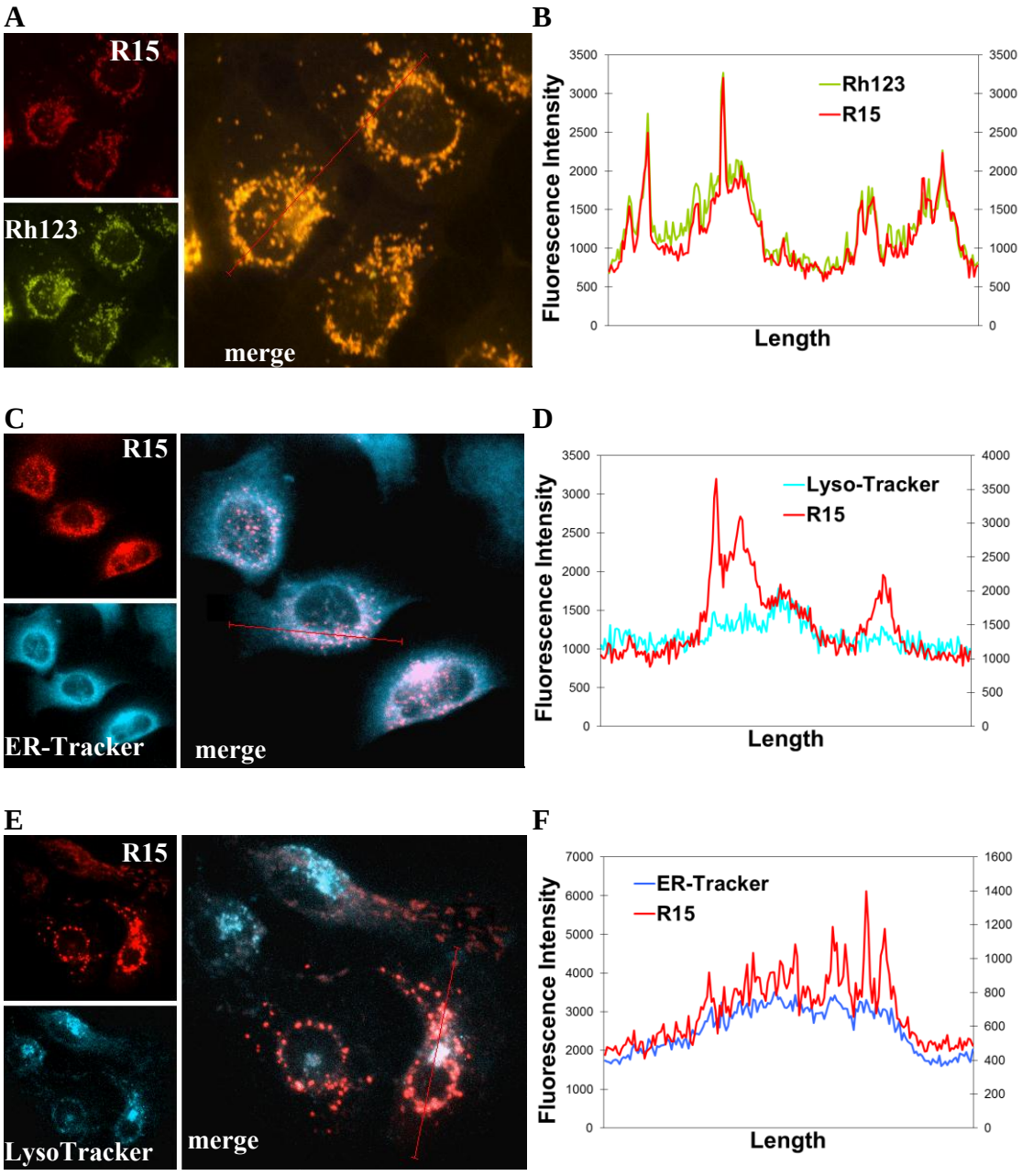

Figure 5.1 Intracellular localisation of **R15** in HSC2 cells. (**A**, **C**, **E**) Confocal images and (**B**, **D**, **F**) fluorescence topographic profiles of HSC2 cells double-stained with 100 nM of **R15** and organelle probes. (**A**, **B**) Mitochondria were labeled with 100 nM Rh123, excited at 494 nm. (**C**, **D**) Endoplasmic reticulum were labeled with 100 nM ER-Tracker, excited at 365 nm. (**E**, **F**) Lysosomes were labeled with 500 nM LysoTracker, excited at 365 nm. **R15** was excited at 575 nm. Topographic profiles revealed that **R15** localised predominantly in mitochondria but partially in both lysosomes and endoplasmic reticulum. Line segment indicates the longitudinal transcellular axis analysed to generate the topography fluorescence profiles. Objective magnification × 60.

5.3.4 Apoptosis and Cell Cycle Arrest

The induction of apoptosis was quantified in flow cytometry experiments measuring the externalisation of membrane phosphatidylserine through annexin V-FITC staining, an event considered to be characteristic of cell undergoing apoptosis (Figure 5.2). Flow cytometric analysis of HSC2 cells treated with 0.5 μM of **R15** showed the onset of apoptosis by 8 h of incubation with 16% of the cells stained positive for annexin V compared to less than 10% at 0 h or 4 h time-points. The proportion of cells undergoing apoptosis continued to increase rapidly to 58% within 24 h (p<0.05). Meanwhile, the cell cycle profile of HSC2 treated with 0.25 μM of R15 was examined in a time course experiment. From Figure 5.3 (A and B), HSC2 cell population in S phase was shown to increase significantly (p<0.05) from 17.9% in the control group to 29.4%, 28.5%, 30.2%, respectively, at 12, 16 and 24 h after treatment. This findings indicate that the apoptosis cell death induced were associated with S-phase cell cycle arrest by **R15**.

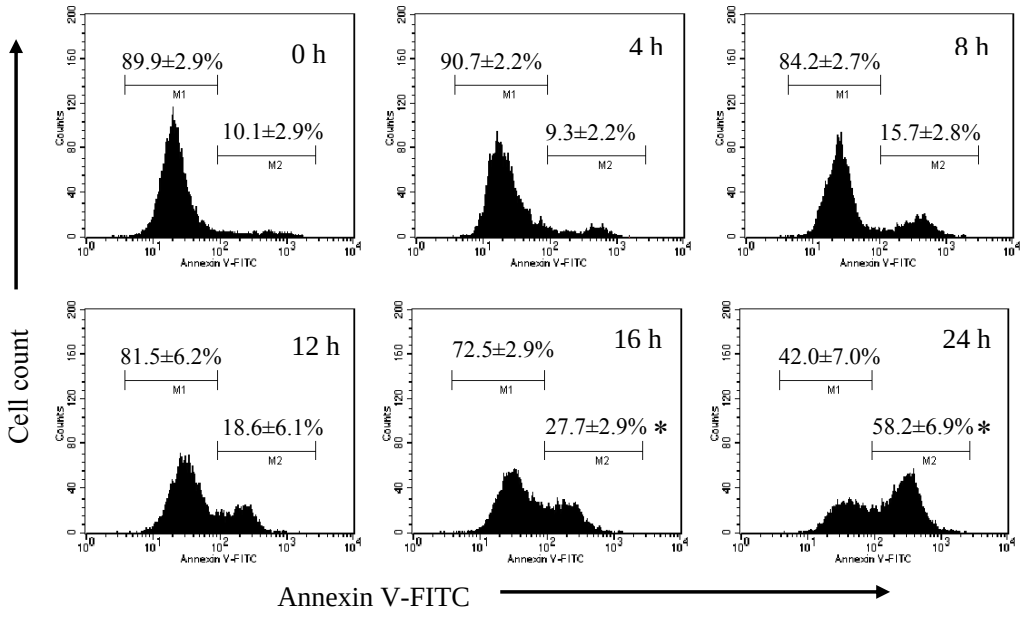

Figure 5.2 Apoptotic cell death induced by **R15.** A representative histograms of event of annexin V-FITC binding to PS as an indicator of apoptosis in HSC2 cells treated with 0.5 μM of **R15** at different duration. Onset of apoptosis was observed 8 h following treatment. M1 represents viable cell population, M2 represents apoptotic cell population. *indicates difference is with p<0.05 compared to 0 h control.

A

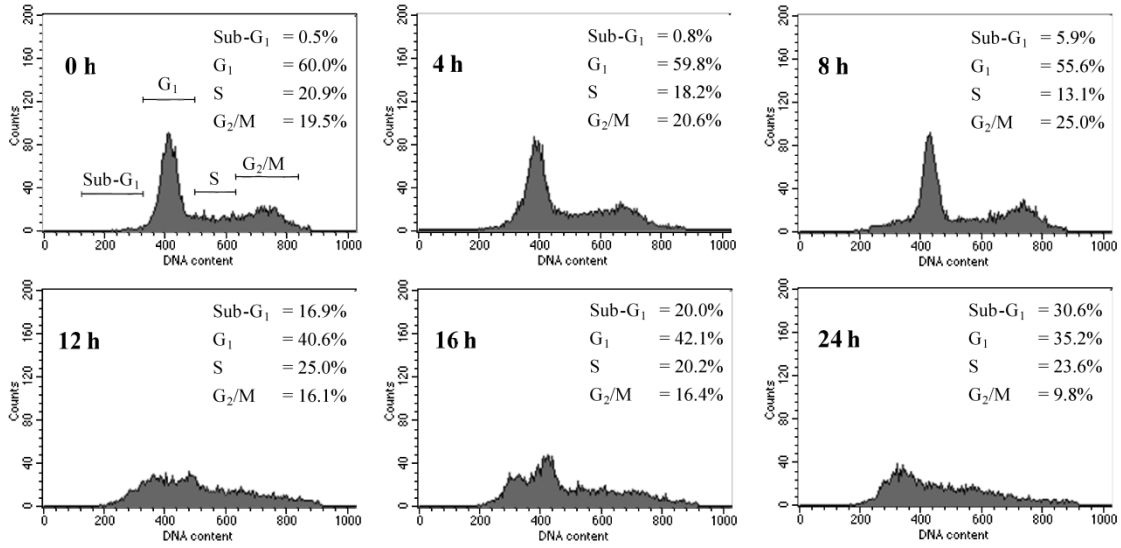

B

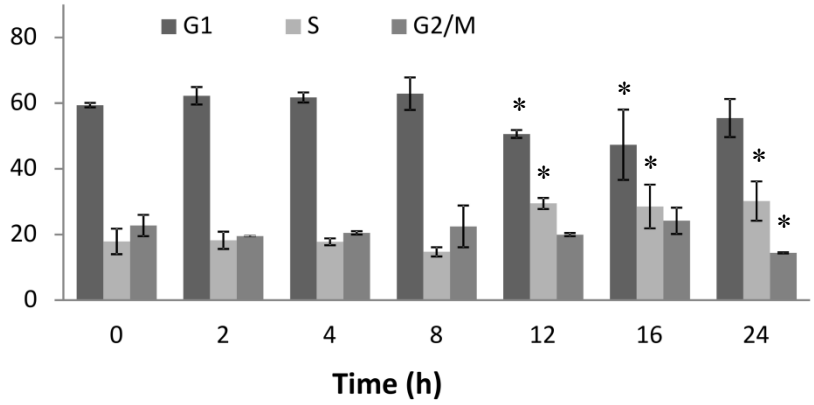

Figure 5.3 Cell cycle arrest induced by **R15. (A)** A representative histograms of event of HSC2 cell cycle phase after treated with 0.25 µM of compound **R15** for various intervals analysed using flow cytometry. (**B**) Mean percentage of proportion of cell population in G_1, S and G_2/M phases, following subtraction of sub-G_1 phase population. An increased of cell population arrested in S phase cell cycle was observed from 12-24 h following treatment. *Difference with $p<0.05$ compared to 0 h control at each cell cycle phase.

5.3.5 Rosamines Interfered the Energy Redox

Accumulation of cytotoxic lipophilic cations is known to alter mitochondrial transmembrane potentials (Don and Hogg 2004; Toogood 2008). The alteration of mitochondrial membrane potential caused by rosamines were monitored based on the accumulation of potential-dependent JC-1 dye which resulted in a shift of fluorescence emission from green (~525 nm) to red (~590 nm) due to the formation of J-aggregates. From the study, approximately 21% of the HSC2 cells treated with **R10** at 0.1 μM were affected in the first hour and the percentage increased drastically to 34% in 8 h. Meanwhile, for HSC2 cells treated with **R15** at 0.1 μM, 9% of the cell population exhibited the onset of mitochondrial transmembrane potential loss within 1 h after treatment and gradually increased to 19% (p<0.05) in 8 h (Figure 5.4). For the untreated control cells, the population of depolarized cells at 8 h remained at approximately 8 %. Meanwhile, cells treated with 5 μM of CCCP for 5 min resulted in loss of membrane potential in 70% (p<0.05) of cell population. CCCP is an oxidative phosphorylation decoupling agent which acts as a positive control for the experiment.

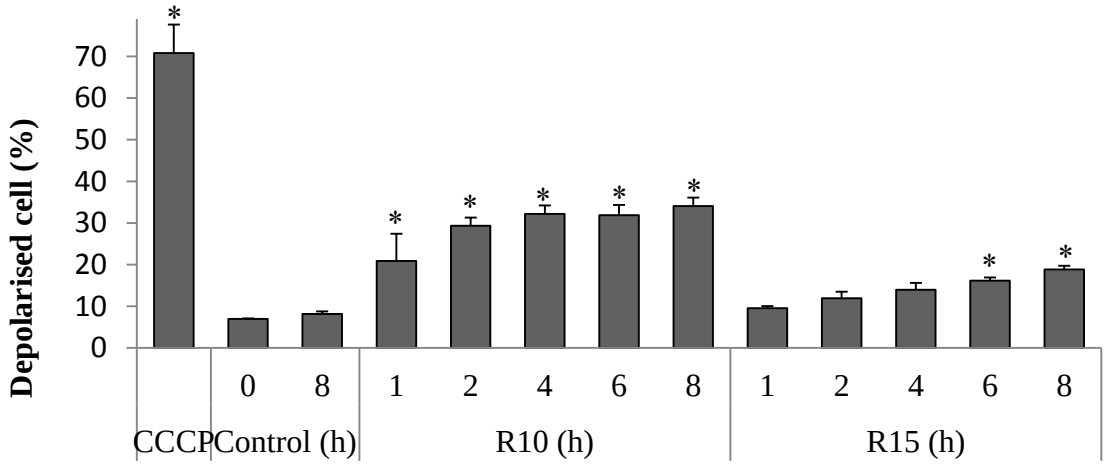

Figure 5.4 Loss of mitochondrial transmembrane potential in HSC2 cells treated with **R10** and **R15** at 0.1 μM for various intervals analysed using flow cytometry. Cells treated with 5 μM of carbonyl cyanide 3-chlorophenylhydrazone (CCCP) for 5 min was included as a positive control. *Difference with p<0.05 compared to control at 0 h.

Since the rosamines were shown to primarily localise in the mitochondria and they induced loss of mitochondrial membrane potential, their effect on the oxidative phosphorylation pathway was therefore investigated. By using immunocapture ELISA microplate assay, the mitochondrial redox carriers namely Complex I, Complex II, Complex IV and ATP-synthase were monitored for their enzyme kinetics upon treatment with **R10** and **R15**. From Figure 5.5, the activity of Complex II was partially inhibited by **R10** with IC_{50} value of 9.6 ± 0.1 μM whereas for **R15**, inhibition was observed but with undetermined IC_{50} value. Meanwhile, both **R10** and **R15** displayed inhibition of ATP synthase activities with IC_{50} values of 3.0 ± 0.8 μM and 3.9 ± 0.3 μM respectively. The activity of Complex I and Complex IV were not affected by the rosamines at treated concentrations (highest at 10 μM). This data indicates that these rosamines act by compromising the mitochondrial bioenergetics function primarily by inhibiting ATP synthase, a proton-driven enzyme that produces ATP from ADP and inorganic phosphate. Similar biochemical interaction was observed in Rh123 and this effect is expected as the compound has close structural similarity with the rosamine (Modica-Napolitano et al. 1984).

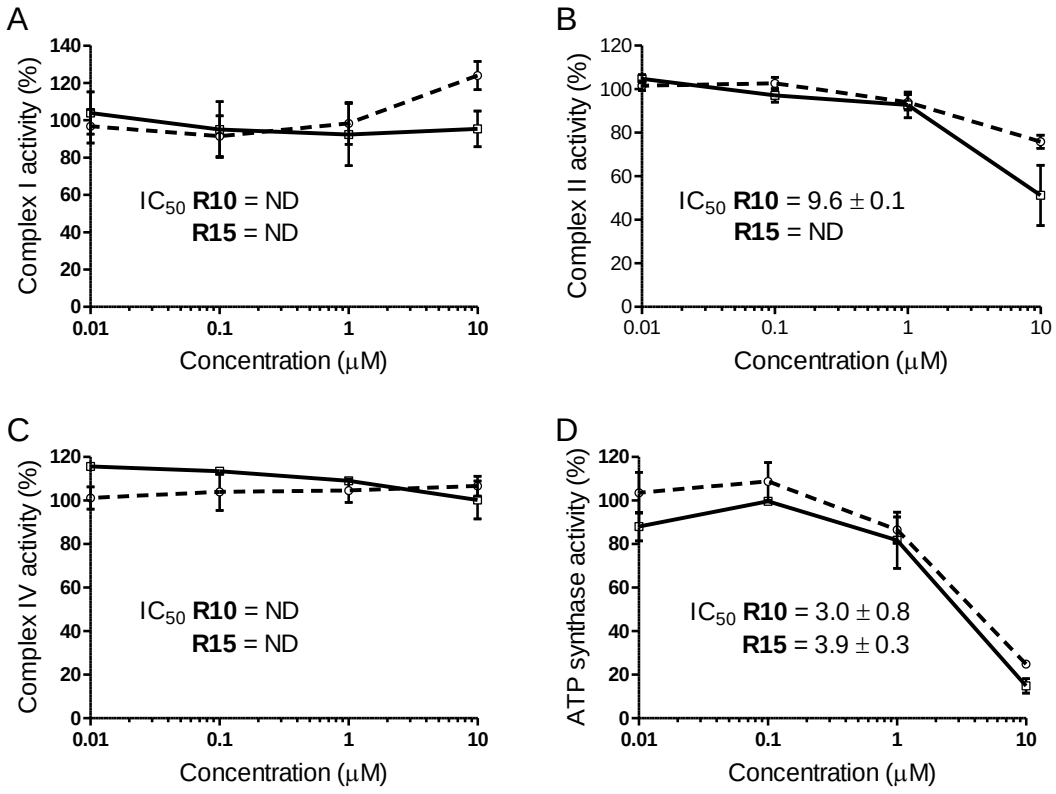

Figure 5.5 Inhibition of mitochondrial oxidative phosphorylation complexes. The dose-response inhibition of mitochondrial oxidative phosphorylation Complex 1 (A), Complex II (B), Complex IV (C) and ATP synthase (D) activities by rosamine **R10** (solid line) and **R15** (dotted line). IC_{50} values depict concentrations that inhibit the complexes activity by 50%. ND - indicate non-determined IC_{50} values based on the concentration used.

5.3.6 *In Vivo* Antitumour Effect of Rosamines

R10 was selected for further evaluation in *in vivo* tumour model given its *in vitro* potency and ability to achieve aqueous solubility large enough for preparing an intravenous injection. As illustrated in Figure 5.6, tumour growth attenuation was observed at experimental end-point (day 14) when the mice received a single bolus of 5 mg/kg of **R10** i.v. compared to the control group (*p*-value=0.08). The tumour growth attenuation effect is further enhanced (*p*-value=0.029) when the mice received a rosamine treatment regimen of 3mg/kg, once every two day, for six times (q2d×6). The

median day for 4T1 tumour in attaining two-doubling growth (RTV=4) were approximately 9, 11 and 13 days in control mice, mice receiving 5 mg/kg and 3 mg/kg (q2d×6) respectively. The percentage of two-doubling tumour growth delay (T-C)/C in mice treated with 5 mg/kg and 3 mg/kg (q2d×6) of **R10** were determined to be 22% and 38%, respectively.

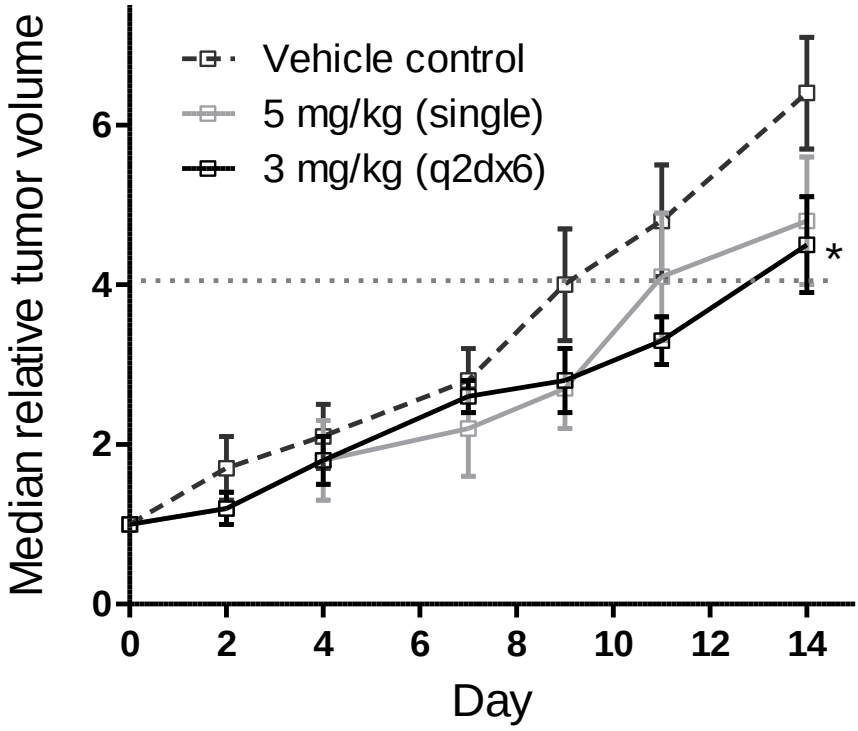

Figure 5.6 *In vivo* antitumour effects of rosamine. The relative tumour volume (RTV) – time profile of 4T1 murine breast carcinoma in BALB/c mice following intravenous dosing of **R10** or saline as vehicle control. Each point represents median ± 95% confidence interval of RTV to staging day (n = 8). The terminal % T/C value for mice receiving 5 mg/kg and 3 mg/kg (q2d×6) of **R10** were 72% and 66% respectively. The two doubling tumour growth delay (T-C)/C (dotted line, RTV=4) for mice receiving a single bolus of 5 mg/kg and multiple doses of 3 mg/kg (q2d×6) of **R10** were 22% and 38%, respectively. T and C refer to RTV for treatment and control groups, respectively. *Difference with $p<0.05$ compared to control animal.

Meanwhile, the terminal percent test/control (% T/C) values calculated at the end of experiment were 72% and 66% in mice receiving 5 mg/kg and 3 mg/kg (q2d×6) respectively. The antitumour efficacy of **R10** was modest as the % T/C attained after treatment had ended was not ≤ 40% activity, the minimal rating for a compound to be considered active (Plowman et al. 1997). Loss of body weight (Figure 5.7) was observed in mice treated with **R10** throughout the experimental period, however the reduction at any time were not statistically significant compared to the untreated mice. None of the mice suffered weight loss of more that 15%, the cut-off limit set in the experiment (Workman et al. 2010). From this study, the *in vivo* anticancer effect showed by **R10** is modest, probably because 4T1 was an aggressive tumour cell line and the dose of compound **R10** used was not high. However, the use of a higher concentration was not possible because of unacceptable adverse effects such as weight loss, diarrhea and sudden death which were observed at 10 mg/kg dose.

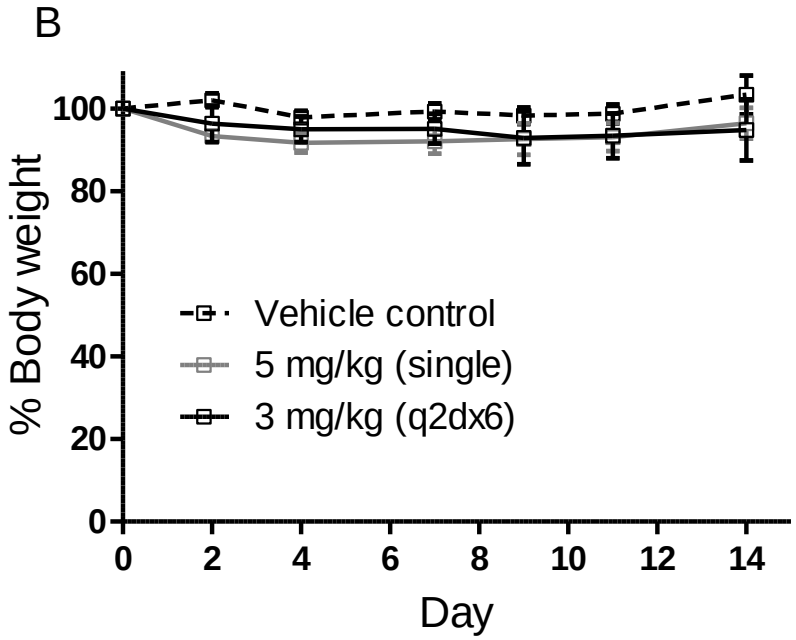

Figure 5.7 Effects of rosamine on mice body weight. Percentage of mean body weight of mice receiving 5 mg/kg or 3 mg/kg (q2d×6) of **R10** compared to untreated mice. Body weight loss was observed in treatment groups but none of these mice experienced weight loss of more than 15%.

Even though these rosamines (i.e **2** and **5**) are more cytotoxic against cancer cells compared with normal epithelial cells (previously published data (Lim et al. 2009)), their effects on normal cells could still lead to undesirable side effects as a result of increase lactic acid accumulation in cells following decreased ATP synthase activity and a shift in metabolic pathways from aerobic to anaerobic metabolism. Accumulation of lactic acid has been shown to cause depressive cardiovascular function, cardiac arrhythmias and multiple organ failure. Therefore, risk minimisation measures to deal with lactic acidosis such as those employed in the management of patients prescribed with metformin, a commonly used antidiabetic drug with similar toxic side effects, need to be outlined to prevent this serious complication (Kraut and Madias 2012; Renda et al. 2013).

Another documented side effect commonly associated with DLC such as rosamines is selective accumulation of these compounds in cardiac muscle cells that can lead to fatal deterioration in the function of the heart muscle (Kurtoglu and Lampidis 2009). Studies have shown that cardiac muscle cells are similar to cancer cells in exhibiting high negative plasma membrane potentials and therefore have increased uptake of DLC. In connection to this, doxorubicin which is a positively charged antracycline antitumour agent, is also shown to target the cardiac muscle cells and causes serious and occasionally fatal cardiotoxicity in a significant number of treated cancer patient (Aiken et al. 2009). However, following liposomal encapsulation of doxorubicin, cardiotoxicity was diminished in cancer patients receiving the formulation with no loss of efficacy (Kesterson et al. 2010). It therefore remains to be investigated whether a similar encapsulation approach (i.e. encapsulation of rosamine with liposomal formulation) may limit the toxicity to sufficiently allow higher dose to be safely used in preclinical study.

5.3.7 NCI-60 Screen

Screening of compounds against the NCI-60 cell line panel gives a wealth of information on the growth inhibitory effects of molecules across a wide variety of human tumour cell lines including cell type specific effects (selective growth inhibition or cytotoxic properties), correlation with specific genes or protein expression levels, and comparison of the mode of action with compound of known action by COMPARE (Computerised Pattern-recognition algorithm) analysis (Weinstein et al. 1997).

5.3.7.1 Compounds Selection and Submission

A total of seven rosamines namely **R10-R16** were submitted online to NCI Development Therapeutic Programme (DTP) for request to be tested against 60 different human cancer cell lines, representing leukemia, melanoma and cancers of the lung, colon, central nervous system, ovary, breast, prostate, and renal subpanel. The seven compounds which consist of two analogs class with different heterocyclic and phenyl-halide substitution at the *para* position were selected based on their potency from in-house screening. From the seven rosamines, three were shortlisted by the DTP staff for testing based on defined guidelines i.e. compound ability to add diversity to the NCI small molecule collection, and compounds with drug-like properties designed utilising the concept of privileged scaffolds or structures based on computer-aided design.

5.3.7.2 NCI *In Vitro* Screen

In NCI *in vitro* screen, three response parameters (GI_{50}, TGI, and LC_{50}) were determined for each cell line. The GI_{50} value (growth inhibitory activity) corresponds to

the concentration of the compounds causing 50% decrease in net cell growth, the TGI value (cytostatic activity) is the concentration of the compounds resulting in total growth inhibition and the LC_{50} value (cytotoxic activity) is the concentration of the compounds causing net 50% loss of initial cells at the end of the incubation period (48 h). A mean graph for each parameter was tabulated to illustrate the rosamine-activity pattern, with bars representing the response deviation of individual tumour cell lines from the overall mean value for all the cells tested. Positive values project to the right of the vertical line represent cellular sensitivities to the test agent that exceed the mean. Whereas, negative values project to the left represent cell line sensitivities to the test agent that are less than the average value (Figure 5.8 - 5.10).

From the mean graphs, mean GI_{50} values generated from the NCI-60 cell lines screen indicated that **R10**, **R11** and **R13** exhibited similar 50% growth inhibitory potency with $Log_{10}GI_{50}$ (M) values of -7.16, -7.28 and -7.02, respectively (GI_{50} = 0.069 μM, 0.052 μM and 0.095 μM, respectively). Meanwhile, the mean value that induced total growth inhibition ($Log_{10}TGI$) for **R10**, **R11** and **R13** was achieved at concentration (M) of -6.58, -6.51 and -6.52, respectively (TGI = 0.26 μM, 0.31 μM and 0.30 μM, respectively). The mean concentration (M) for **R10**, **R11** and **R13** to induce 50% killing of initial cells ($Log_{10}LC_{50}$) was achieved at -5.94, -5.78 and -5.95 respectively (LC_{50} = 1.2 μM, 1.7 μM and 1.1 μM, respectively). From the activity pattern, all the three rosamines were particularly more effective against a colorectal cancer subpanel across the three response parameters (except for HCT-15). The renal cancer subpanel was also more sensitive to **R11** in all the three response parameters. Meanwhile, the leukemia subpanel is less sensitive towards rosamines treatment at TGI and LC_{50} concentrations compared with other tested cell lines.

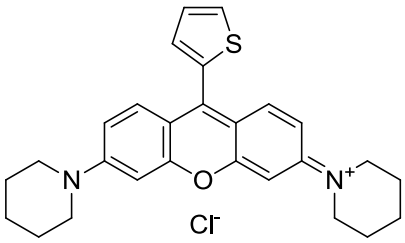

Panel/Cell Line	Log_{10}GI50	Log_{10}TGI	Log_{10}LC50
Leukemia			
CCRF-CEM	-7.30	-5.97	-5.00
HL-60(TB)	-6.87	-6.32	-5.00
K-562	-7.26	-5.91	-5.00
MOLT-4	-7.29	-6.32	-5.00
SR	-7.50	-6.46	-5.00
Non-Small Cell Lung Cancer			
A549/ATCC	-7.53	-6.95	-5.97
EKVX	-7.20	-6.45	-5.68
HOP-62	-7.32	-6.75	-6.29
HOP-92	-7.00	-6.58	-6.17
NCI-H226	-6.72	-5.98	-5.37
NCI-H23	-6.86	-6.44	-6.01
NCI-H322M	-7.55	-7.08	-5.93
NCI-H460	-7.50	-6.98	-6.30
Colon Cancer			
COLO 205	-7.16	-6.64	-6.19
HCC-2998	-7.41	-6.85	-6.41
HCT-116	-7.49	-6.98	-6.44
HCT-15	-6.58	-5.88	-5.27
HT29	-7.56	-7.03	-6.18
KM12	-7.46	-6.90	-6.40
SW-620	-7.40	-6.83	-6.34
CNS Cancer			
SF-268	-7.20	-6.63	-6.16
SF-295	-7.51	-7.06	-6.04
SF-539	-7.35	-6.71	-6.07
SNB-19	-6.92	-6.56	-6.20
SNB-75	-7.04	-6.36	-5.58
U251	-7.60	-7.07	-6.45
Melanoma			
LOX IMVI	-7.53	-7.02	-6.46
MALME-3M	-7.57	-7.09	-6.40
M14	-7.30	-6.75	-6.32
MDA-MB-435	-6.99	-6.58	-6.18
SK-MEL-2	-6.88	-6.45	-6.01
SK-MEL-28	-6.77	-6.33	-5.72
SK-MEL-5	-6.90	-6.59	-6.27
UACC-257	-7.01	-6.49	-5.96
UACC-62	-6.83	-6.47	-6.11
Ovarian Cancer			
IGROV1	-6.93	-6.47	-6.00
OVCAR-3	-7.06	-6.63	-6.23
OVCAR-4	-6.67	-5.81	-5.27
OVCAR-5	-6.64	-5.98	-5.46
OVCAR-8	-7.58	-7.10	-6.39
NCI/ADR-RES	-6.84	-6.23	-5.11
SK-OV-3	-6.78	-6.30	-5.73
Renal Cancer			
786-0	-7.22	-6.72	-6.35
A498	-7.65	-6.75	-5.84
ACHN	-6.93	-6.60	-6.27
CAKI-1	-6.81	-6.45	-6.08
RXF 393	-6.90	-6.58	-6.26
SN12C	-7.35	-6.78	-6.31
TK-10	-7.47	-6.55	-5.00
UO-31	-6.88	-6.57	-6.26
Prostate Cancer			
PC-3	-7.43	-6.75	-5.95
DU-145	-7.29	-6.70	-6.21
Breast Cancer			
MCF7	-7.21	-6.58	-6.03
MDA-MB-231/ATCC	-7.17	-6.45	-5.59
BT-549	-6.84	-6.48	-6.13
T-47D	-7.08	-6.49	-5.72
MDA-MB-468	-7.22	-6.67	-6.22
Mean	-7.16	-6.58	-5.94

Figure 5.8 NCI mean graphs that illustrate the pattern activity at GI50 (50% growth inhibition), TGI (total growth inhibition) and LC50 (50% lethal concentration) response parameters in the NCI-60 cell line screen for **R10**.

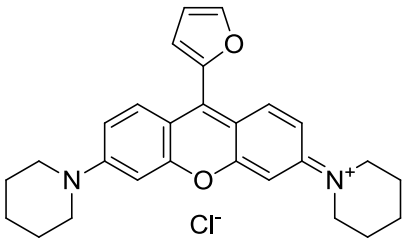

Panel/Cell Line	$Log_{10}GI50$	GI50	$Log_{10}TGI$	TGI	$Log_{10}LC50$	LC50
Leukemia						
CCRF-CEM	-7.51		-5.95		-5.00	
HL-60(TB)	-6.94		-6.32		-5.00	
K-562	-7.27		-5.94		-5.00	
MOLT-4	-7.34		-6.22		-5.00	
SR	-7.46		-6.22		-5.00	
Non-Small Cell Lung Cancer						
A549/ATCC	-7.53		-6.94		-5.48	
EKVX	-7.46		-6.67		-5.66	
HOP-62	-7.32		-6.58		-5.75	
HOP-92	-7.65		-7.04		-6.21	
NCI-H226	-6.77		-5.80		-5.00	
NCI-H23	-7.27		-6.39		-5.59	
NCI-H322M	-6.82		-6.34		-5.75	
NCI-H460	-7.46		-6.86		-5.86	
Colon Cancer						
COLO 205	-7.24		-6.71		-6.28	
HCC-2998	-7.53		-6.99		-6.42	
HCT-116	-7.57		-6.97		-6.48	
HCT-15	-7.04		-5.92		-5.33	
HT29	-7.59		-6.99		-6.22	
KM12	-7.37		-6.79		-6.35	
SW-620	-7.46		-6.85		-6.36	
CNS Cancer						
SF-268	-7.35		-6.66		-5.97	
SF-295	-7.07		-6.42		-5.70	
SF-539	-7.41		-6.73		-5.99	
SNB-19	-6.70		-5.80		-5.35	
SNB-75	-6.77		-5.94		-5.37	
U251	-7.56		-6.96		-6.38	
Melanoma						
LOX IMVI	-7.52		-6.99		-6.49	
MALME-3M	-7.62		-7.17		-6.47	
M14	-7.42		-6.76		-6.18	
MDA-MB-435	-7.43		-6.83		-6.27	
SK-MEL-2	-6.92		-5.96		-5.40	
SK-MEL-28	-7.04		-5.97		-5.40	
SK-MEL-5	-6.84		-6.47		-6.10	
UACC-257	-7.41		-6.73		-6.15	
UACC-62	-6.99		-5.96		-5.42	
Ovarian Cancer						
IGROV1	-7.31		-6.62		-5.87	
OVCAR-3	-7.44		-6.87		-6.36	
OVCAR-4	-7.17		-6.15		-5.28	
OVCAR-5	-7.17		-5.99		-5.47	
OVCAR-8	-7.54		-6.99		-6.26	
NCI/ADR-RES	-6.98		-6.28		-5.39	
SK-OV-3	-6.64		-6.14		-5.58	
Renal Cancer						
786-0	-7.43		-6.83		-6.25	
A498	-7.60		-6.62		-5.68	
ACHN	-7.47		-6.91		-6.42	
CAKI-1	-7.50		-6.98		-6.06	
RXF 393	-7.41		-6.75		-6.18	
SN12C	-7.23		-6.56		-5.95	
TK-10	-7.41		-6.06		-5.00	
UO-31	-7.58		-6.98		-6.38	
Prostate Cancer						
PC-3	-7.22		-6.08		-5.44	
DU-145	-7.14		-6.50		-5.86	
Breast Cancer						
MCF7	-7.36		-5.81		-5.00	
MDA-MB-231/ATCC	-7.42		-6.80		-6.29	
BT-549	-6.71		-6.17		-5.59	
T-47D	-7.38		-6.45		-5.37	
MDA-MB-468	-7.05		-6.41		-5.58	
Mean	-7.28		-6.51		-5.78	

3 2 1 0 -1 -2 -3 | 3 2 1 0 -1 -2 -3 | 3 2 1 0 -1 -2 -3

Figure 5.9 NCI mean graphs that illustrate the pattern activity at GI50 (50% growth inhibition), TGI (total growth inhibition) and LC50 (50% lethal concentration) response parameters in the NCI-60 cell line screen for **R11**.

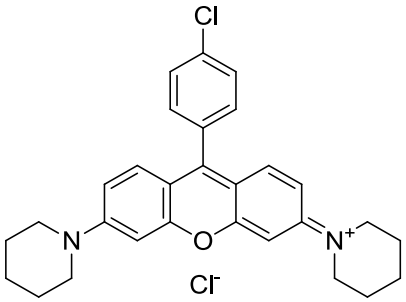

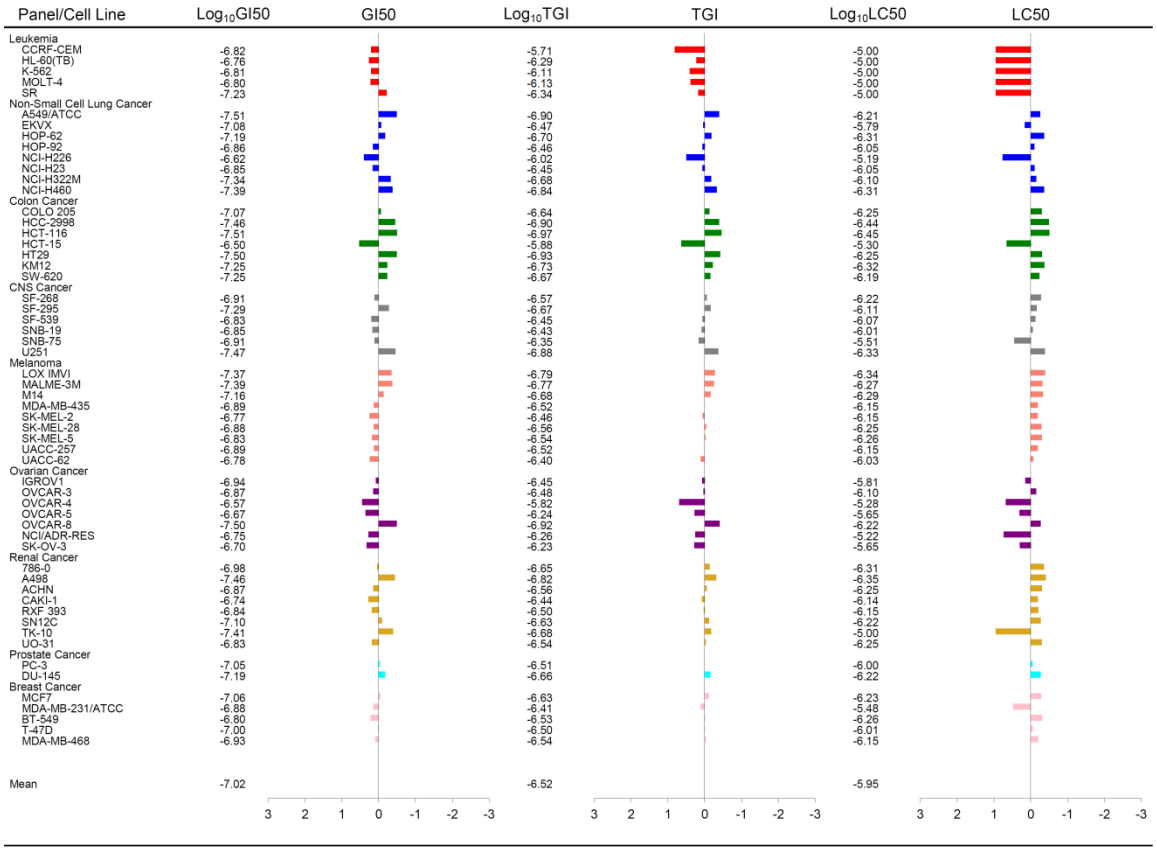

Figure 5.10 The mean graphs that illustrate the pattern activity at GI50 (50% growth inhibition), TGI (total growth inhibition) and LC50 (50% lethal concentration) response parameters in the NCI-60 cell line screen for **R13**.

For better illustration of tumour-type selectivity, box and whisker plots were constructed (Figure 5.11-5.13). Dotted line across the plot represents overall mean value of all the tested cell lines and the significant differences (p<0.05) between cell-type subpanel mean and overall mean values were determined using one sample t-test. The leukemia subpanel was significantly less sensitive towards rosamines treatment at TGI

and LC_{50} concentrations compared with other tested cell lines. Meanwhile, significant increase in sensitivity was observed in the melanoma subpanel treated with **R10** at LC_{50} value; in renal and colon subpanel treated with **R11** at TGI and LC_{50}, respectively; and in melanoma treated with **R13** at LC_{50} value.

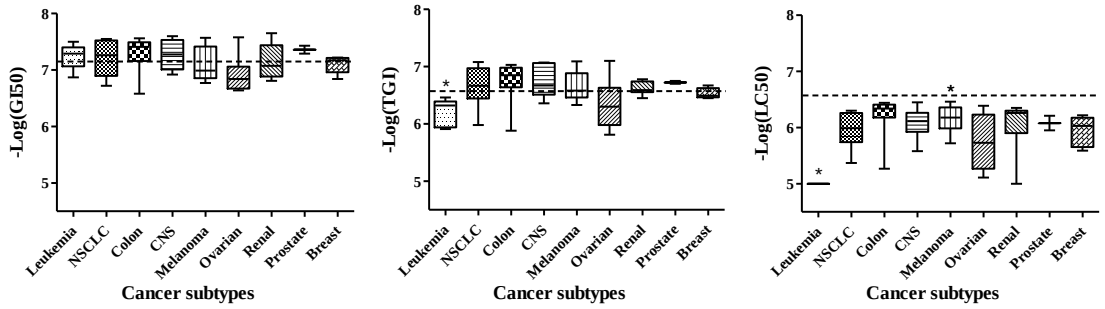

Figure 5.11 Cytotoxicity of **R10** on NCI-60 cancer subtypes. Box and whisker plots of **R10** cytotoxicity against NCI-60 cancer subtypes at GI50, TGI and LC50 values. *Difference with $p<0.05$ compared to mean value across panel of cell lines (dotted line) determined using one-sample t-tests.

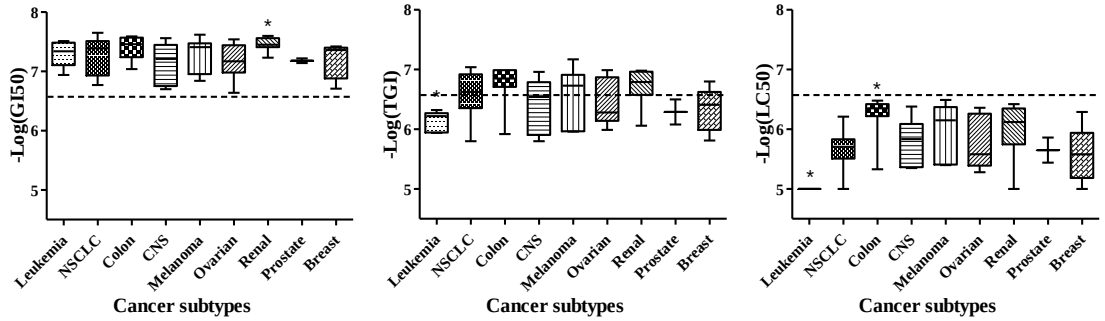

Figure 5.12 Cytotoxicity of **R11** on NCI-60 cancer subtypes. Box and whisker plots of **R11** cytotoxicity against NCI-60 cancer subtypes at A) GI50, B) TGI and C) LC50 values. *Difference with $p<0.05$ compared to mean value across panel of cell lines (dotted line) determined using one-sample t-tests.

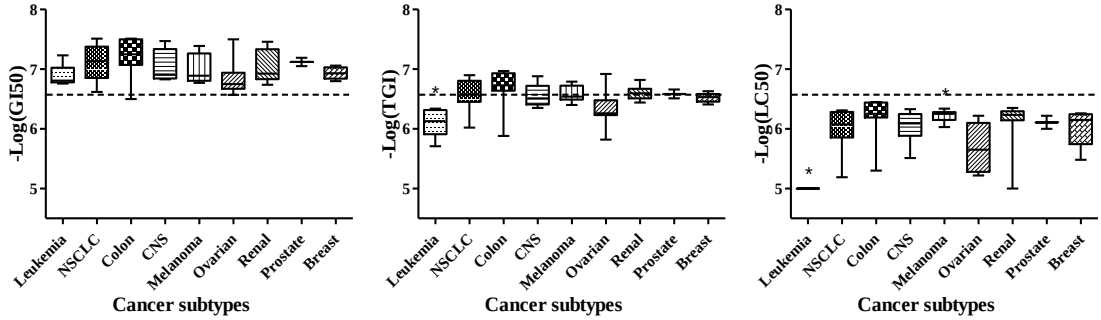

Figure 5.13 Cytotoxicity of **R13** on NCI-60 cancer subtypes. Box and whisker plots of **R13** cytotoxicity against NCI-60 cancer subtypes at A) GI50, B) TGI and C) LC50 values. *Difference with $p<0.05$ compared to mean value across panel of cell lines (dotted line) determined using one-sample t-tests.

5.3.7.3 COMPARE Analysis

The NCI COMPARE analysis allows the probable mode of action to be inferred by comparing the drug-activity patterns against standard anticancer agents with known targeting characteristics (Shoemaker 2006). COMPARE (computerised pattern-recognition algorithm) analysis utilises the mean graph profiles generated from the NCI-60 cell line screen to determine and express the degree of activity patterns similarity with Pearson Correlation Coefficient (PCC) values. PCC values >0.6 are considered to indicate similarities on the basis of chemical structure and mechanism of action to known agents (van Osdol et al. 1994; Weinstein et al. 1997).

In Table 5.3, COMPARE analyses indicated that both the rosamines **R10** and **R13** shared strong similarities in activity patterns with methyl violet (NSC271967), a cationic triarylmethane dye which has been formerly used in medicine for its antimicrobial, antifungal and antihelmintic properties. This class of dyes had been shown to promote mitochondrial respiratory inhibition by inhibiting ATP synthesis, dissipating mitochondrial membrane potential and inducing mitochondrial permeability

Table 5.3 COMPARE analysis of **R10**, **R11** and **R13** with standard agents at GI50 values

Rosamine (NSC No.)	PCC[a]	Compound/Class (NSC No.)	Mechanisms of action (Ref)[b]
R10 (751817)	0.72	Methyl violet dye (NSC271967) 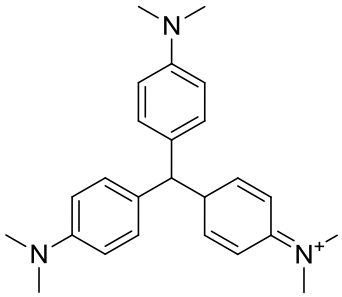	Mitochondrial respiratory inhibitor (Spikes and Bommer 1993)
	0.611	Aclacinomycin HCl (NSC654508) 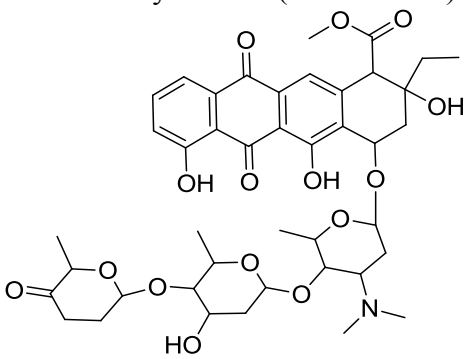	Topoisomerase II inhibitor (Nitiss et al. 1997)
	0.598	(NSCS140380) 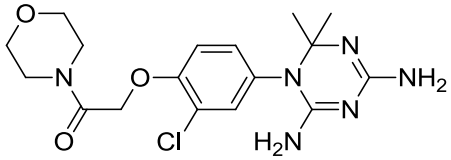	Antifolate (Andrea and Kalayeh 1991)
R11 (751818)	0.728	Acridine thioether (NSC751818) 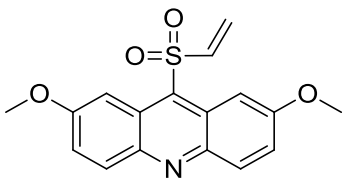	Topoisomerase I/II inhibitors (Santelli-Rouvier et al. 2004)
	0.657	Acridine thioether (NSC699927) 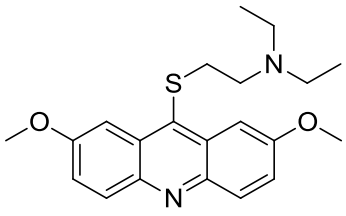	Topoisomerase I/II inhibitors (Santelli-Rouvier et al. 2004)

Table 5.3, continued

	0.657	(NSC698379) 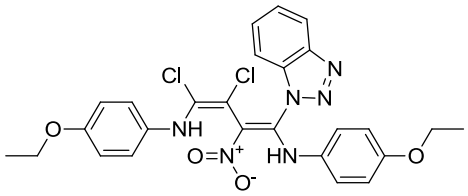	Unknown
R13 (751819)	0.767	Methyl violet dye (S271967) 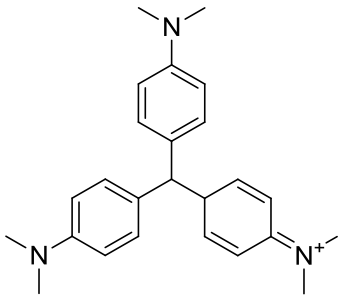	Mitochondrial respiratory inhibitor (Kowaltowski et al. 1999)
	0.644	Methyl violet BASIC BLUE 1 (S83193) 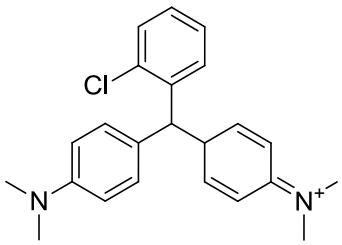	Possible mitochondrial respiratory inhibitor (Kowaltowski et al. 1999)
	0.585	Methyl violet BASIC VIOLET 3 (NSC 3090) 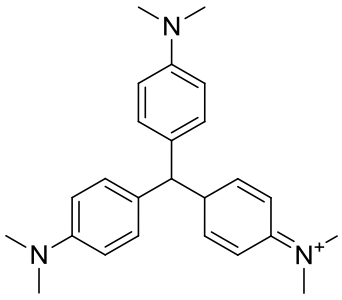	Mitochondrial respiratory inhibitor (Kowaltowski et al. 1999)

[a] PCC – Pearson correlation coefficient and PCC values >0.6 are considered to indicate a significant similarity to known agents (Weinstein et al., 1997). [b] Ref – reference.

transition (Moreno et al. 1988; Kowaltowski et al. 1999). Thus the NCI-60 cell lines screen indicated the compounds tested had a signature unique to energy metabolism-targeting anticancer agents. Data from the COMPARE analysis further confirmed our earlier findings, indicating that rosamines interfered with energy redox. Furthermore,

both the rosamines share basic structural similarity with triarylmethane dye, deferring only in the presence of an oxygen bridge.

Meanwhile, the activity patterns for **R10** also showed strong correlation with aclacinomycin, whereas **R11** was strongly correlated with acridine thioethers, where both aclacinomycin and acridine thioethers are topoisomerase I/II inhibitors (Nitiss et al. 1997; Santelli-Rouvier et al. 2004). These findings suggest that another possible anticancer mechanism of rosamines is through the inhibition of topoisomerase activity. It is thought that the planar structure of **R10** and **R11** is the contributing factor for their topoisomerase inhibition.

5.3.7.4 Cancer Genes Mutations and Drug Activity

Recent studies have indicated that mutations in cancer genes may influence cellular sensitivity to chemotherapy. For examples, p53 mutations correlate significantly with resistance to platinum-based chemotherapy in ovarian cancer patient (Reles et al. 2001), and PIK3CA mutations have been correlated with altered sensitivity to taxanes in human cancer cell lines and with treatment outcome of patients (Santarpia et al. 2008). Data from the NCI-60 screen can be used to correlate activity to specific genes mutation or differential protein expression level (Weinstein et al. 1997). A database such as the Catalogue of Somatic Mutations in Cancer (COSMIC) provides a comprehensive list of genetic mutations for the NCI-60 cell-panel (http://www.sanger.ac.uk/genetics/CGP/NCI60). Using the information obtained from COSMIC, the effects of mutations in 7 individual genes and 5 gene combinations on drug-activity were tested. The 7 individual genes consist of *TP53*, *CDKN2A*, *PTEN*, *KRAS*, *BRAF*, *APC* and *PICK3CA* which represent the most common mutations found in the NCI-60 cell-panel (Ikediobi et al. 2006). Meanwhile, the 5 gene combinations

were selected to assess the effect of mutations of multiple genes involved in the same pathway on drug activity (Ikediobi et al. 2008). For example, compound that may act on proliferative signaling pathway, cell lines mutant for either *RAS* and/or *BRAF* were group together. The following are the gene combinations and their related pathway in parenthesis: *RAS* and/or *BRAF* (MAPK signaling pathway in regulating cell proliferation); *RB1* and/or *CDKN2A* (retinoblastoma pathway in regulating cell proliferation); *KRAS* and/or *PIK3CA* (PI3K/AKT pathway in suppressing senescence); *PIK3CA* and/or *PTEN* (phosphoinositide 3-kinase pathway which regulates growth, survival, and proliferation); and *KRAS* and/or *PIK3CA* and/or *PTEN* (mTOR signaling pathway which promotes cell survival).

From the analysis (Figure 5.14 - 5.16), no statistically significant differences (Student's t-test, $p<0.05$) were observed in the activity of rosamines against cell lines with mutations either in individual genes or in combinations compared to cell lines with correspond wild-type genes. This finding indicates that the anticancer activity of rosamines was not affected by present of mutations and that they do not particularly target any signaling pathway involves in tumourigenesis. Since we have shown that rosamines inhibit the oxidative phosphorylation pathway, it would be interesting to investigate if different cellular bioenergetics of the NCI-60 cell lines such as mitochondrial respiration and glycolysis levels would affect rosamines activity. However, at present time, there is no report on the cellular bioenergetics of NCI-60.

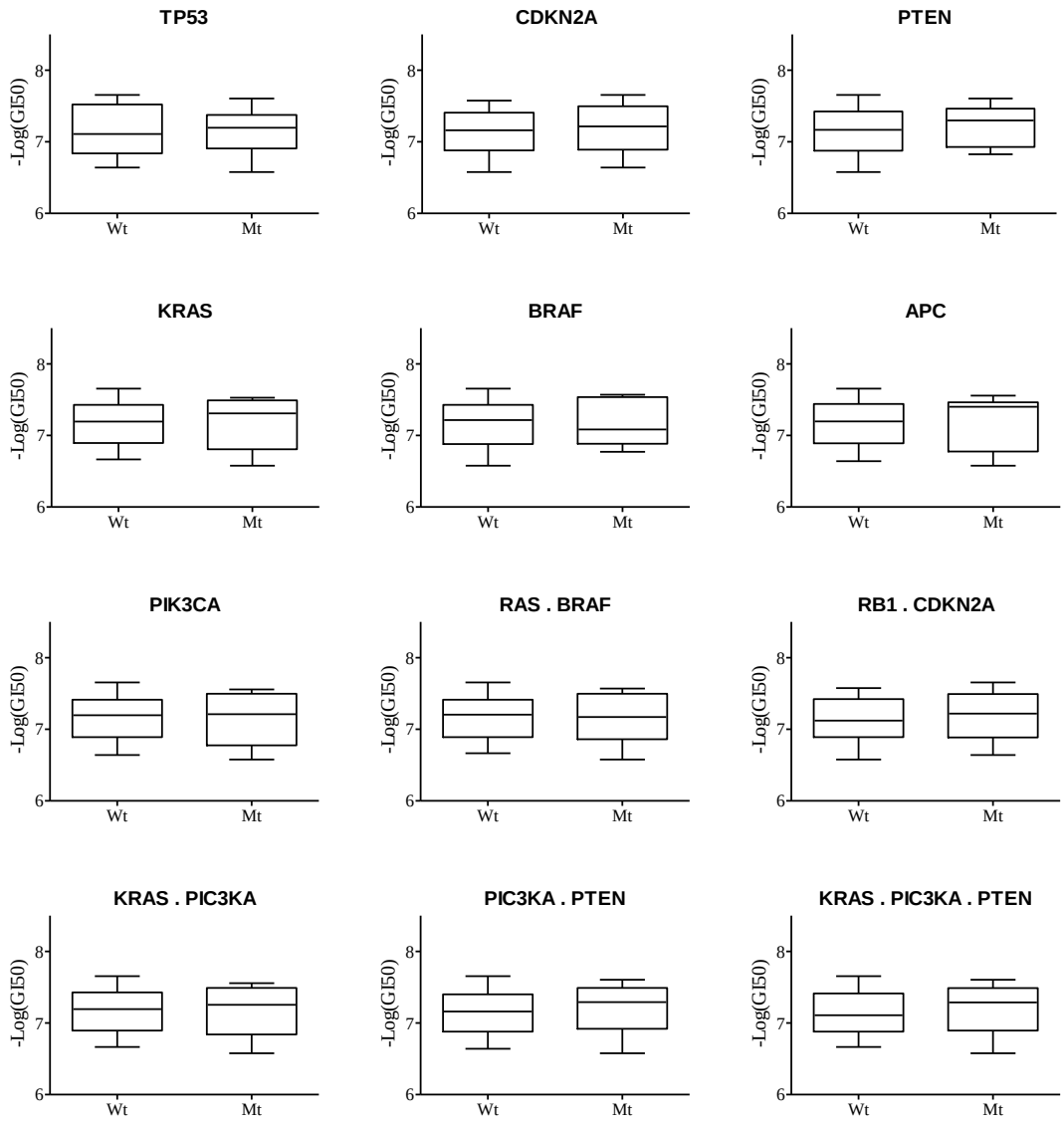

Figure 5.14 Box and whisker plots of the -$\log_{10}$ (GI50) values of **R10** tested in wild type (Wt) and mutant (Mt) cell lines of the NCI-60 for twelve gene categories. Larger -$\log_{10}$ (GI50) values indicate increased sensitivity to the drug compound.

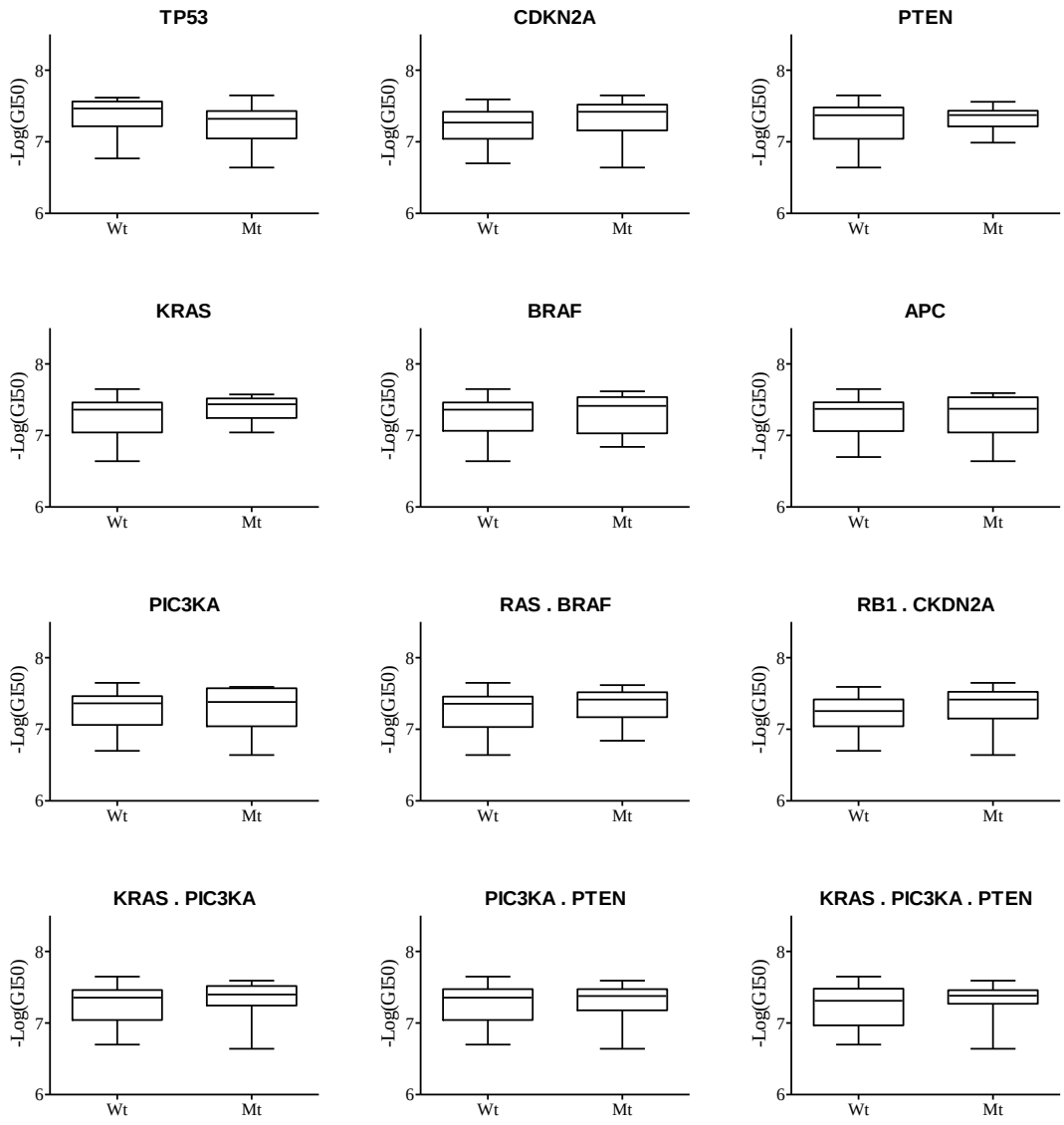

Figure 5.15 Box and whisker plots of the -$\log_{10}$ (GI50) values of **R11** tested in wild type (Wt) and mutant (Mt) cell lines of the NCI-60 for twelve gene categories. Larger -$\log_{10}$ (GI50) values indicate increased sensitivity to the drug compound.

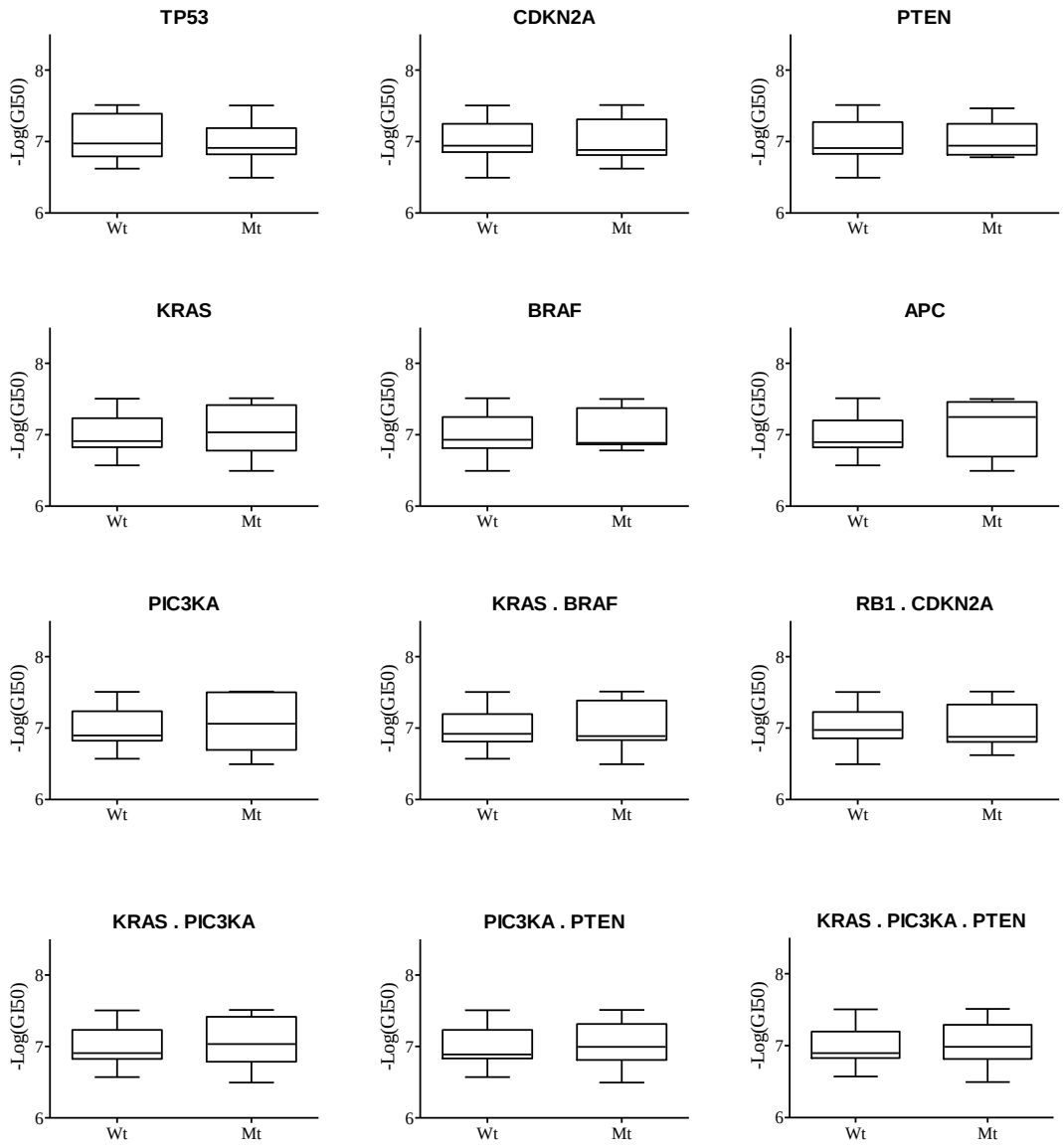

Figure 5.16 Box and whisker plots of the -$\log_{10}$ (GI50) values of R13 tested in wild type (Wt) and mutant (Mt) cell lines of the NCI-60 for twelve gene categories. Larger -$\log_{10}$ (GI50) values indicate increased sensitivity to the drug compound.

5.4 Conclusions

The photophysical properties of rosamine could be fine-tuned by minor modification such as cyclic-amine and meso-aryl substitutions hence rendering them ideal as photosensitiser in contrast to tetrapyrrole-based photosensitiser. However, these modifications did not improved the photodynamic efficiency of rosamine but enhanced their non-PDT induced cytotoxicity. Therefore, their *in vitro* antiproliferative activities against a panel of cell lines from leukemia and solid tumours were investigated instead. SAR study indicated the importance of having hydrophobic substituents at the peripheral cyclic-amines as well as at the *meso*-aryl groups. Structures with aryl substituents at the *meso* position, either directly attached or througha -CH_2- spacer conferred extra activity. The most active compounds **R10** and **R15** were at least 10-fold more potent than Rh123, a structurally similar compound whose anticancer properties have been extensively investigated.

Fluorescence microscopy studies showed that rosamine localises exclusively within the mitochondria. This, together with data from cell cycle analysis and onset of apoptosis studies, suggests that rosamine-induced cell death through mitochondria-dependent apoptosis rather than through damage to nucleic materials. The anticancer effects of these compounds were associated with their ability to compromise mitochondrial membrane potential and to inhibit the oxidative phosphorylation complexes primarily the ATP synthase (Figure 4.18). This observation was further confirmed by COMPARE analysis of the NCI-60 screen data that rosamine activity had a strong correlation in growth inhibitory pattern with that exhibited by a mitochondrial respiratory inhibitor i.e. crystal violet.

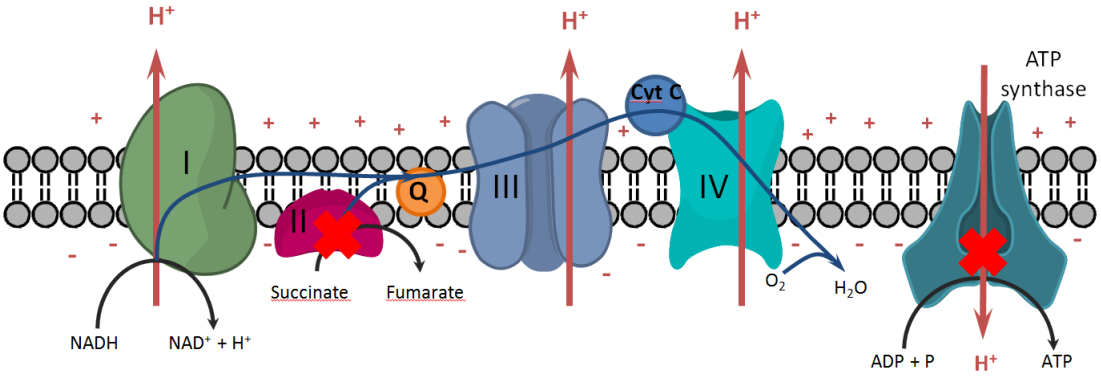

Figure 5.17 The inhibition of rosamines on the oxidative phosphorylation pathway complexes i.e Complex II and ATP synthase which were associated with cell death and loss of mitochondrial transmembrane potential.

Although the *in vivo* antitumour effects of **R10** was moderate against 4T1 murine mammary tumour, it may be worthwhile to test the compound in colon cancer models for example models based on HCT-116 and HT-29 cell lines as both were more sensitive to **R10** based on the NCI-60 cell line screen. Without a doubt, proper strategies need to be devised to deliver and enhance tumour uptake of rosamines for example by integration to carrier molecules to improve safety and therapeutic outcome. Overall, our results suggest that these compounds offer a unique potential for the design of mitochondrial targeting agents that either directly kill or deliver cytotoxic drugs to selectively kill cancer cells.

CHAPTER 6

General Discussion and Recommendation of Future Research

6.1 General Discussion

The discovery and development pathway of photosensitisers in general is very similar to that for conventional therapeutics. The major difference lies in the incorporation of photo-property assays into the development schedule. As with conventional therapeutics, one of the major reasons for new compound synthesis is to improve selectivity, and therefore therapeutic efficacy. New compounds may have altered hydrophilic/lipophilic balance that may improve cellular uptake and pharmacology /pharmacokinetic profiles. New compound synthesis may also affect the photosensitising properties of the compounds. The main goal of photosensitiser design is to develop photosensitisers with the most ideal characteristics as mentioned in Section 2.3.1.

Throughout the modern era of PDT research, the discovery and development of photosensitiser had evolved around porphyrins. As discussed in Section 2.3.2, much of these efforts focus on optimising or synthesis of tetrapyrrole-based chromophores such as chlorins, bacteriochlorins and phthalocyanines as potential improvements for anticancer application. However, challenges in synthesis and purification of tetrapyrroles have restricted modulation of their photophysical and biological properties through chemical derivatisation during drug development. Therefore, there is an interest among photodynamic research groups in discovering other tetrapyrrole and non-tetrapyrrole photosensitisers that might be more synthetically accessible.

One of the approaches of discovering new photosensitiser chromophore is through natural product screening. It cannot be denied that natural product has made invaluable contribution to drug discovery for potential anticancer agents and as source for photosensitiser discovery used in modern PDT. However, bio-assay guided isolation for photosensitiser from natural resources often leads to identification of known or derivatives of cyclic tetrapyrrolic based photosensitiser. In our attempts to tap into Malaysia natural resources for new photosensitisers, approximately 300 plant extracts that exhibited photocytotoxicity were subjected to dereplication by using liquid chromatography mass spectrometry coupled with principal component analysis (LCMS-PCA) technique. From the study, only eight photosensitisers were identified and importantly, they were all based on the cyclic tetrapyrrole structure. These photosensitisers were probably degradation products from the ubiquitous plant chlorophylls (Kessel 1992).

On the other hand, biological stains mainly used as fluorescence probes or histological stains may be an alternative source for photosensitiser drug discovery. Such examples include the class of compounds belonging to acridine, phenothiazinium, xanthene and BODIPY (see Section 2.3.3). Typically, they have high absorption extinction coefficients, high quantum efficiencies of fluorescence, relative insensitivity to environment and resistance to photobleaching. As fluorescence occurs through relaxation from singlet excited state, high quantum yield for fluorescence is undesirable since much of the energy absorbed on excitation would not cross to the triplet states. However, fluorescence quantum yield could be converted to singlet-to-triplet intersystem crossing quantum yield (to facilitate generation of reactive singlet oxygen) through compound modification. More importantly, their ease in synthesis (through chromophoric extension and auxochromic functionalisation) and purification allows for

large quantities of pure photosensitiser to be prepared, thereby making them more commercially viable.

In Chapter 3, we had shown that conjugation of G2 with ionisable amino acids was able to alter their photosensitising efficacies by modifying multiple parameters i.e absorption coefficient, singlet oxygen quantum yield, cellular uptake, photostability and intracellular localisation. These G2-derived photosensitisers had absorption wavelength > 660 nm wavelength which allow deeper access into biological tissue for effective treatment of larger or deep-seated lesion. Although both the lysine and aspartic acid conjugation successfully increased the aqueous solubility of G2, the conjugation had resulted in the loss *in vitro* PDT efficiencies especially with lysine. When evaluated in physiological setting, G2-Asp however was able to achieve equivalent *in vivo* PDT efficacies as G2 in both the CAM model and the *in vivo* mouse tumour model. Given the hydrophilic nature of G2-Asp, the photosensitiser is a pharmaceutically advantageous candidate as it can be formulated easily for administration and reduces the risk of vascular aggregation.

In Chapter 4, we had shown that BODIPY is a good chomophore candidate to be developed as a photosensitiser since their photophysical properties such as λ_{abs} and molar extinction coefficient of BODIPY could be fine-tuned by minor modification to the chromophore core for examples; iodination on the BODIPY pyrollic carbon resulted in red-shift λ_{abs} and higher singlet oxygen generation, while extended conjugation at similar position shifts the λ_{abs} to the red. BODIPY was found to induce cell death through mitochondria-dependent apoptosis following photosensitisation and was able to occlude the vasculature network in the CAM *in vivo* model. These findings further substantiated its potential to be explored as a clinically useful agent for PDT of cancer.

The BODIPY studied here had a relatively short absorption wavelength ranging from 500-580 nm. Although photosensitisers with excitation > 600 nm wavelength allow deeper access into biological tissue for effective treatment of larger or deep-seated lesion, these shorter wavelength absorbing BODIPYs may be preferred in treatment of superficial lesion tissues such as basal cell carcinoma, melanoma or mucosal carcinoma of hollow organs. For example, rose Bengal with 549 nm excitation wavelength has been used successfully for the treatment of metastatic melanoma in a Phase II clinical trial and is currently being investigated in Phase I trial for treatment of cutaneous and subcutaneous tumours under compassionate use. In addition, in a clinical PDT study for superficial cancer in the esophagus and bronchi with porfimer sodium, treatment regime with light corresponding to the 514 nm excitation wavelength exhibited similar effectiveness as that with 630 nm in terms of tumour eradication but, significantly, with less damage of the deep tissues which could cause perforation on the esophagus (Grosjean et al. 1998).

Another group of compounds that we evaluated for PDT efficacy belongs to a new class of rosamine derivatives (Chapter 5). Like the BODIPY, their photophysical properties such as λ_{abs} and molar extinction coefficient could be modulated by minor modification to the chromophore core for examples; cyclic-amine substitution particularly with piperidine drastically improved the compound absorptivity, while, substitution of meso-aryl with heterocyclic or phenyl-halide red-shifted the λ_{abs}. Such modifications however were not sufficient for the compounds to produce potent photo-induced cytotoxicity. Probably this could be due to the lack of conversion yield of the compounds to triplet excited state following light irradiation, a process that controls the singlet oxygen production. To overcome this, conjugation of heavy atom such as chlorine, bromine and iodine to the chromophore core, or substitution of the oxygen

bridge with heavier chalcogen atoms may enhance the crossing of singlet to triplet state, a phenomenon known as “heavy atom effects”.

Despite lack of photodynamic efficacies, several of the rosamines having hydrophobic cyclic-amines and meso-aryl substituents exhibited potent cytotoxic effects. These compounds were found to localise in the mitochondria and induced apoptotic cell death which was associated with membrane potential loss and inhibition of oxidative phosphorylation enzymes activity. Nevertheless, the lead rosamine (**R10**) evaluated in *in vivo* model only exhibited modest antitumour activity probably due to insufficient drugs concentration administered. However the use of higher drug doses in the study was limited by adverse side-effects. As in the case of doxorubin as discussed in Section 5.3.7, liposomal formulation possibly may reduce the adverse side-effects and higher drug doses could then be used to evaluate its antitumour efficacies.

It is interesting to point out that both the BODIPY and rosamine localised particularly well in the mitochondria. Numerous studies have shown that the mitochondrial membrane potential of carcinoma cells is higher than in normal epithelial cells and that the accumulation and retention of lipophilic cations correlated with the mitochondrial membrane potential (Lampidis et al. 1985; Modica-Napolitano and Aprille 2001). The increase in mitochondrial membrane potential in carcinoma cells had led to selective accumulation of toxic lipophilic cations, thereby providing a rationale for treatment selectivity. This is feasible because mitochondria are the main energy generators which maintain cell life and are involved in diverse cellular events by being an integral part of multiple signaling cascades in regulation of metabolism, cell cycle control, development, and cell death (McBride et al. 2006). Furthermore, reprogramming of energy metabolism has been identified as one of the emerging hallmarks of cancer and mitochondria are recognised as a potential anticancer targets (Hanahan and Weinberg 2011).

Targeting the mitochondria is a viable strategy because the lack of selectivity of current conventional cancer chemotherapy that acts by interrupting DNA replication, i.e. by inhibiting the synthesis or function of new nucleic materials, or by causing irreparable damage to vital nucleic acids through intercalation, alkylation or enzymatic inhibition had resulted in unwarranted side-effects. On the other hand, contemporary chemotherapeutic strategies that target signaling pathways or particular gene products tend to be limited to cancers driven by a dominant oncogene and are often vulnerable to resistance through the multiplicity of tumourigenesis signaling pathways (Lemmon and Schlessinger 2010). For example, most of the HER-2 positive metastatic breast cancer patients who initially responded to treatment with trastuzumab developed secondary trastuzumab resistance within a year after the treatment began (Nahta and Esteva 2007). Similar observations have been made for BRAF-targeted vemurafenib for melanoma therapy (Alcala and Flaherty 2012) and EGFR-targeted gefitinib or erlotinib for the treatment of non-small cell lung cancer (Ayoola et al. 2012). In contrast, mitochondria is a cellular targets that all cancer cells have in common, especially those in metastatic cancers and therefore, shutting down the mitochondria either by photosensitisation or toxic lipophilic cations insult, will disrupt essential cellular functions that subsequently can lead to cell death.

Over the years, the used of PDT for cancer treatment has increased tremendously as clinicians started to recognise the advantages that PDT holds over conventional therapy for cancer such as surgery, chemotherapy and radiotherapy. The non-invasive procedure of PDT is specifically useful for treating lesions which are anatomical challenging, for favorable cosmetic outcomes and repeat treatments can be performed when necessary without the risk of resistance development. In a recent match cohort comparison study, it has shown that PDT is able to achieve disease control and survival at comparable rates to trans-oral surgery in treating patients with early stage

oral cavity squamous cell cancer (Karakullukcu et al. 2013). Because of the tissue sparing properties of PDT, this has rendered the used of PDT as an alternative treatment for early stage cancer especially attractive in patients with extensive malignant lesions. It is hope that in the future, PDT may become an integrated part of the mainstays for cancer therapy.

6.2 Recommendation of Future Research

Data from G2 study showed that complete tumour regression was observed in two out of eight mice treated with G2-Asp. Therefore, it would be interesting to investigate whether higher number of complete tumour regression could be achieved by performing multiple PDT. Unlike chemotherapy and radiotherapy, PDT has no cumulative toxicity or does not cause the development of resistance clones. In addition, the photosensitiser pharmacokinetics parameters for example uptake/clearance in tumour tissues need to be understood further to ascertain the optimal time interval between drug administration and light irradiation.

Data from our study offer invaluable SAR information for synthesis of second generation BODIPY and rosamines with improved PDT efficacies. For BODIPY, the relatively short λ_{abs} could be increased by benzylation at the position as shown in Figure 6.1. Attachment of electron donating groups (i.e. benzyl) is known to red-shift the absorption though with the expense of increasing lipophilicity. Highly lipophilic photosensitisers tend to have poor aqueous solubility and might pose a challenge in drug delivery during clinical development. Therefore, attachment of hydrophilic substituents such as carboxylates or sulphonates may be considered to improve their solubility.

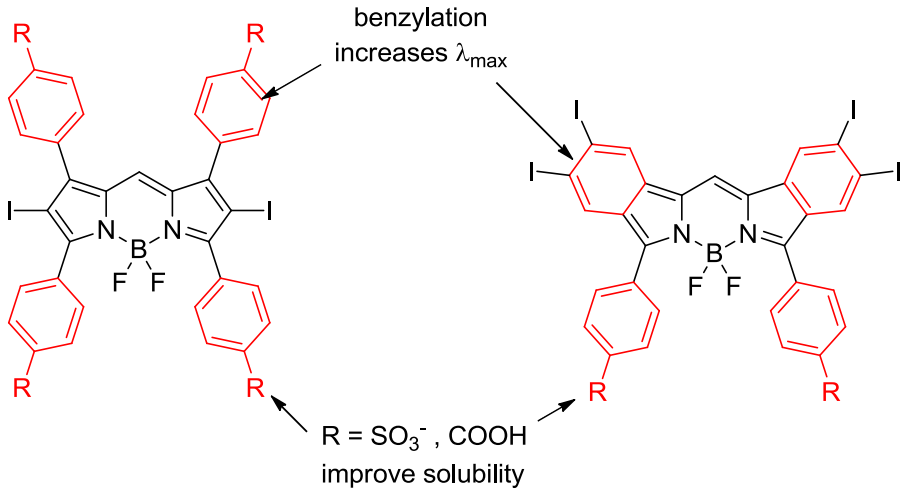

Figure 6.1 Potential structural modification (in red) on BOBIPY chromophore to improve its PDT efficacies.

Meanwhile for the cyclic-amine rosamines, their photosensitising efficacy i.e. singlet oxygen production could be increased by heavy chalcogen atoms substitution at the central heteroatom or by halogenation of carbon adjacent to the core. The additions of akyl or aryl moieties to the chromophore will extent the λ_{abs} to the red. It is also essential to consider the addition of hydrophilic substituents such as carboxylates or sulphonates to improve the hydrophilicity of these rosamines (Figure 6.2).

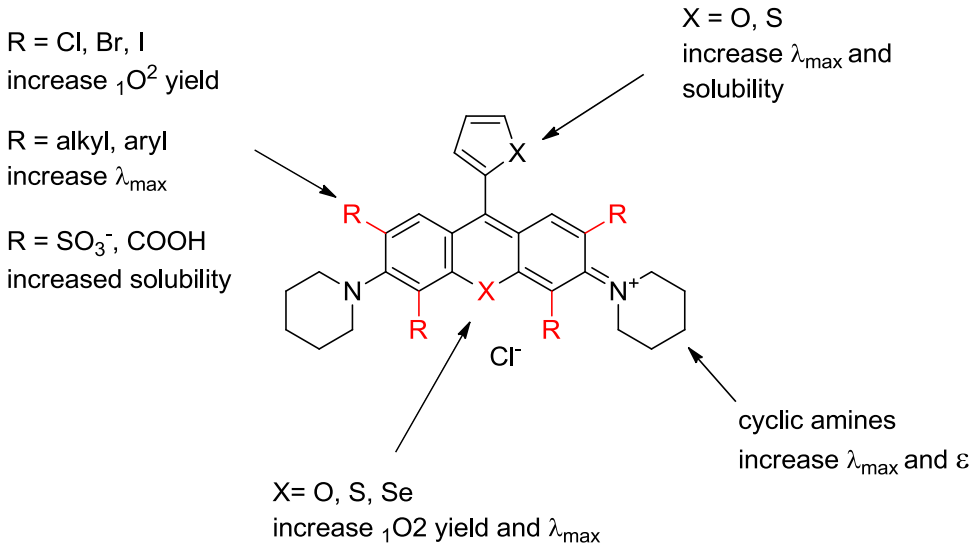

Figure 6.2 Potential structural modification (in red) on rosamine chromophore to improve its PDT efficacies.

For downstream development of BODIPY as photosensitiser, it would be interesting to investigate their efficacy in *in vivo* tumour model. Since the BODIPY studied here possessed slightly shorter excitation wavelength and that non-invasive delivery of light was almost limited to the skin and oral cavity, it is recommended to evaluate their efficiency in superficial embedded tumour model. For this, we would propose the use of dimethylbenz[a]anthracene (DBMA) -induced hamster cheek pouch tumour model which is a well-characterised squamous cell carcinoma model that histologically mimics human oral cancers. Furthermore, the check pouch can be readily inverted for local irradiation and macroscopic follow up. As for the rosamines, it is suggested that their *in vivo* antitumour efficacies are evaluated in the sensitive HCT-116 and HT-29 tumour cell lines based on the NCI-60 *in vitro* screen data. Further formulation would be required to reduce the toxicity of the rosamines, which may also improve their potency and pharmacokinetic properties.

References

Abdel-Hady, E. S., Martin-Hirsch, P., Duggan-Keen, M., Stern, P. L., Moore, J. V., Corbitt, G., Kitchener, H. C. & Hampson, I. N. (2001) Immunological and viral factors associated with the response of vulval intraepithelial neoplasia to photodynamic therapy. *Cancer Res.* **61**(1): 192-196.

Agarwal, M. L., Clay, M. E., Harvey, E. J., Evans, H. H., Antunez, A. R. & Oleinick, N. L. (1991) Photodynamic therapy induces rapid cell death by apoptosis in L5178Y mouse lymphoma cells. *Cancer Res.* **51**(21): 5993-5996.

Agostinis, P., Berg, K., Cengel, K. A., Foster, T. H., Girotti, A. W., Gollnick, S. O., Hahn, S. M., Hamblin, M. R., Juzeniene, A., Kessel, D., Korbelik, M., Moan, J., Mroz, P., Nowis, D., Piette, J., Wilson, B. C. & Golab, J. (2011) Photodynamic therapy of cancer: an update. *CA Cancer J Clin.* **61**(4): 250-281.

Aiken, M. J., Suhag, V., Garcia, C. A., Acio, E., Moreau, S., Priebat, D. A., Chennupati, S. P. & Van Nostrand, D. (2009) Doxorubicin-induced cardiac toxicity and cardiac rest gated blood pool imaging. *Clin Nucl Med.* **34**(11): 762-767.

Alcala, A. M. & Flaherty, K. T. (2012) BRAF inhibitors for the treatment of metastatic melanoma: clinical trials and mechanisms of resistance. *Clin Cancer Res.* **18**(1): 33-39.

Ali, H. & van Lier, J. E. (1999) Metal complexes as photo- and radiosensitizers. *Chem Rev.* **99**(9): 2379-2450.

Allison, R. R. & Sibata, C. H. (2010) Oncologic photodynamic therapy photosensitizers: a clinical review. *Photodiagnosis Photodyn Ther.* **7**(2): 61-75.

Andrea, T. A. & Kalayeh, H. (1991) Applications of neural networks in quantitative structure-activity relationships of dihydrofolate reductase inhibitors. *J Med Chem.* **34**(9): 2824-2836.

Atilgan, S., Ekmekci, Z., Dogan, A. L., Guc, D. & Akkaya, E. U. (2006) Water soluble distyryl-boradiazaindacenes as efficient photosensitizers for photodynamic therapy. *Chem Commun (Camb).*(42): 4398-4400.

Aveline, B. M., Hasan, T. & Redmond, R. W. (1994) Photophysical and photosensitizing properties of benzoporphyrin derivative monoacid ring A (BPD-MA). *Photochem Photobiol.* **59**(3): 328-335.

Aveline, B. M., Hasan, T. & Redmond, R. W. (1995) The effects of aggregation, protein binding and cellular incorporation on the photophysical properties of benzoporphyrin derivative monoacid ring A (BPDMA). *J Photochem Photobiol B.* **30**(2-3): 161-169.

Ayoola, A., Barochia, A., Belani, K. & Belani, C. P. (2012) Primary and acquired resistance to epidermal growth factor receptor tyrosine kinase inhibitors in non-small cell lung cancer: an update. *Cancer Invest.* **30**(5): 433-446.

Belitchenko, I., Melnikova, V., Bezdetnaya, L., Rezzoug, H., Merlin, J. L., Potapenko, A. & Guillemin, F. (1998) Characterization of photodegradation of meta-tetra(hydroxyphenyl)chlorin (mTHPC) in solution: biological consequences in human tumor cells. *Photochem Photobiol.* **67**(5): 584-590.

Berthod, A. & Carda-Broch, S. (2004) Determination of liquid-liquid partition coefficients by separation methods. *J Chromatogr A.* **1037**(1-2): 3-14.

Betrouni, N., Lopes, R., Puech, P., Colin, P. & Mordon, S. (2011) A model to estimate the outcome of prostate cancer photodynamic therapy with TOOKAD Soluble WST11. *Phys Med Biol.* **56**(15): 4771-4783.

Biasutto, L., Dong, L. F., Zoratti, M. & Neuzil, J. (2010) Mitochondrially targeted anti-cancer agents. *Mitochondrion.* **10**(6): 670-681.

Boyd, M. R. & Paull, K. D. (1995) Some practical considerations and applications of the national cancer institute in vitro anticancer drug discovery screen. *Drug Dev Res.* **34**(2): 91-109.

Brancaleon, L. & Moseley, H. (2002) Laser and non-laser light sources for photodynamic therapy. *Lasers Med Sci.* **17**(3): 173-186.

Brown, S. B. & Truscott, T. G. (1993) " New light on cancer therapy". *Chem Br.* **29**: 955-958.

Burghart, A., Kim, H. R., Welch, M. B., Thoresen, L. H., Reibenspies, J., Burgess, K., Bergström, F. & Johansson, L. B. Å. (1999) 3,5-Diaryl-4,4-difluoro-4-bora-3a,4a-diaza-s-indacene (BODIPY) Dyes: Synthesis, Spectroscopic, Electrochemical, and Structural Properties. *J Org Chem.* **64**(21): 7813-7819.

Buytaert, E., Dewaele, M. & Agostinis, P. (2007) Molecular effectors of multiple cell death pathways initiated by photodynamic therapy. *Biochim Biophys Acta.* **1776**(1): 86-107.

Byrne, A. T., O'Connor, A. E., Hall, M., Murtagh, J., O'Neill, K., Curran, K. M., Mongrain, K., Rousseau, J. A., Lecomte, R., McGee, S., Callanan, J. J., O'Shea, D. F. & Gallagher, W. M. (2009) Vascular-targeted photodynamic therapy with BF2-chelated Tetraaryl-Azadipyrromethene agents: a multi-modality molecular imaging approach to therapeutic assessment. *Br J Cancer.* **101**(9): 1565-1573.

Calitree, B., Donnelly, D. J., Holt, J. J., Gannon, M. K., Nygren, C. L., Sukumaran, D. K., Autschbach, J. & Detty, M. R. (2007) Tellurium Analogues of Rosamine and Rhodamine Dyes: Synthesis, Structure, 125Te NMR, and Heteroatom Contributions to Excitation Energies. *Organometallics.* **26**(25): 6248-6257.

Castano, A. P., Demidova, T. N. & Hamblin, M. R. (2004) Mechanisms in photodynamic therapy: part one - photosensitizers, photochemistry and cellular localization. *Photodiag Photodyn Ther.* **1**: 279-293.

Castano, A. P., Demidova, T. N. & Hamblin, M. R. (2005) Mechanisms in photodynamic therapy: part two—cellular signaling, cell metabolism and modes of cell death. *Photodiag Photodyn Ther.* **2**(1): 1-23.

Castano, A. P., Mroz, P. & Hamblin, M. R. (2006) Photodynamic therapy and anti-tumour immunity. *Nat Rev Cancer.* **6**(7): 535-545.

Celli, J. P., Solban, N., Liang, A., Pereira, S. P. & Hasan, T. (2011) Verteporfin-based photodynamic therapy overcomes gemcitabine insensitivity in a panel of pancreatic cancer cell lines. *Lasers Surg Med.* **43**(7): 565-574.

Chee, C. F., Lee, H. B., Ong, H. C. & Ho, A. S. (2005) Photocytotoxic pheophorbide-related compounds from Aglaonema simplex. *Chem Biodivers.* **2**(12): 1648-1655.

Chen, B., Pogue, B. W., Hoopes, P. J. & Hasan, T. (2006a) Vascular and cellular targeting for photodynamic therapy. *Crit Rev Eukaryot Gene Expr.* **16**(4): 279-305.

Chen, B., Pogue, B. W., Luna, J. M., Hardman, R. L., Hoopes, P. J. & Hasan, T. (2006b) Tumor vascular permeabilization by vascular-targeting photosensitization: effects, mechanism, and therapeutic implications. *Clin Cancer Res.* **12**(3 Pt 1): 917-923.

Chen, M., Liu, X. & Fahr, A. (2011) Skin penetration and deposition of carboxyfluorescein and temoporfin from different lipid vesicular systems: In vitro study with finite and infinite dosage application. *Int J Pharm.* **408**(1-2): 223-234.

Cruess, A. F., Zlateva, G., Pleil, A. M. & Wirostko, B. (2009) Photodynamic therapy with verteporfin in age-related macular degeneration: a systematic review of efficacy, safety, treatment modifications and pharmacoeconomic properties. *Acta Ophthalmol.* **87**(2): 118-132.

David, E., Lejeune, J., Pellet-Rostaing, S., Schulz, J., Lemaire, M., Chauvin, J. & Deronzier, A. (2008) Synthesis of fluorescent rhodamine dyes using an extension of the Heck reaction. *Tetrahedron Letters.* **49**(11): 1860-1864.

Davidson, S. R., Weersink, R. A., Haider, M. A., Gertner, M. R., Bogaards, A., Giewercer, D., Scherz, A., Sherar, M. D., Elhilali, M., Chin, J. L., Trachtenberg, J. & Wilson, B. C. (2009) Treatment planning and dose analysis for interstitial photodynamic therapy of prostate cancer. *Phys Med Biol.* **54**(8): 2293-2313.

De Felice, E. (2010) Shedding light: laser physics and mechanism of action. *Phlebology.* **25**(1): 11-28.

Debefve, E., Cheng, C., Schaefer, S. C., Yan, H., Ballini, J. P., van den Bergh, H., Lehr, H. A., Ruffieux, C., Ris, H. B. & Krueger, T. (2010) Photodynamic therapy induces selective extravasation of macromolecules: Insights using intravital microscopy. *J Photochem Photobiol B.* **98**(1): 69-76.

DeRosa, M. C. & Crutchley, R. J. (2002) Photosensitized singlet oxygen and its applications. *Coordination Chem Rev.* **233–234**(0): 351-371.

Detty, M. R., Prasad, P. N., Donnelly, D. J., Ohulchanskyy, T., Gibson, S. L. & Hilf, R. (2004) Synthesis, properties, and photodynamic properties in vitro of heavy-chalcogen analogues of tetramethylrosamine. *Bioorg Med Chem.* **12**(10): 2537-2544.

Dewaele, M., Maes, H. & Agostinis, P. (2010) ROS-mediated mechanisms of autophagy stimulation and their relevance in cancer therapy. *Autophagy.* **6**(7): 838-854.

Dimofte, A., Zhu, T. C., Hahn, S. M. & Lustig, R. A. (2002) In vivo light dosimetry for motexafin lutetium-mediated PDT of recurrent breast cancer. *Lasers Surg Med.* **31**(5): 305-312.

Dolmans, D. E., Fukumura, D. & Jain, R. K. (2003) Photodynamic therapy for cancer. *Nat Rev Cancer.* **3**(5): 380-387.

Don, A. S. & Hogg, P. J. (2004) Mitochondria as cancer drug targets. *Trends Mol Med.* **10**(8): 372-378.

Ethirajan, M., Saenz, C., Gupta, A., Dobhal, M. P. & Pandey, R. K. (2008) Photosensitizers for photodynamic therapy and imaging. Advances in photodynamic therapy: Basic, translational, and clinical. R. H. Michael and M. Pawel. Boston, MA, USA, Artech House**:** 13-39.

Feng, X. & Senge, M. O. (2001) An efficient synthesis of highly functionalized asymmetric porphyrins with organolithium reagents. *Journal of the Chemical Society, Perkin Transactions 1.*(9): 1030-1038.

Fernandez, J. M., Bilgin, M. D. & Grossweiner, L. I. (1997) Singlet oxygen generation by photodynamic agents. *J Photochem Photobiol B.* **37**(1): 131-140.

Fotinos, N., Campo, M. A., Popowycz, F., Gurny, R. & Lange, N. (2006) 5-Aminolevulinic acid derivatives in photomedicine: Characteristics, application and perspectives. *Photochem Photobiol.* **82**(4): 994-1015.

Frezza, C., Cipolat, S. & Scorrano, L. (2007) Organelle isolation: functional mitochondria from mouse liver, muscle and cultured fibroblasts. *Nat Protoc.* **2**(2): 287-295.

Garg, A. D., Nowis, D., Golab, J. & Agostinis, P. (2010) Photodynamic therapy: illuminating the road from cell death towards anti-tumour immunity. *Apoptosis.* **15**(9): 1050-1071.

Garland, M. J., Cassidy, C. M., Woolfson, D. & Donnelly, R. F. (2009) Designing photosensitizers for photodynamic therapy: strategies, challenges and promising developments. *Future Med Chem.* **1**(4): 667-691.

Gelderblom, H., Verweij, J., Nooter, K. & Sparreboom, A. (2001) Cremophor EL: the drawbacks and advantages of vehicle selection for drug formulation. *Eur J Cancer.* **37**(13): 1590-1598.

Gerebtzoff, G., Li-Blatter, X., Fischer, H., Frentzel, A. & Seelig, A. (2004) Halogenation of drugs enhances membrane binding and permeation. *Chembiochem.* **5**(5): 676-684.

Godal, A., Nilsen, N. O., Klaveness, J., Branden, J. E., Nesland, J. M. & Peng, Q. (2006) New derivatives of 5-aminolevulinic acid for photodynamic therapy: chemical synthesis and porphyrin production in in vitro and in vivo biological systems. *J Environ Pathol Toxicol Oncol.* **25**(1-2): 109-126.

Gollnick, S. O., Vaughan, L. & Henderson, B. W. (2002) Generation of effective antitumor vaccines using photodynamic therapy. *Cancer Res.* **62**(6): 1604-1608.

Gorman, A., Killoran, J., O'Shea, C., Kenna, T., Gallagher, W. M. & O'Shea, D. F. (2004) In vitro demonstration of the heavy-atom effect for photodynamic therapy. *J Am Chem Soc.* **126**(34): 10619-10631.

Grahn, M. F., McGuinness, A., Benzie, R., Boyle, R., de Jode, M. L., Dilkes, M. G., Abbas, B. & Williams, N. S. (1997) Intracellular uptake, absorption spectrum and stability of the bacteriochlorin photosensitizer 5,10,15, 20-tetrakis (m-hydroxyphenyl) bacteriochlorin (mTHPBC). Comparison with 5,10,15,20-tetrakis (m-hydroxyphenyl) chlorin (mTHPC). *J Photochem Photobiol B.* **37**(3): 261-266.

Grosjean, P., Wagnieres, G., Fontolliet, C., van den Bergh, H. & Monnier, P. (1998) Clinical photodynamic therapy for superficial cancer in the oesophagus and the bronchi: 514 nm compared with 630 nm light irradiation after sensitization with Photofrin II. *Br J Cancer.* **77**(11): 1989-1995.

Hackbarth, S., Horneffer, V., Wiehe, A., Hillenkamp, F. & Röder, B. (2001) Photophysical properties of pheophorbide-a-substituted diaminobutane poly-propylene-imine dendrimer. *Chem Phys.* **269**: 339-346.

Hadjur, C., Lange, N., Rebstein, J., Monnier, P., van den Bergh, H. & Wagnieres, G. (1998) Spectroscopic studies of photobleaching and photoproduct formation of meta(tetrahydroxyphenyl)chlorin (m-THPC) used in photodynamic therapy. The production of singletoxygen by m-THPC. *J Photochem Photobiol B.* **45**(170-8).

Hainaut, P. & Plymoth, A. (2013) Targeting the hallmarks of cancer: towards a rational approach to next-generation cancer therapy. *Curr Opin Oncol.* **25**(1): 50-51.

Hammer-Wilson, M. J., Cao, D., Kimel, S. & Berns, M. W. (2002) Photodynamic parameters in the chick chorioallantoic membrane (CAM) bioassay for photosensitizers administered intraperitoneally (IP) into the chick embryo. *Photochem Photobiol Sci.* **1**(9): 721-728.

Hanahan, D. & Weinberg, R. A. (2011) Hallmarks of cancer: the next generation. *Cell.* **144**(5): 646-674.

Harris, F., Chatfield, L. K. & Phoenix, D. A. (2005) Phenothiazinium based photosensitisers--photodynamic agents with a multiplicity of cellular targets and clinical applications. *Curr Drug Targets.* **6**(5): 615-627.

Hatz, S., Lambert, J. D. & Ogilby, P. R. (2007) Measuring the lifetime of singlet oxygen in a single cell: addressing the issue of cell viability. *Photochem Photobiol Sci.* **6**(10): 1106-1116.

Henderson, B. W. & Fingar, V. H. (1987) Relationship of tumor hypoxia and response to photodynamic treatment in an experimental mouse tumor. *Cancer Res.* **47**(12): 3110-3114.

Hockel, M. & Vaupel, P. (2001) Biological consequences of tumor hypoxia. *Semin Oncol.* **28**(2 Suppl 8): 36-41.

Hollingshead, M. G. (2008) Antitumor efficacy testing in rodents. *J Natl Cancer Inst.* **100**(21): 1500-1510.

Holt, J. J., Gannon, M. K., Tombline, G., McCarty, T. A., Page, P. M., Bright, F. V. & Detty, M. R. (2006) A cationic chalcogenoxanthylium photosensitizer effective in vitro in chemosensitive and multidrug-resistant cells. *Bioorg Med Chem.* **14**(24): 8635-8643.

Hongying, Y., Fuyuan, W. & Zhiyi, Z. (1999) Photobleaching of chlorins in homogeneous and heterogeneous media. *Dyes Pigments.* **43**(2): 109-117.

Hopkinson, H. J., Vernon, D. I. & Brown, S. B. (1999) Identification and partial characterization of an unusual distribution of the photosensitizer meta-tetrahydroxyphenyl chlorin (temoporfin) in human plasma. *Photochem Photobiol.* **69**(4): 482-488.

Houle, J. M. & Strong, A. (2002) Clinical pharmacokinetics of verteporfin. *J Clin Pharmacol.* **42**(5): 547-557.

Huang, Y. Y., Mroz, P., Zhiyentayev, T., Sharma, S. K., Balasubramanian, T., Ruzie, C., Krayer, M., Fan, D., Borbas, K. E., Yang, E., Kee, H. L., Kirmaier, C., Diers, J. R., Bocian, D. F., Holten, D., Lindsey, J. S. & Hamblin, M. R. (2010) In vitro photodynamic therapy and quantitative structure-activity relationship studies with stable synthetic near-infrared-absorbing bacteriochlorin photosensitizers. *J Med Chem.* **53**(10): 4018-4027.

Ichikawa, K., Takeuchi, Y., Yonezawa, S., Hikita, T., Kurohane, K., Namba, Y. & Oku, N. (2004) Antiangiogenic photodynamic therapy (PDT) using Visudyne causes effective suppression of tumor growth. *Cancer Lett.* **205**(1): 39-48.

Ikediobi, O. N., Davies, H., Bignell, G., Edkins, S., Stevens, C., O'Meara, S., Santarius, T., Avis, T., Barthorpe, S., Brackenbury, L., Buck, G., Butler, A., Clements, J., Cole, J., Dicks, E., Forbes, S., Gray, K., Halliday, K., Harrison, R., Hills, K., Hinton, J., Hunter, C., Jenkinson, A., Jones, D., Kosmidou, V., Lugg, R., Menzies, A., Mironenko, T., Parker, A., Perry, J., Raine, K., Richardson, D., Shepherd, R., Small, A., Smith, R., Solomon, H., Stephens, P., Teague, J., Tofts, C., Varian, J., Webb, T., West, S., Widaa, S., Yates, A., Reinhold, W., Weinstein, J. N., Stratton, M. R., Futreal, P. A. & Wooster, R. (2006) Mutation analysis of 24 known cancer genes in the NCI-60 cell line set. *Mol Cancer Ther.* **5**(11): 2606-2612.

Ikediobi, O. N., Reimers, M., Durinck, S., Blower, P. E., Futreal, A. P., Stratton, M. R. & Weinstein, J. N. (2008) In vitro differential sensitivity of melanomas to phenothiazines is based on the presence of codon 600 BRAF mutation. *Mol Cancer Ther.* **7**(6): 1337-1346.

Isakau, H. A., Parkhats, M. V., Knyukshto, V. N., Dzhagarov, B. M., Petrov, E. P. & Petrov, P. T. (2008) Toward understanding the high PDT efficacy of chlorin e6-polyvinylpyrrolidone formulations: photophysical and molecular aspects of photosensitizer-polymer interaction in vitro. *J Photochem Photobiol B.* **92**(3): 165-174.

Jalili, A., Makowski, M., Switaj, T., Nowis, D., Wilczynski, G. M., Wilczek, E., Chorazy-Massalska, M., Radzikowska, A., Maslinski, W., Bialy, L., Sienko, J., Sieron, A., Adamek, M., Basak, G., Mroz, P., Krasnodebski, I. W., Jakobisiak, M. & Golab, J. (2004) Effective photoimmunotherapy of murine colon carcinoma induced by the combination of photodynamic therapy and dendritic cells. *Clin Cancer Res.* **10**(13): 4498-4508.

Jin, W., Kim, G. M., Kim, M. S., Lim, M. H., Yun, C., Jeong, J., Nam, J. S. & Kim, S. J. (2010) TrkC plays an essential role in breast tumor growth and metastasis. *Carcinogenesis.* **31**(11): 1939-1947.

Juarranz, A., Jaen, P., Sanz-Rodriguez, F., Cuevas, J. & Gonzalez, S. (2008) Photodynamic therapy of cancer. Basic principles and applications. *Clin Transl Oncol.* **10**(3): 148-154.

Juzeniene, A., Nielsen, K. P. & Moan, J. (2006) Biophysical aspects of photodynamic therapy. *J Environ Pathol Toxicol Oncol.* **25**(1-2): 7-28.

Kabingu, E., Oseroff, A. R., Wilding, G. E. & Gollnick, S. O. (2009) Enhanced systemic immune reactivity to a Basal cell carcinoma associated antigen following photodynamic therapy. *Clin Cancer Res.* **15**(13): 4460-4466.

Kamal, N., Sabaratnam, V., Abdullah, N., Ho, A. S., Teo, S. H. & Lee, H. B. (2009) Light-activated cytotoxic compounds from Malaysian microorganisms for photodynamic therapy of cancer. *Antonie Van Leeuwenhoek.* **95**(2): 179-188.

Kamarulzaman, F. A., Shaari, K., Ho, A. S., Lajis, N. H., Teo, S. H. & Lee, H. B. (2011) Derivatives of pheophorbide-a and pheophorbide-b from photocytotoxic Piper penangense extract. *Chem Biodivers.* **8**(3): 494-502.

Karakullukcu, B., Stoker, S. D., Wildeman, A. P., Copper, M. P., Wildeman, M. A. & Tan, I. B. (2013) A matched cohort comparison of mTHPC-mediated photodynamic therapy and trans-oral surgery of early stage oral cavity squamous cell cancer. *Eur Arch Otorhinolaryngol.* **270**(3): 1093-1097.

Kennedy, J. C. & Pottier, R. H. (1992) Endogenous protoporphyrin IX, a clinically useful photosensitizer for photodynamic therapy. *J Photochem Photobiol B.* **14**(4): 275-292.

Kereiakes, D. J., Szyniszewski, A. M., Wahr, D., Herrmann, H. C., Simon, D. I., Rogers, C., Kramer, P., Shear, W., Yeung, A. C., Shunk, K. A., Chou, T. M., Popma, J., Fitzgerald, P., Carroll, T. E., Forer, D. & Adelman, D. C. (2003) Phase I drug and light dose-escalation trial of motexafin lutetium and far red light activation (phototherapy) in subjects with coronary artery disease undergoing percutaneous coronary intervention and stent deployment: procedural and long-term results. *Circulation.* **108**(11): 1310-1315.

Kessel, D. (1989a) Determinants of photosensitization by mono-L-aspartyl chlorin e6. *Photochem Photobiol.* **49**(4): 447-452.

Kessel, D. (1989b) Determinants of photosensitization by purpurins. *Photochem Photobiol.* **50**(2): 169-174.

Kessel, D. (1992) Properties of cremophor EL micelles probed by fluorescence. *Photochem Photobiol.* **56**(4): 447-451.

Kessel, D., Luo, Y., Mathieu, P. & Reiners, J. J., Jr. (2000) Determinants of the apoptotic response to lysosomal photodamage. *Photochem Photobiol.* **71**(2): 196-200.

Kessel, D. & Poretz, R. D. (2000) Sites of photodamage induced by photodynamic therapy with a chlorin e6 triacetoxymethyl ester (CAME). *Photochem Photobiol.* **71**(1): 94-96.

Kessel, D. & Reiners, J. J., Jr. (2007) Apoptosis and autophagy after mitochondrial or endoplasmic reticulum photodamage. *Photochem Photobiol.* **83**(5): 1024-1028.

Kessel, D., Vicente, M. G. & Reiners, J. J., Jr. (2006) Initiation of apoptosis and autophagy by photodynamic therapy. *Lasers Surg Med.* **38**(5): 482-488.

Kesterson, J. P., Odunsi, K. & Lele, S. (2010) High cumulative doses of pegylated liposomal doxorubicin are not associated with cardiac toxicity in patients with gynecologic malignancies. *Chemotherapy.* **56**(2): 108-111.

Kiesslich, T., Berlanda, J., Plaetzer, K., Krammer, B. & Berr, F. (2007) Comparative characterization of the efficiency and cellular pharmacokinetics of Foscan- and Foslip-based photodynamic treatment in human biliary tract cancer cell lines. *Photochem Photobiol Sci.* **6**(6): 619-627.

Kim, H. R., Luo, Y., Li, G. & Kessel, D. (1999) Enhanced apoptotic response to photodynamic therapy after bcl-2 transfection. *Cancer Res.* **59**(14): 3429-3432.
Kim, K. K., Kawano, Y. & Yamazaki, Y. (2003) A novel porphyrin photosensitizer from bamboo leaves that induces apoptosis in cancer cell lines. *Anticancer Res.* **23**(3B): 2355-2361.
Kimel, S., Tromberg, B. J., Roberts, W. G. & Berns, M. W. (1989) Singlet oxygen generation of porphyrins, chlorins, and phthalocyanines. *Photochem Photobiol.* **50**(2): 175-183.
Kloek, J., Akkermans, W. & Beijersbergen van Henegouwen, G. M. (1998) Derivatives of 5-aminolevulinic acid for photodynamic therapy: enzymatic conversion into protoporphyrin. *Photochem Photobiol.* **67**(1): 150-154.
Kochevar, I. E. & Redmond, R. W. (2000) Photosensitized production of singlet oxygen. *Methods Enzymol.* **319**: 20-28.
Korbelik, M. (2006) PDT-associated host response and its role in the therapy outcome. *Lasers Surg Med.* **38**(5): 500-508.
Kowaltowski, A. J., Turin, J., Indig, G. L. & Vercesi, A. E. (1999) Mitochondrial effects of triarylmethane dyes. *J Bioenerg Biomembr.* **31**(6): 581-590.
Krammer, B. (2001) Vascular effects of photodynamic therapy. *Anticancer Res.* **21**(6B): 4271-4277.
Kraut, J. A. & Madias, N. E. (2012) Treatment of acute metabolic acidosis: a pathophysiologic approach. *Nat Rev Nephrol.* **8**(10): 589-601.
Krosl, G., Korbelik, M. & Dougherty, G. J. (1995) Induction of immune cell infiltration into murine SCCVII tumour by photofrin-based photodynamic therapy. *Br J Cancer.* **71**(3): 549-555.
Kurohane, K., Tominaga, A., Sato, K., North, J. R., Namba, Y. & Oku, N. (2001) Photodynamic therapy targeted to tumor-induced angiogenic vessels. *Cancer Lett.* **167**(1): 49-56.
Kurtoglu, M. & Lampidis, T. J. (2009) From delocalized lipophilic cations to hypoxia: blocking tumor cell mitochondrial function leads to therapeutic gain with glycolytic inhibitors. *Mol Nutr Food Res.* **53**(1): 68-75.
Kwitniewski, M., Juzeniene, A., Ma, L. W., Glosnicka, R., Graczyk, A. & Moan, J. (2009) Diamino acid derivatives of PpIX as potential photosensitizers for photodynamic therapy of squamous cell carcinoma and prostate cancer: in vitro studies. *J Photochem Photobiol B.* **94**(3): 214-222.
Kwitniewski, M., Kunikowska, D., Dera-Tomaszewska, B., Tokarska-Pietrzak, E., Dziadziuszko, H., Graczyk, A. & Glosnicka, R. (2005) Influence of diamino acid derivatives of protoporphyrin IX on mouse immunological system: preliminary results. *J Photochem Photobiol B.* **81**(3): 129-135.
Lampidis, T. J., Hasin, Y., Weiss, M. J. & Chen, L. B. (1985) Selective killing of carcinoma cells "in vitro" by lipophilic-cationic compounds: a cellular basis. *Biomed Pharmacother.* **39**(5): 220-226.
Lange, N., Ballini, J. P., Wagnieres, G. & van den Bergh, H. (2001) A new drug-screening procedure for photosensitizing agents used in photodynamic therapy for CNV. *Invest Ophthalmol Vis Sci.* **42**(1): 38-46.
Lee, H. B., Ho, A. S. & Teo, S. H. (2006) p53 Status does not affect photodynamic cell killing induced by hypericin. *Cancer Chemother Pharmacol.* **58**(1): 91-98.
Lemmon, M. A. & Schlessinger, J. (2010) Cell signaling by receptor tyrosine kinases. *Cell.* **141**(7): 1117-1134.
Li, L., Han, J., Nguyen, B. & Burgess, K. (2008) Syntheses and spectral properties of functionalized, water-soluble BODIPY derivatives. *J Org Chem.* **73**(5): 1963-1970.

Lim, S. H., Lee, H. B. & Ho, A. S. (2011) A new naturally derived photosensitizer and its phototoxicity on head and neck cancer cells. *Photochem Photobiol.* **87**(5): 1152-1158.

Lim, S. H., Nowak-Sliwinska, P., Kamarulzaman, F. A., van den Bergh, H., Wagnieres, G. & Lee, H. B. (2010) The neovessel occlusion efficacy of 15-hydroxypurpurin-7-lactone dimethyl ester induced with photodynamic therapy. *Photochem Photobiol.* **86**(2): 397-402.

Lim, S. H., Wu, L., Burgess, K. & Lee, H. B. (2009) New cytotoxic rosamine derivatives selectively accumulate in the mitochondria of cancer cells. *Anticancer Drugs.* **20**(6): 461-468.

Lobel, J., MacDonald, I. J., Ciesielski, M. J., Barone, T., Potter, W. R., Pollina, J., Plunkett, R. J., Fenstermaker, R. A. & Dougherty, T. J. (2001) 2-[1-hexyloxyethyl]-2-devinyl pyropheophorbide-a (HPPH) in a nude rat glioma model: implications for photodynamic therapy. *Lasers Surg Med.* **29**(5): 397-405.

Lou, P. J., Jager, H. R., Jones, L., Theodossy, T., Bown, S. G. & Hopper, C. (2004) Interstitial photodynamic therapy as salvage treatment for recurrent head and neck cancer. *Br J Cancer.* **91**(3): 441-446.

Loudet, A. & Burgess, K. (2007) BODIPY dyes and their derivatives: syntheses and spectroscopic properties. *Chem Rev.* **107**(11): 4891-4932.

Lozovaya, G. I., Masinovsky, Z. & Sivash, A. A. (1990) Protoporphyrin ix as a possible ancient photosensitizer: Spectral and photochemical studies *Origins of Life Evol Biosph.* **20**: 321-330.

Lui, H., Hobbs, L., Tope, W. D., Lee, P. K., Elmets, C., Provost, N., Chan, A., Neyndorff, H., Su, X. Y., Jain, H., Hamzavi, I., McLean, D. & Bissonnette, R. (2004) Photodynamic therapy of multiple nonmelanoma skin cancers with verteporfin and red light-emitting diodes: two-year results evaluating tumor response and cosmetic outcomes. *Arch Dermatol.* **140**(1): 26-32.

Macalpine, J. K., Boch, R. & Dolphin, D. (2002) Evaluation of tetraphenyl-2,3-dihydroxychlorins as potential photosensitizers. *J Porphyr Phthalocyanines.* **6**(2): 146-155.

MacDonald, I. J. & Dougherty, T. J. (2001) Basic principles of photodynamic therapy. *J Porphyr Phthalocyanines.* **5**: 105-129.

Madar-Balakirski, N., Tempel-Brami, C., Kalchenko, V., Brenner, O., Varon, D., Scherz, A. & Salomon, Y. (2010) Permanent occlusion of feeding arteries and draining veins in solid mouse tumors by vascular targeted photodynamic therapy (VTP) with Tookad. *PLoS One.* **5**(4): e10282.

Mang, T. S. (2008) Dosimetric concepts for PDT. *Photodiagnosis Photodyn Ther.* **5**(3): 217-223.

Marchal, S., Francois, A., Dumas, D., Guillemin, F. & Bezdetnaya, L. (2007) Relationship between subcellular localisation of Foscan and caspase activation in photosensitised MCF-7 cells. *Br J Cancer.* **96**(6): 944-951.

Margaron, P., Gregoire, M. J., Scasnar, V., Ali, H. & van Lier, J. E. (1996) Structure-photodynamic activity relationships of a series of 4-substituted zinc phthalocyanines. *Photochem Photobiol.* **63**(2): 217-223.

Marshall, N. J., Goodwin, C. J. & Holt, S. J. (1995) A critical assessment of the use of microculture tetrazolium assays to measure cell growth and function. *Growth Regul.* **5**(2): 69-84.

McBride, H. M., Neuspiel, M. & Wasiak, S. (2006) Mitochondria: more than just a powerhouse. *Curr Biol.* **16**(14): R551-560.

Minamikawa, T., Sriratana, A., Williams, D. A., Bowser, D. N., Hill, J. S. & Nagley, P. (1999) Chloromethyl-X-rosamine (MitoTracker Red) photosensitises

mitochondria and induces apoptosis in intact human cells. *J Cell Sci.* **112 (Pt 14)**: 2419-2430.

Moan, J. & Berg, K. (1991) The photodegradation of porphyrins in cells can be used to estimate the lifetime of singlet oxygen. *Photochem Photobiol.* **53**(4): 549-553.

Moan, J. & Sommer, S. (1985) Oxygen dependence of the photosensitizing effect of hematoporphyrin derivative in NHIK 3025 cells. *Cancer Res.* **45**(4): 1608-1610.

Modica-Napolitano, J. S. & Aprille, J. R. (1987) Basis for the selective cytotoxicity of rhodamine 123. *Cancer Res.* **47**(16): 4361-4365.

Modica-Napolitano, J. S. & Aprille, J. R. (2001) Delocalized lipophilic cations selectively target the mitochondria of carcinoma cells. *Adv Drug Deliv Rev.* **49**(1-2): 63-70.

Modica-Napolitano, J. S., Weiss, M. J., Chen, L. B. & Aprille, J. R. (1984) Rhodamine 123 inhibits bioenergetic function in isolated rat liver mitochondria. *Biochem Biophys Res Commun.* **118**(3): 717-723.

Moreno, S. N., Gadelha, F. R. & Docampo, R. (1988) Crystal violet as an uncoupler of oxidative phosphorylation in rat liver mitochondria. *J Biol Chem.* **263**(25): 12493-12499.

Morgan, J. & Oseroff, A. R. (2001) Mitochondria-based photodynamic anti-cancer therapy. *Adv Drug Deliv Rev.* **49**(1-2): 71-86.

Mosmann, T. (1983) Rapid colorimetric assay for cellular growth and survival: application to proliferation and cytotoxicity assays. *J Immunol Methods.* **65**(1-2): 55-63.

Mousavi, S. H., Tavakkol-Afshari, J., Brook, A. & Jafari-Anarkooli, I. (2009) Direct toxicity of Rose Bengal in MCF-7 cell line: role of apoptosis. *Food Chem Toxicol.* **47**(4): 855-859.

Mroz, P., Huang, Y. Y. & Hamblin, M. R. (2010) Photodynamic therapy for cancer and activation of immune response. Biophotonics and Immune Responses V. W. R. Chen. San Francisco, Ca, SPIE.

Mroz, P., Yaroslavsky, A., Kharkwal, G. B. & Hamblin, M. R. (2011) Cell death pathways in photodynamic therapy of cancer. *Cancers.* **3**(2): 2516-2539.

Nadanaciva, S., Bernal, A., Aggeler, R., Capaldi, R. & Will, Y. (2007) Target identification of drug induced mitochondrial toxicity using immunocapture based OXPHOS activity assays. *Toxicol In Vitro.* **21**(5): 902-911.

Nahta, R. & Esteva, F. J. (2007) Trastuzumab: triumphs and tribulations. *Oncogene.* **26**(25): 3637-3643.

Nitiss, J. L., Pourquier, P. & Pommier, Y. (1997) Aclacinomycin A stabilizes topoisomerase I covalent complexes. *Cancer Res.* **57**(20): 4564-4569.

Nyman, E. S. & Hynninen, P. H. (2004) Research advances in the use of tetrapyrrolic photosensitizers for photodynamic therapy. *J Photochem Photobiol B.* **73**(1-2): 1-28.

Ong, C. Y., Ling, S. K., Ali, R. M., Chee, C. F., Samah, Z. A., Ho, A. S., Teo, S. H. & Lee, H. B. (2009) Systematic analysis of in vitro photo-cytotoxic activity in extracts from terrestrial plants in Peninsula Malaysia for photodynamic therapy. *J Photochem Photobiol B.* **96**(3): 216-222.

Ormond, A. & Freeman, H. (2013) Dye Sensitizers for Photodynamic Therapy. *Materials.* **6**(3): 817-840.

Pal, P., Zeng, H., Durocher, G., Girard, D., Li, T., Gupta, A. K., Giasson, R., Blanchard, L., Gaboury, L., Balassy, A., Turmel, C., Laperrière, A. & Villeneuve, L. (1996) Phototoxicity of some bromine-substituted rhodamine dyes: Synthesis, photophysical properties and application as photosensitizers. *Photochem Photobiol.* **63**(2): 161-168.

Palmer, G. M., Fontanella, A. N., Shan, S., Hanna, G., Zhang, G., Fraser, C. L. & Dewhirst, M. W. (2011) In vivo optical molecular imaging and analysis in mice using dorsal window chamber models applied to hypoxia, vasculature and fluorescent reporters. *Nat Protoc.* **6**(9): 1355-1366.

Pandey, R. K., Jagerovic, N., Ryan, J. M., Dougherty, T. J. & Smith, K. M. (1994) Efficient syntheses of new classes of regiochemically pure benzoporphyrin derivatives. *Bioorg Med Chem Lett.* **3**(12): 2615-2618.

Patel, H., Mick, R., Finlay, J., Zhu, T. C., Rickter, E., Cengel, K. A., Malkowicz, S. B., Hahn, S. M. & Busch, T. M. (2008) Motexafin lutetium-photodynamic therapy of prostate cancer: short- and long-term effects on prostate-specific antigen. *Clin Cancer Res.* **14**(15): 4869-4876.

Plowman, J., Dykes, D. J., Hollingshead, M., Simpson-Herren, L. & Alley, M. C. (1997) Human tumor xenograft models. Anticancer Drug Development Guide: Preclinical Screening, Clinical Trials, and Approval. B. Teicher. Totowa, NJ, Humana Press**:** 101–125.

Reers, M., Smith, T. W. & Chen, L. B. (1991) J-aggregate formation of a carbocyanine as a quantitative fluorescent indicator of membrane potential. *Biochemistry.* **30**(18): 4480-4486.

Reiners, J. J., Jr., Agostinis, P., Berg, K., Oleinick, N. L. & Kessel, D. (2010) Assessing autophagy in the context of photodynamic therapy. *Autophagy.* **6**(1): 7-18.

Reiners, J. J., Jr., Caruso, J. A., Mathieu, P., Chelladurai, B., Yin, X. M. & Kessel, D. (2002) Release of cytochrome c and activation of pro-caspase-9 following lysosomal photodamage involves Bid cleavage. *Cell Death Differ.* **9**(9): 934-944.

Reles, A., Wen, W. H., Schmider, A., Gee, C., Runnebaum, I. B., Kilian, U., Jones, L. A., El-Naggar, A., Minguillon, C., Schonborn, I., Reich, O., Kreienberg, R., Lichtenegger, W. & Press, M. F. (2001) Correlation of p53 mutations with resistance to platinum-based chemotherapy and shortened survival in ovarian cancer. *Clin Cancer Res.* **7**(10): 2984-2997.

Renda, F., Mura, P., Finco, G., Ferrazin, F., Pani, L. & Landoni, G. (2013) Metformin-associated lactic acidosis requiring hospitalization. A national 10 year survey and a systematic literature review. *Eur Rev Med Oharmaco Sci.* **17** ((Suppl 1)): 45-49.

Ribatti, D., Nico, B., Vacca, A. & Presta, M. (2006) The gelatin sponge-chorioallantoic membrane assay. *Nat Protoc.* **1**(1): 85-91.

Ribatti, D., Nico, B., Vacca, A., Roncali, L., Burri, P. H. & Djonov, V. (2001) Chorioallantoic membrane capillary bed: a useful target for studying angiogenesis and anti-angiogenesis in vivo. *Anat Rec.* **264**(4): 317-324.

Richmond, R. C. & O'Hara, J. A. (1993) Effective photodynamic action by rhodamine 123 leading to photosensitized killing of Chinese hamster ovary cells in tissue culture and a proposed mechanism. *Photochem Photobiol.* **57**(2): 291-297.

Roberts, W. G., Shiau, F. Y., Nelson, J. S., Smith, K. M. & Berns, M. W. (1988) In vitro characterization of monoaspartyl chlorin e6 and diaspartyl chlorin e6 for photodynamic therapy. *J Natl Cancer Inst.* **80**(5): 330-336.

Röder, B., Hanke, T., Oelckers, S., Hackbarth, S. & Symietz, C. (2000) Photophysical properties of pheophorbide a in solution and in model membrane systems. *J Porphyrins Phthalocyanines.* **4**(1): 37-44.

Rook, A. H., Wood, G. S., Duvic, M., Vonderheid, E. C., Tobia, A. & Cabana, B. (2010) A phase II placebo-controlled study of photodynamic therapy with topical hypericin and visible light irradiation in the treatment of cutaneous T-cell lymphoma and psoriasis. *J Am Acad Dermatol.* **63**(6): 984-990.

Rotomskis, R., Bagdonas, S. & Streckyte, G. (1996) Spectroscopic studies of photobleaching and photoproduct formation of porphyrins used in tumour therapy. *J Photochem Photobiol B.* **33**(1): 61-67.

Rück, A., Böhmler, A. & Steiner, R. (2005) PDT with TOOKAD® studied in the chorioallantoic membrane of fertilized eggs. *Photodiag Photodyn Ther.* **2**(1): 79-90.

Santarpia, M., Altavilla, G., Margeli, M., Cirauqui, B., Mesiti, M., Cavallari, V., Ramirez, J. L., Sanchez-Ronco, M., Santarpia, L., Taron, M. & Rosell, R. (2008) PIK3CA mutations and BRCA1 expression in breast cancer: potential biomarkers for chemoresistance. *Cancer Invest.* **26**(10): 1044-1051.

Santelli-Rouvier, C., Barret, J. M., Farrell, C. M., Sharples, D., Hill, B. T. & Barbe, J. (2004) Synthesis of 9-acridinyl sulfur derivatives: sulfides, sulfoxides and sulfones. Comparison of their activity on tumour cells. *Eur J Med Chem.* **39**(12): 1029-1038.

Sasnouski, S., Kachatkou, D., Zorin, V., Guillemin, F. & Bezdetnaya, L. (2006) Redistribution of Foscan from plasma proteins to model membranes. *Photochem Photobiol Sci.* **5**(8): 770-777.

Sekkat, N., van den Bergh, H., Nyokong, T. & Lange, N. (2012) Like a bolt from the blue: phthalocyanines in biomedical optics. *Molecules.* **17**(1): 98-144.

Senge, M. O. & Brandt, J. C. (2011) Temoporfin (Foscan(R), 5,10,15,20-tetra(m-hydroxyphenyl)chlorin)--a second-generation photosensitizer. *Photochem Photobiol.* **87**(6): 1240-1296.

Serra, V. V., Zamarron, A., Faustino, M. A., Cruz, M. C., Blazquez, A., Rodrigues, J. M., Neves, M. G., Cavaleiro, J. A., Juarranz, A. & Sanz-Rodriguez, F. (2010) New porphyrin amino acid conjugates: synthesis and photodynamic effect in human epithelial cells. *Bioorg Med Chem.* **18**(16): 6170-6178.

Shandura, M. P., Poronik, Y. M. & Kovtun, Y. P. (2007) New heterocyclic analogues of rhodamines. *Dyes and Pigments.* **73**(1): 25-30.

Sharman, W. M., Allen, C. M. & van Lier, J. E. (1999) Photodynamic therapeutics: basic principles and clinical applications. *Drug Discov Today.* **4**(11): 507-517.

Shliakhtsin, S. V., Trukhachova, T. V., Isakau, H. A. & Istomin, Y. P. (2009) Pharmacokinetics and biodistribution of Photolon (Fotolon) in intact and tumor-bearing rats. *Photodiagnosis Photodyn Ther.* **6**(2): 97-104.

Shoemaker, R. H. (2006) The NCI60 human tumour cell line anticancer drug screen. *Nat Rev Cancer.* **6**(10): 813-823.

Singh, G., Alqawi, O. & Espiritu, M. (2010) Metronomic PDT and cell death pathways. Photodynamic Therapy. C. J. Gomer, Humana Press. **635:** 65-78.

Spikes, J. D. (1992) Quantum yields and kinetics of the photobleaching of hematoporphyrin, Photofrin II, tetra(4-sulfonatophenyl)-porphine and uroporphyrin. *Photochem Photobiol.* **55**(6): 797-808.

Spikes, J. D. & Bommer, J. C. (1993) Photosensitizing properties of mono-L-aspartyl chlorin e6 (NPe6): a candidate sensitizer for the photodynamic therapy of tumors. *J Photochem Photobiol B.* **17**(2): 135-143.

Sternberg, E. D., Dolphin, D. & Brückner, C. (1998) Porphyrin-based photosensitizers for use in photodynamic therapy. *Tetrahedron.* **54**(17): 4151-4202.

Strickley, R. G. (2004) Solubilizing excipients in oral and injectable formulations. *Pharm Res.* **21**(2): 201-230.

Szokalska, A., Makowski, M., Nowis, D., Wilczynski, G. M., Kujawa, M., Wojcik, C., Mlynarczuk-Bialy, I., Salwa, P., Bil, J., Janowska, S., Agostinis, P., Verfaillie, T., Bugajski, M., Gietka, J., Issat, T., Glodkowska, E., Mrowka, P., Stoklosa, T., Hamblin, M. R., Mroz, P., Jakobisiak, M. & Golab, J. (2009) Proteasome inhibition potentiates antitumor effects of photodynamic therapy in mice through

induction of endoplasmic reticulum stress and unfolded protein response. *Cancer Res.* **69**(10): 4235-4243.

Tan, P. J., Ong, C. Y., Danial, A., Yusof, H. M., Neoh, B. K. & Lee, H. B. (2011) Cyclic Tetrapyrrolic Photosensitisers from the leaves of Phaeanthus ophthalmicus. *Chem Cent J.* **5**: 32.

Tanaka, F., Tsumura, K., Furuta, T., Iwamoto, K. & Okamoto, M. (2008) Efficiencies of singlet oxygen production and rate constants for oxygen quenching in the S1 state of dicyanonaphthalenes and related compounds. *Photochem Photobiol Sci.* **7**(1): 56-62.

Tanaka, M., Kinoshita, M., Yoshihara, Y., Shinomiya, N., Seki, S., Nemoto, K., Hirayama, T., Dai, T., Huang, L., Hamblin, M. R. & Morimoto, Y. (2012) Optimal photosensitizers for photodynamic therapy of infections should kill bacteria but spare neutrophils. *Photochem Photobiol.* **88**(1): 227-232.

Thong, P. S., Ong, K. W., Goh, N. S., Kho, K. W., Manivasager, V., Bhuvaneswari, R., Olivo, M. & Soo, K. C. (2007) Photodynamic-therapy-activated immune response against distant untreated tumours in recurrent angiosarcoma. *Lancet Oncol.* **8**(10): 950-952.

Toogood, P. L. (2008) Mitochondrial drugs. *Curr Opin Chem Biol.* **12**(4): 457-463.

Tuchin, V. V. (1997) Light scattering study of tissues. *Physics -Uspekhi.* **40**(5): 495-515.

Usuda, J., Chiu, S. M., Murphy, E. S., Lam, M., Nieminen, A. L. & Oleinick, N. L. (2003) Domain-dependent photodamage to Bcl-2. A membrane anchorage region is needed to form the target of phthalocyanine photosensitization. *J Biol Chem.* **278**(3): 2021-2029.

Usuda, J., Kato, H., Okunaka, T., Furukawa, K., Tsutsui, H., Yamada, K., Suga, Y., Honda, H., Nagatsuka, Y., Ohira, T., Tsuboi, M. & Hirano, T. (2006) Photodynamic therapy (PDT) for lung cancers. *J Thorac Oncol.* **1**(5): 489-493.

van der Bruggen, P. & van den Eynde, B. J. (2006) Processing and presentation of tumor antigens and vaccination strategies. *Curr Opin Immunol.* **18**(1): 98-104.

van Osdol, W. W., Myers, T. G., Paull, K. D., Kohn, K. W. & Weinstein, J. N. (1994) Use of the Kohonen self-organizing map to study the mechanisms of action of chemotherapeutic agents. *J Natl Cancer Inst.* **86**(24): 1853-1859.

Vantieghem, A., Xu, Y., Assefa, Z., Piette, J., Vandenheede, J. R., Merlevede, W., De Witte, P. A. & Agostinis, P. (2002) Phosphorylation of Bcl-2 in G2/M phase-arrested cells following photodynamic therapy with hypericin involves a CDK1-mediated signal and delays the onset of apoptosis. *J Biol Chem.* **277**(40): 37718-37731.

Vargas, A., Zeisser-Labouebe, M., Lange, N., Gurny, R. & Delie, F. (2007) The chick embryo and its chorioallantoic membrane (CAM) for the in vivo evaluation of drug delivery systems. *Adv Drug Deliv Rev.* **59**(11): 1162-1176.

Wachowska, M., Muchowicz, A., Firczuk, M., Gabrysiak, M., Winiarska, M., Wańczyk, M., Bojarczuk, K. & Golab, J. (2011) Aminolevulinic acid (ALA) as a prodrug in photodynamic therapy of cancer. *Molecules.* **16**(5): 4140-4164.

Wainwright, M. (2005) The development of phenothiazinium photosensitisers. *Photodiag Photodyn Ther.* **2**(4): 263-272.

Wainwright, M. (2009) Photosensitisers in biomedicine. West Sussex, UK, John Wiley & Sons Ltd.

Wainwright, M. & Giddens, R. M. (2003) Phenothiazinium photosensitisers: choices in synthesis and application *Dyes Pigments.* **57**(3): 245-257.

Wainwright, M., Phoenix, D. A., Rice, L., Burrow, S. M. & Waring, J. (1997) Increased cytotoxicity and phototoxicity in the methylene blue series via chromophore methylation. *J Photochem Photobiol B.* **40**(3): 233-239.

Wang, F., Ogasawara, M. A. & Huang, P. (2010) Small mitochondria-targeting molecules as anti-cancer agents. *Molecular Aspects of Medicine.* **31**(1): 75-92.

Wang, H. M., Jiang, J. Q., Xiao, J. H., Gao, R. L., Lin, F. Y. & Liu, X. Y. (2008) Porphyrin with amino acid moieties: a tumor photosensitizer. *Chem Biol Interact.* **172**(2): 154-158.

Wang, I., Bendsoe, N., Klinteberg, C. A., Enejder, A. M., Andersson-Engels, S., Svanberg, S. & Svanberg, K. (2001) Photodynamic therapy vs. cryosurgery of basal cell carcinomas: results of a phase III clinical trial. *Br J Dermatol.* **144**(4): 832-840.

Warren, C. B., Karai, L. J., Vidimos, A. & Maytin, E. V. (2009) Pain associated with aminolevulinic acid-photodynamic therapy of skin disease. *J Am Acad Dermatol.* **61**(6): 1033-1043.

Webber, J., Kessel, D. & Fromm, D. (1997) Plasma levels of protoporphyrin IX in humans after oral administration of 5-aminolevulinic acid. *J Photochem Photobiol B.* **37**(1-2): 151-153.

Weersink, R. A., Forbes, J., Bisland, S., Trachtenberg, J., Elhilali, M., Brun, P. H. & Wilson, B. C. (2005) Assessment of cutaneous photosensitivity of TOOKAD (WST09) in preclinical animal models and in patients. *Photochem Photobiol.* **81**(1): 106-113.

Weinstein, J. N., Myers, T. G., O'Connor, P. M., Friend, S. H., Fornace, A. J., Jr., Kohn, K. W., Fojo, T., Bates, S. E., Rubinstein, L. V., Anderson, N. L., Buolamwini, J. K., van Osdol, W. W., Monks, A. P., Scudiero, D. A., Sausville, E. A., Zaharevitz, D. W., Bunow, B., Viswanadhan, V. N., Johnson, G. S., Wittes, R. E. & Paull, K. D. (1997) An information-intensive approach to the molecular pharmacology of cancer. *Science.* **275**(5298): 343-349.

Wenzel, J., Zeisig, R. & Fichtner, I. (2010) Inhibition of metastasis in a murine 4T1 breast cancer model by liposomes preventing tumor cell-platelet interactions. *Clin Exp Metastasis.* **27**(1): 25-34.

Whitacre, C. M., Feyes, D. K., Satoh, T., Grossmann, J., Mulvihill, J. W., Mukhtar, H. & Oleinick, N. L. (2000) Photodynamic therapy with the phthalocyanine photosensitizer Pc 4 of SW480 human colon cancer xenografts in athymic mice. *Clin Cancer Res.* **6**(5): 2021-2027.

Wirz, A., Meier, B. & Sticher, O. (2002) Solubility of hypericin in methanol and methanol-pyridine. *Pharmazie.* **57**(8): 543-545.

Woodburn, K. W., Engelman, C. J. & Blumenkranz, M. S. (2002) Photodynamic therapy for choroidal neovascularization: a review. *Retina.* **22**(4): 391-405; quiz 527-398.

Workman, P., Aboagye, E. O., Balkwill, F., Balmain, A., Bruder, G., Chaplin, D. J., Double, J. A., Everitt, J., Farningham, D. A., Glennie, M. J., Kelland, L. R., Robinson, V., Stratford, I. J., Tozer, G. M., Watson, S., Wedge, S. R., Eccles, S. A. & Committee of the National Cancer Research, I. (2010) Guidelines for the welfare and use of animals in cancer research. *Br J Cancer.* **102**(11): 1555-1577.

Wu, L. & Burgess, K. (2008a) A new synthesis of symmetric boraindacene (BODIPY) dyes. *Chem Commun (Camb).*(40): 4933-4935.

Wu, L. & Burgess, K. (2008b) Synthesis and spectroscopic properties of rosamines with cyclic amine substituents. *J Org Chem.* **73**(22): 8711-8718.

Xue, L. Y., Chiu, S. M., Azizuddin, K., Joseph, S. & Oleinick, N. L. (2007) The death of human cancer cells following photodynamic therapy: apoptosis competence is necessary for Bcl-2 protection but not for induction of autophagy. *Photochem Photobiol.* **83**(5): 1016-1023.

Xue, L. Y., Chiu, S. M. & Oleinick, N. L. (2010) Atg7 deficiency increases resistance of MCF-7 human breast cancer cells to photodynamic therapy. *Autophagy*. **6**(2): 248-255.

Yogo, T., Urano, Y., Ishitsuka, Y., Maniwa, F. & Nagano, T. (2005) Highly efficient and photostable photosensitizer based on BODIPY chromophore. *J Am Chem Soc*. **127**(35): 12162-12163.

Zhu, T. C. & Finlay, J. C. (2008) The role of photodynamic therapy (PDT) physics. *Med Phys*. **35**(7): 3127-3136.

Zilberstein, J., Salomon, Y., Scherz, A. & Bromberg, A. (2001) Direct and Continuous Measurements of Oxygen Partial Pressure Using a Tissue-Inserted Optical Oxygen Microsensor: During Photodynamic Therapy. Novel Approaches in Biosensors and Rapid Diagnostic Assays. Z. Liron, A. Bromberg and M. Fisher, Springer US**:** 273-284.

Zuluaga, M. F., Mailhos, C., Robinson, G., Shima, D. T., Gurny, R. & Lange, N. (2007) Synergies of VEGF inhibition and photodynamic therapy in the treatment of age-related macular degeneration. *Invest Ophthalmol Vis Sci*. **48**(4): 1767-1772.

List of Appendices

Appendix A

Animal ethics approval letter

UNIVERSITY OF MALAYA
KUALA LUMPUR
The Leader In Research and Innovation

يونيورسيتي مالايا

PEJABAT KETUA

14 Julai 2010

Lim Siang Hui
Jabatan Farmasi
Fakulti Perubatan
Universiti Malaya

Tuan,

EVALUATION OF EFFICACY AND PHARMACOKINETIC PROPERTIES OF 3 NOVEL SMALL MOLECULES FOR ANTICANCER PHOTODYNAMIC THERAPY

Dengan sukacitanya Jawatankuasa Etika Penjagaan dan Penggunaan Haiwan, Fakulti Perubatan, Universiti Malaya telah meluluskan permohonan untuk penyelidikan tersebut di atas.

No rujukan etika: **FAR/14/07/2010/LSH (R)**

Sila ambil perhatian bahawa nombor rujukan etika yang diberi adalah sah untuk tempoh **dua tahun sehingga 13 Julai 2012.**

Sekian, terima kasih.

Yang benar,

Dr. Haji Azizuddin Bin Haji Kamaruddin
Ketua
Pusat Haiwan Makmal
Fakulti Perubatan
Merangkap Setiausaha Jawatankuasa Etika Penjagaan dan Penggunaan Haiwan

SK : Puan Zura Syazleena Hamizan
Setiausaha MCRC
Pejabat Dekan
Fakulti Perubatan

MS ISO 9001:2000 REG. NO. AR 2760

Ketua, Pusat Haiwan Makmal
Fakulti Perubatan, Universiti Malaya, 50603 Kuala Lumpur, Malaysia
Head, Laboratory Animal Centre
Faculty of Medicine, University of Malaya, 50603, Kuala Lumpur, Malaysia
Tel: (603) 7967 4792 Faks: (603) 7955 9886
E-mail: azizud@um.edu.my Website: http://www.um.edu.my

Appendix B

Conference Attended

In vitro and *in vivo* photo-cytotoxicity of BODIPY derivatives for photodynamic therapy

S. H. Lim[1], C. Thivierge[2], P. Nowak-Sliwinska[3], J. Han[2], H. van den Bergh[3], G. Wagnieres[3], K. Burgess[2], H. B. Lee[1]

[1]Cancer Research Initiatives Foundation, Subang Jaya, Selangor, Malaysia. [2]Department of Chemistry, Texas A&M University, Texas, USA. [3]Medical Photonics Group, Swiss Federal Institute of Technology, Lausanne, Switzerland.

13th IPA World Congress
International Photodynamic Association
Innsbruck, Austria 10-14 May 2011

Abstract

Photodynamic therapy (PDT) is now a well-recognised treatment modality for cancer and precancerous lesions. One class of photosensitisers that is currently investigated for PDT is the boron-dipyrromethene difluoride (BODIPY). BODIPYs have many ideal photosensitiser characteristics including high extinction coefficients, high fluorescence quantum efficiencies, relatively insensitive to environment and resistance to photobleaching. In this study, two structural variations of BODIPY were investigated for their efficacies as photosensitisers. In the first variation, functionalisations such as meso-substitution and sulphonation to improve hydrophilicity were tested to fine-tune the activity of iodinated BODIPY. The second variation consisted of compounds with extended conjugation at the 4-pyrollic position which had not been studied before. The PDT efficacies of BODIPYs were evaluated by means of singlet oxygen generation rate and in vitro microculture MTT assay. The most potent BODIPY was further investigated for its intracellular localisation using confocal microscopy technique, cell cycle and apoptosis by flow cytometry and vascular occlusion efficiency in a chorioallantoic membrane (CAM) model. Among the 16 BODIPY structures studied, the iodinated compound **5** was the most effective in terms of photo-induced cytotoxicity and singlet oxygen production. The compound was also shown to localise exclusively in the mitochondria, induced G2/M-phase cell cycle block and apoptosis. In addition, a formulated preparation of compound **5** was found to extensively occlude the CAM vascular network following PDT, a feature that correlate with tumor regression in mouse tumor models. In conclusion, iodinated BODIPY structures such as compound **5** have promising potential to be developed as new PDT agents for cancer treatment.

Rosamines target the cancer oxidative phosphorylation pathway: *In vitro* and *in vivo*

S. H. Lim[1,4], L. Wu[2], L. V. Kiew[3], K. Burgess[2], L. Y. Chung[4], H. B. Lee[1]

[1]Cancer Research Initiatives Foundation, Subang Jaya, Selangor, Malaysia. [2]Department of Chemistry, Texas A&M University, Texas, USA. [3]Department of Pharmacology, Faculty of Medicine, University Malaya, Kuala Lumpur, Malaysia. [4]Department of Pharmacy, Faculty of Medicine, University Malaya, Kuala Lumpur, Malaysia.

26th Scientific Meeting of Malaysia Society of Pharmacology & Physiology on "Translation research for sustainable wellness: From perception to reality".
Penang, Malaysia. 18-20 May 2012.

Abstract

Reprogramming of energy metabolism has recently been identified as one of the hallmarks of cancer and therefore, mitochondria offer a unique target for cancer therapy. Previously, we had demonstrated the antiproliferative activity of a new class of mitochondria-targeting known as rosamines. These compounds were shown to was found to localize exclusively within the mitochondria and induced apoptosis as the major mode of cell death. We now described the *in vitro* cytotoxicity efficacy of a second generation rosamine analogs, the studies to identify the molecular targets of these molecules and their *in vivo* efficacy in a mouse allograft model. Experiments conducted on analogues KB14 and KB15 indicated inhibition of Complex II and ATP synthase activities of the mitochondrial oxidative phosphorylation pathway machinery which results in the loss of mitochondrial transmembrane potential. *In vivo* animal experiments showed that KB15 was able to inhibit the tumour growth of Balb/C mice implanted with 4T1 mouse mammary carcinoma cells by 23% compared to the untreated control. Our data suggests that rosamine analogues such as KB15 are good lead structures for the design of mitochondrial-targeting agents.

Photodynamic characterisation of amino acids conjugated 15[1]-hydroxypurpurin-7-lactone for cancer treatment

S. H. Lim[1,3], M. L. Yam[1], M. L. Lam[1], F.A. Kamarulzaman[1], N. Samat[1], L. V. Kiew[2], L. Y. Chung[3], H. B. Lee[1]

[1]Cancer Research Initiatives Foundation, Subang Jaya, Selangor, Malaysia. [2]Department of Pharmacology, Faculty of Medicine, University Malaya, Kuala Lumpur, Malaysia. [3]Department of Pharmacy, Faculty of Medicine, University Malaya, Kuala Lumpur, Malaysia.

University Of Malaya Researchers' Conference 2013.
University of Malaya
Kuala Lumpur. 19-20th November.

Abstract

This study aims to improve the physicochemical properties and biological effectiveness of 151-hydroxypurpurin-7-lactone dimethyl ester (G2), a semisynthetic photosensitiser, for the PDT treatment of cancer. The strategy undertook was by conjugating G2 with amino acids moieties such as aspartic acid and lysine. The photophysical properties, singlet oxygen generation, distribution coefficiency (LogD) and photostability of these analogues and their in vitro bioactivities such as cellular uptake, intracellular localization and photo-induced cytotoxicity were evaluated. In addition, selected analogues were also investigated for their PDT-induced vasculature occlusion in CAM model and antitumour efficacies in Balb/C mice bearing 4T1-mouse mammary tumour. From the study, conjugation with Asp improved the aqueous solubility G2 without affecting its photophysicochemical characteristics. G2-Asp showed similar in vitro and in vivo antitumour efficacies compared to the parent compound. Given the hydrophilic nature of G2-Asp, the photosensitiser is a pharmaceutically advantageous candidate as it can be formulated easily for administration and reduces the risk of vascular aggregation.

Appendix C

Published articles

1. Kamkaew A, Lim SH, Lee HB, Kiew LV, Chung LY, Burgess K. 2013. BODIPY dyes in photodynamic therapy. Chem Soc Rev. 42: 77-88. doi: 10-1039/c2cs35216h.

2. Lim SH, Thivierge C, Nowak-Sliwinska P, Han J, van den Bergh H, Wagnières G, Burgess K, Lee HB. 2010. In vitro and in vivo photo-cytotoxicity of BODIPY derivatives for photodynamic therapy. J. Med. Chem. 53: 2865-2874.

3. Lim SH, Yam ML, Lam ML, Kamarulzaman FA, Samat N, Kiew LV, Chung LY, Lee HB. 2014. Photodynamic characterisation of amino acids conjugated 151-hydroxypurpurin-7-lactone for cancer treatment. Mol Pharm. 11: 3164-3173.

4. Lim SH, Wu L, Kiew LV, Chung LY, Burgess K, Lee HB. Rosamines targeting the cancer oxidative phosphorylation pathway. PLoS ONE. 9(3): e82934.